

1. Report No. TX-95+987-4		2. Government Accession No.		3. Recipient's Catalog No.	
4. Title and Subtitle Initial Performance of Asphalt Overlays on Overlaid Jointed Concrete Pavement (JCP) and on Flexible Pavements in Field Test Sections in Lufkin, Texas				5. Report Date January 1995	
				6. Performing Organization Code	
7. Author(s) Yoon-Ho Cho, José Weissmann, and B. Frank McCullough				8. Performing Organization Report No. Research Report 987-4	
9. Performing Organization Name and Address Center for Transportation Research The University of Texas at Austin 3208 Red River, Suite 200 Austin, Texas 78705-2650				10. Work Unit No. (TRAIS)	
				11. Contract or Grant No. Research Study 3-110-89/94-987	
12. Sponsoring Agency Name and Address Texas Department of Transportation Research and Technology Transfer Office P. O. Box 5051 Austin, Texas 78763-5051				13. Type of Report and Period Covered Interim	
				14. Sponsoring Agency Code	
15. Supplementary Notes Study conducted in cooperation with the Texas Department of Transportation Research study title: "A Long-Range Plan for the Rehabilitation of U.S. 59 in District 11"					
16. Abstract <p>This report focuses on the performance of the various rehabilitation strategies implemented in the test sections placed on US 59 by the Lufkin District. Specific chapters discuss traffic, temperature, deflections, rutting, profiles, and the effectiveness of each rehabilitation strategy. The two sets of test sections constructed for this study have served as representative sections of rigid and flexible pavements in the Lufkin District.</p> <p>A Weigh in Motion (WIM) station was installed to collect such traffic information as axle classification, weight, speed, lateral distribution, and temperature — all of which can contribute to pavement damage. The WIM records both air and pavement temperature within the control sections.</p> <p>We surveyed, measured, and recorded at set intervals the rutting, profiles, and various kinds of cracks. Deflection measurements were recorded during the three stages of construction: before milling of the existing overlay, after milling, and after construction of the new overlay. These data summarize the structural response of the different pavement systems. Backcalculating the stiffness for the different layers of each test section shows the stiffness variation under repeated traffic loads. The rut depth survey verified that a pavement that has had rutting problems in the original pavement continues to have rutting problems. It also showed that the flexible base layer does not prevent rutting, even though it can prevent some reflective cracking. After analyzing the condition surveys, we concluded that all transverse cracks in the rigid sections are reflective cracks, while the transverse cracks in the flexible section are a combination of fatigue-related cracking and reflective cracking. The open grade mix (or Arkansas mix) performed better than the other rehabilitation methods. The pavement roughness was summarized using the International Roughness Index (IRI) and Pavement Serviceability Index (PSI). The crack and seat method showed the poorest serviceability after 2 years of traffic loading and exposure to the environment. This and other performance information will be used to identify optimal rehabilitation strategies for the rigid and flexible pavements throughout the Lufkin District.</p>					
17. Key Words Asphalt overlays, jointed concrete overlays, deflection measurements, backcalculation of pavement properties, rutting, condition surveys, roughness, rehabilitation strategies, US 59			18. Distribution Statement No restrictions. This document is available to the public through the National Technical Information Service, Springfield, Virginia 22161.		
19. Security Classif. (of this report) Unclassified		20. Security Classif. (of this page) Unclassified		21. No. of Pages 159	22. Price

**INITIAL PERFORMANCE OF ASPHALT OVERLAYS ON OVERLAID JOINTED
CONCRETE PAVEMENT (JCP) AND ON FLEXIBLE PAVEMENTS IN FIELD TEST
SECTIONS IN LUFKIN, TEXAS**

by

Yoon-Ho Cho
José Weissmann
B. Frank McCullough

Research Report Number 987-4

Research Project 3-110-89/94-987

A Long-Range Plan for the Rehabilitation of US 59 in District 11

conducted for the

Texas Department of Transportation

by the

CENTER FOR TRANSPORTATION RESEARCH

Bureau of Engineering Research

THE UNIVERSITY OF TEXAS AT AUSTIN

JANUARY 1995

IMPLEMENTATION

The long-range rehabilitation plan developed as part of this project will be directed toward the needs of US 59 within the Lufkin District. Although this long-range plan is being developed for the Lufkin District, the framework of this plan may be utilized for the cost-effective rehabilitation of pavements throughout Texas.

Prepared in cooperation with the Texas Department of Transportation.

DISCLAIMERS

The contents of this report reflect the view of the authors, who are responsible for the facts and the accuracy of the data presented herein. The contents do not necessarily reflect the official views or policies of the Texas Department of Transportation. This report does not constitute a standard, specification, or regulation.

**NOT INTENDED FOR CONSTRUCTION,
BIDDING, OR PERMIT PURPOSES**

B. Frank McCullough, P.E. (Texas No. 19914)
Research Supervisor

TABLE OF CONTENTS

IMPLEMENTATION STATEMENT.....	iii
SUMMARY	ix
CHAPTER 1. INTRODUCTION	1
1.1. BACKGROUND.....	1
1.2. STUDY OBJECTIVES.....	1
1.3. REPORT ORGANIZATION.....	2
CHAPTER 2. CONSTRUCTION AND MAINTENANCE OF TEST SECTION.....	3
2.1. EXISTING PAVEMENT STRUCTURE	3
2.2. CONSTRUCTION OF TEST SECTION.....	4
2.2.1. Overview.....	4
2.2.2. Rigid Section	4
2.2.3. Flexible Sections.....	6
2.3. DISTRESS AND MAINTENANCE OF THE TEST SECTIONS.....	6
CHAPTER 3. WEIGH IN MOTION INFORMATION.....	9
3.1. INTRODUCTION.....	9
3.2. INSTALLATION OF THE WIM STATION.....	9
3.3. DESCRIPTION OF THE WIM STATION	11
3.4. TRAFFIC DATA ANALYSIS	11
3.4.1. Average Daily Traffic Statistics.....	11
3.4.2. ESAL Summaries	13
3.4.3. Lateral Distribution.....	18
3.5. TEMPERATURE DISTRIBUTION IN THE TEST SECTION.....	19
3.5.1. Hourly Temperature Variations.....	19
3.5.2 Daily Temperature Variations.....	24
3.5.3. Monthly Variation of Temperature.....	27
CHAPTER 4. PAVEMENT DEFLECTION MEASUREMENTS.....	29
4.1. BACKGROUND.....	29
4.2. TEST EQUIPMENT AND DATA COLLECTION	29
4.3. PAVEMENT DEFLECTIONS BEFORE OVERLAY CONSTRUCTION.....	31
4.3.1 Rigid Section	31
4.3.2 Flexible Sections.....	34
4.4. DEFLECTIONS FOR THE RIGID TEST SECTIONS	35
4.4.1. Deflections during Construction.....	36
4.4.2. Deflections after Construction	40

4.4.3. Load Transfer for the Composite Pavement.....	42
4.4.4. Deflection Variation within the Lane	46
4.5. DEFLECTIONS FOR THE FLEXIBLE TEST SECTIONS	46
4.5.1. Deflection Variation after Construction	46
4.5.2. Deflection Variations within Lanes.....	48
4.6. SUMMARY	49
CHAPTER 5. BACKCALCULATION OF PAVEMENT PROPERTIES USING DEFLECTION DATA.....	51
5.1. BACKGROUND.....	51
5.2. DATA REQUIREMENTS	52
5.3. BACKCALCULATION PROCEDURE.....	52
5.4. BACKCALCULATION RESULTS FOR THE RIGID SECTIONS.....	55
5.4.1. Stiffness before Overlay	55
5.4.2. After Milling.....	58
5.4.3. Results after Construction.....	59
5.4.4. Results of 2 Years of Traffic Load Applications.	62
5.4.5. Structural Numbers for the Rigid Sections.....	65
5.5. BACKCALCULATION RESULTS FOR THE FLEXIBLE SECTION	66
5.5.1. Stiffness Variation for Flexible Sections.	66
5.5.2. Structural Number Calculation	69
5.6. SUMMARY	69
CHAPTER 6. RUTTING OF THE TESTS SECTIONS	71
6.1. BACKGROUND.....	71
6.2. MECHANISM OF RUTTING	71
6.3. FACTORS AFFECTING RUTTING PROGRESSION.....	71
6.4. RUTTING MEASUREMENT EQUIPMENT	73
6.5. RUTTING MEASUREMENTS BEFORE OVERLAY	74
6.5.1. Rut Depths for the Rigid Section.....	74
6.5.2. Rut Depth for the Flexible Section.....	76
6.6. RUT DEPTHS AFTER NEW OVERLAY.....	77
6.6.1. Rigid Section	77
6.6.2. Flexible Section	80
6.7. RELATIONSHIP BETWEEN RUT DEPTHS VERSUS DEFLECTIONS.....	83
6.7.1. Rigid Sections.....	83
6.7.2. Flexible Sections.....	89
6.7.3. Summary.....	91
CHAPTER 7. CONDITION SURVEY.....	93

7.1. INTRODUCTION.....	93
7.2. RIGID SECTIONS BEFORE CONSTRUCTION	93
7.2.1. Transversal Cracking.....	93
7.2.2. Longitudinal Cracking	94
7.3. FLEXIBLE SECTIONS BEFORE CONSTRUCTION	95
7.3.1. Transversal Cracking.....	95
7.3.2. Longitudinal Cracking	96
7.4. SURVEY AFTER MILLING OF THE EXISTING OVERLAY.....	97
7.4.1. Transversal Cracking.....	98
7.4.2. Longitudinal Cracking	98
7.5. CONDITION SURVEYS AFTER CONSTRUCTION FOR THE RIGID SECTIONS.....	98
7.5.1. Transversal Cracking.....	99
7.5.2. Longitudinal Cracking	102
7.5.3. Other Distresses	105
7.6. SUMMARY OF CONDITION SURVEY RESULTS FOR RIGID SECTIONS	107
7.7. CONDITION SURVEYS AFTER CONSTRUCTION FOR FLEXIBLE SECTIONS	109
 CHAPTER 8. ROUGHNESS.....	 113
8.1. BACKGROUND.....	113
8.1.1. Equipment for Measuring Roughness.....	113
8.1.2. Data Collection Procedure	115
8.2. PROFILE DATA COLLECTION BEFORE CONSTRUCTION.....	115
8.2.1. Rigid Sections.....	115
8.2.2. Flexible Sections.....	117
8.2.3. PSI for the Rigid and Flexible Sections.....	118
8.3. RIGID TEST SECTION ROUGHNESS PERFORMANCE AFTER OVERLAY.....	120
8.4. PERFORMANCE OF THE RIGID TEST SECTIONS AFTER OVERLAY	123
8.5 . FLEXIBLE SECTION ROUGHNESS PERFORMANCE AFTER OVERLAY.....	124
8.6. PERFORMANCE OF THE FLEXIBLE TEST SECTIONS AFTER OVERLAY.....	126
8.7. SUMMARY	127
 CHAPTER 9. CONCLUSIONS AND RECOMMENDATIONS	 129
9.1. CONSTRUCTION AND MAINTENANCE OF THE TEST SECTIONS	129
9.2. INFORMATION RECORDED BY THE WIM STATION.....	129
9.3. PERFORMANCE OF THE ASPHALT OVERLAYS ON THE	

TEST SECTIONS	129
9.4. PERFORMANCE EVALUATION OF EACH REHABILITATION ALTERNATIVE FOR THE RIGID SECTIONS.	132
9.5. PERFORMANCE EVALUATION OF EACH REHABILITATION ALTERNATIVE FOR THE FLEXIBLE SECTIONS.	134
REFERENCES	137
APPENDIX A.....	141
APPENDIX B	147

SUMMARY

This report focuses on the performance of the various rehabilitation strategies implemented in the test sections placed on US 59 by the Lufkin District. Specific chapters discuss traffic, temperature, deflections, rutting, profiles, and the effectiveness of each rehabilitation strategy. The two sets of test sections constructed for this study have served as representative sections of rigid and flexible pavements in the Lufkin District.

A Weigh in Motion (WIM) station was installed to collect such traffic information as axle classification, weight, speed, lateral distribution, and temperature — all of which can contribute to pavement damage. The WIM records both air and pavement temperature within the control sections.

We surveyed, measured, and recorded at set intervals the rutting, profiles, and various kinds of cracks. Deflection measurements were recorded during the three stages of construction: before milling of the existing overlay, after milling, and after construction of the new overlay. These data summarize the structural response of the different pavement systems. Backcalculating the stiffness for the different layers of each test section shows the stiffness variation under repeated traffic loads. The rut depth survey verified that a pavement that has had rutting problems in the original pavement continues to have rutting problems. It also showed that the flexible base layer does not prevent rutting, even though it can prevent some reflective cracking. After analyzing the condition surveys, we concluded that all transverse cracks in the rigid sections are reflective cracks, while the transverse cracks in the flexible section are a combination of fatigue-related cracking and reflective cracking. The open grade mix (or Arkansas mix) performed better than the other rehabilitation methods. The pavement roughness was summarized using the International Roughness Index (IRI) and Pavement Serviceability Index (PSI). The crack and seat method showed the poorest serviceability after 2 years of traffic loading and exposure to the environment. This and other performance information will be used to identify optimal rehabilitation strategies for the rigid and flexible pavements throughout the Lufkin District.

CHAPTER 1. INTRODUCTION

1.1. BACKGROUND

Carrying more than 19,000 vehicles a day, the US 59 corridor is one of the most heavily traveled highways in Texas and an important link to Houston. Because it is an older highway, however, it is now in need of rehabilitation. One of the objectives of Project 987 is to evaluate rehabilitation alternatives available for this important corridor. This report assesses the performance of a particular rehabilitation strategy — an asphalt overlay — on US 59 near Lufkin, Texas.

Since its construction in the 1940s, US 59 has received several overlays to improve ride quality. The primary distresses observed with the previously employed rehabilitation procedures include reflective cracking in the rigid (jointed concrete pavement, or JCP) sections, rutting in the flexible (hot mix asphalt cement, or HMAC) sections, and fatigue cracking. For this study, test sections were constructed on both the rigid and flexible sections using various rehabilitation methods.

1.2. STUDY OBJECTIVES

The overall objective of this study is to provide a long-range rehabilitation plan for US 59 in the Lufkin District. Within the short term, the study will assist in the planning, design, construction, and performance monitoring of alternative experimental pavement test sections along US 59. Test sections were built to observe pavement performance under actual field conditions (i.e., traffic loading and changing climate). Various designs and construction solutions were applied to prevent observed problems of reflective cracking and rutting. Data collection was performed before the overlay construction, during construction of the test sections, and after overlay construction under a carefully designed monitoring program. Structural factors investigated to explain performance of the overlay included cross sections, core, deflection, and stiffness from the backcalculation procedures. Deflection measurements taken before and after construction are reported to show the overlay effect on the rigid sections. Roughness was expressed with the International Roughness Index (IRI) and the Pavement Serviceability Index (PSI), and condition surveys included cracking and rutting. A weigh-in-motion (WIM) device was installed to collect traffic-related information, including weight per axle, speed, lateral position and headway between two vehicles. Pavement temperature information was also collected at the WIM site.

The long-range rehabilitation plan will include: (1) prediction of the performance during the planning horizon; (2) effects of previous pavement condition on the overlay performance; (3) other factors affecting performance of the different overlay alternatives on rigid and flexible sections; (4) prediction of performance; and (5) determination of an optimal rehabilitation strategy for the different pavement sections along US 59.

1.3. REPORT ORGANIZATION

Chapter 2 describes the selection, design, construction, and maintenance history of the test sections. Chapter 3 then presents the traffic loading information recorded by the WIM station installed at the site, as well as the hour, day, and month pavement temperature variation within the test sections. This chapter also discusses the differences between the estimated traffic and the actual traffic volumes recorded by the WIM station at the site. Other important traffic characteristics, such as lateral position of wheel loading and lane distributions, are also discussed in this chapter.

Chapters 4 through 8 report pavement overlay performance at the test site on US 59. It also contains deflection information for both the rigid and the flexible test sections, while Chapter 5 includes the backcalculation procedure of pavement material properties. Chapter 6 documents all the rutting information; Chapter 7 covers the detailed condition survey. Chapter 8 summarizes the profile data obtained using the International Roughness Index (IRI), while Chapter 9 presents the report's conclusions and recommendations.

CHAPTER 2. CONSTRUCTION AND MAINTENANCE OF TEST SECTION

2.1. EXISTING PAVEMENT STRUCTURE

The asphalt overlay test sections on both the rigid and flexible pavements are located south of Lufkin on US 59. The rigid section was constructed in 1936 using the 22.86-17.78-22.86 cm (9-7-9 inch) design of jointed concrete pavement (JCP), without soil treatment or dowels. It has 4.572-m (15-foot) contraction joints and expansion joints every 36.576 m (120 feet). As traffic on US 59 increased, overlays (as many as five) were applied using a thin asphalt overlay having an average asphalt overlay thickness of 17.78 cm (7 in.). The average daily traffic (ADT) volume was 14,150 in 1991, of which about 20 percent was composed of truck traffic (Ref 2). Based on the condition survey results, the most common distress observed on the test sections before overlay was reflective cracking. These cracks were filled with thin asphalt tar to prevent water from reaching the subgrade.

The flexible test section was built in 1966 with 3.81 cm (1.5 in.) of asphalt concrete on 15.24 cm (6 in.) of cement treated base, with 15.24 cm (6 in.) of lime-treated subgrade. Since the construction, three thin asphalt overlays have been placed. Longitudinal and transverse cracking are found throughout the test section, and water-related problems (e.g., stripings) were observed. The cross section before construction is shown in Figure 2.1.

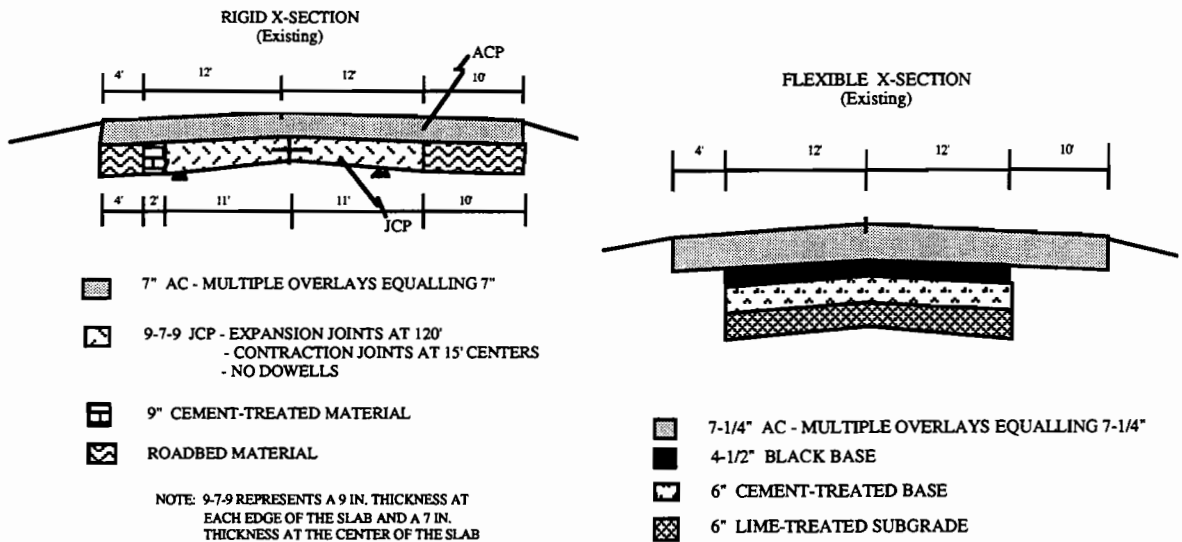


*Figure 2.1 Typical plane section of the test section before construction
(1 inch=2.54 cm; 1 foot=0.304 m)*

2.2. CONSTRUCTION OF TEST SECTION

2.2.1. Overview

The rigid section, running from station number 1490+00 to 1420+00, is 2,133.6 m (7,000 feet) long; the flexible section, running from station number 1060+00 through 990+00, is also 2,133.6 m (7,000 feet) long. Fourteen test sections, each 304.8 m (1,000 feet) long, were constructed to represent potential rehabilitation procedures that merited detailed investigation for application in a long-range rehabilitation plan for US 59 (Ref 2). These test sections, described below, are basically divided into rigid and flexible test sections. These test sections represent the various types of pavements found on US 59.

2.2.2. Rigid Section

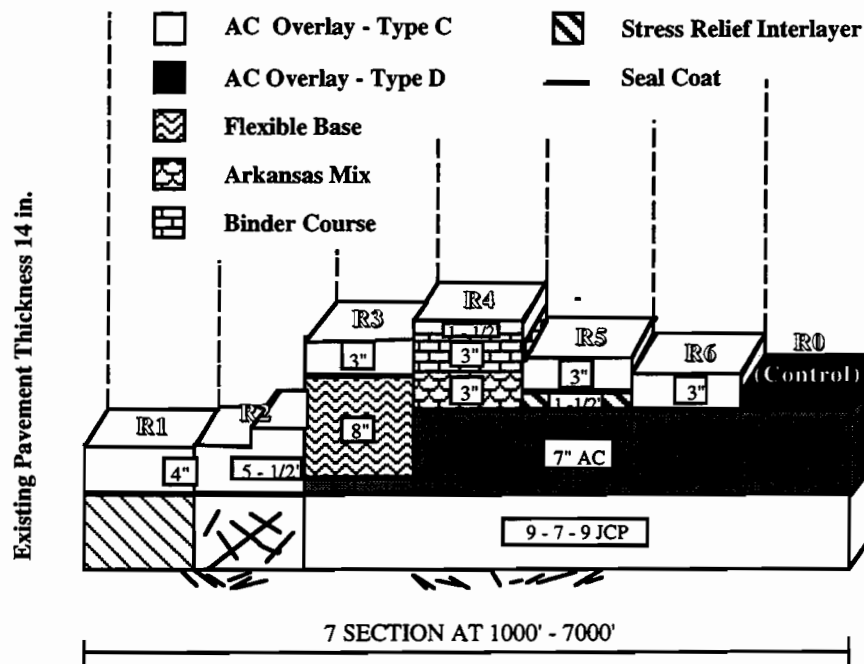
The construction of the rigid sections started in March 1991 and was completed in April 1992. The construction was delayed because the construction sites experienced a high incidence of rain during the summer. During construction, the traffic from the southbound lanes was detoured to the inside lane of the northbound lanes. Details of the traffic detouring procedures were described in a previous report (Ref 3). The rigid test section consists of six test sections and one control section, as shown in Figure 2.2. These sections are classified into two groups: disturbed sections and non-disturbed sections. The disturbed sections are composed of sections R1, R2, and R3, which had the existing asphalt overlay milled off. The non-disturbed sections are composed of the three remaining test sections, and one control section that did not experience surface preparation.

Section R1 was monitored to observe the effects of the existing crack maintenance before the asphalt overlay. The old asphalt overlay on this section was milled off and its cracks and joints then water- and air-blasted. After the cracks and joints were cleaned, black tar was applied as a sealant. A high-molecular-weight monomer was applied to repair the spalling. The inside shoulder was extended 198 cm (72 in.) and was constructed using a 22.8-cm (9-inch) thick JCP. Sawcuts were used to control cracking. The saw cuts started at 79.2 m (260 feet) and ended at 234.6 m (770 feet), with joint spacing every 4.5 m (15 feet), leaving the first 79.248 m (260 feet) and the last 70.1 m (230 feet) with no sawcuts (so that this effect could be studied).

Sections R2A and R2B were included in the experiment to verify the performance of a crack and seat method. In this procedure, the existing JCP was broken into pieces using a large weight hammer; this was followed by seating with the application of a heavy-weight tire roller. This procedure is used to prevent reflective cracking on overlaid pavements. The difference in thickness between R2A and R2B is 3.81 cm (1 1/2 in.).

A flexible base was used on section R3, which had 12.7 cm (5 in.) out of the 17.78 cm (7 in.) of the existing asphalt milled off, followed by 7.62 cm (3 in.) of type C surface. The flexible base was meant to protect the surface layer from the reflective cracking action of the rigid pavement underneath.

Sections R4, R5, R6, and R0 represented the non-disturbed sections in the experiment. Open-graded mix, also known as Arkansas mix, was placed on the existing old asphalt overlay (unmilled) on the R4 test section. Based on previous experience on IH-45 and on the experience of CTR and district staff, 7.62 cm (3 in.) of open-grade mix were followed by 7.62 cm (3 in.) of type B and 3.81 cm (1 1/2 in.) of type C surface material. Section R5 used a 2.54-cm (1-inch) layer of Styrene Butadiene Block Copolymer (SBS) modified-plant mix seal as a stress relief interlayer. Over this stress relief interlayer, a 7.62-cm (3-inch) thick type C asphalt overlay was applied. Sections R6 and R0 had similar asphalt overlay thicknesses, the main difference being the aggregate sizes used in the mix. Section R6 had a type C mix, while the control section R0 had an overlay of type D mix.



- R1 - REPAIR/REPLACE PCC + AC OVERLAY**
- R2 - BREAK AND SEAT**
- R3 - FLEXIBLE BASE + OVERLAY**
- R4 - ARKANSAS MIX**
- R5 - STRESS RELIEF INTERLAYER**
- R6 - AC OVERLAY**
- R0 - AC OVERLAY - TYPE D (CONTROL)**

Figure 2.2 Construction of test section in rigid site (1 inch=2.54 cm; 1 foot=0.304 m)

2.2.3. Flexible Sections

Like the rigid sections, the flexible test sections included six design alternatives and a control section. The preparation of the construction sites started in August 1991, with all construction completed by July 7, 1992. The weather again delayed construction.

Because attempts to construct detours did not prove cost-effective, a decision was made to complete the construction of the flexible sections by rehabilitating one lane at a time. The outside lane was constructed first, followed by the inside lane.

The flexible sections also included milled and non-milled sites. For section F0 and on sections F1 through F4, the existing asphalt overlays were preserved, while on sections F5 and F6 the existing asphalt overlay was milled off. The sections that were not milled have almost the same thickness. But, as shown in Figure 2.3, there were differences in asphalt material design parameters (e.g., aggregate grading and asphalt binder). For example, the only difference between sections F1 and F2 is the aggregate type used, while the only difference between sections F2 and F4 is the AC binder used. Section F3 has a type B asphalt overlay under 3.8 cm (1 1/2 in.) of type C surface. The asphalt binder used in all test sections was AC 20, with the exception of sections F1 and F2, which both used an SBS-modified binder. SBS is an elastomeric polymer that modifies the asphalt properties to improve the slope of the viscosity-versus-temperature curve (Ref 4). The milled sections include one flexible base section (like the rigid sections) and one thicker pavement section that will be used to investigate the effect of thickness. Research Report 987-3 (Ref 5) contains more information regarding test section construction.

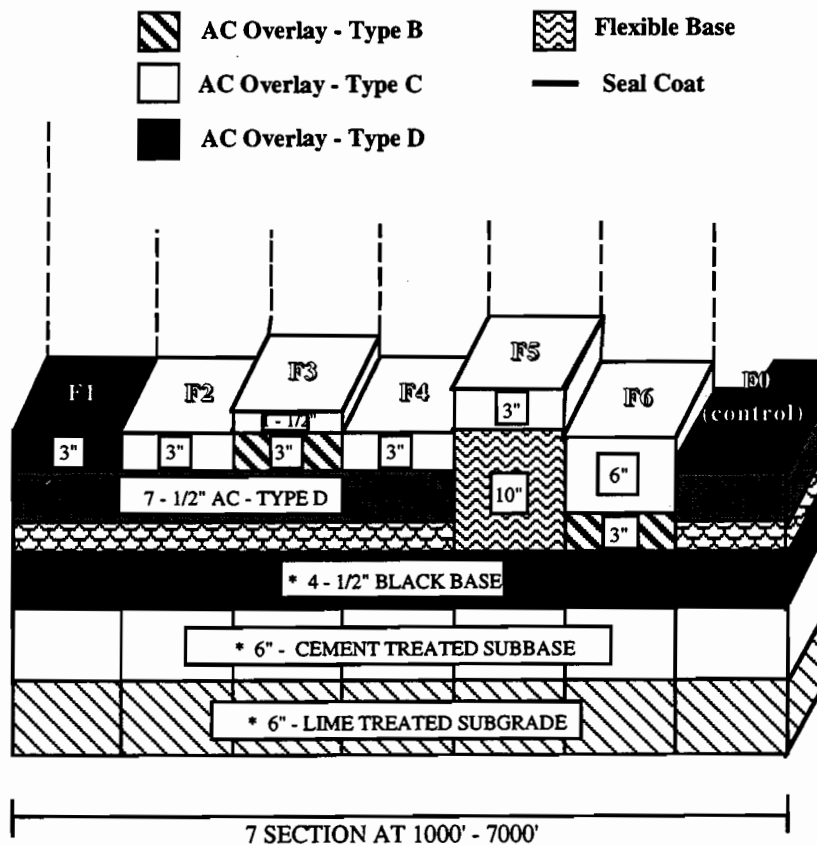
2.3. DISTRESS AND MAINTENANCE OF THE TEST SECTIONS

Several of the test sections performed poorly and cracked extensively after they were opened to traffic. Sections R2A and F5 especially exhibited poor performance, as indicated in Figures 2.4 and 2.5. Severe cracks and areas of pumping were repaired by the district.

In section R2A, a large pothole and some additional fine alligator cracking were repaired by patching in January 1993. The pothole was approximately 0.6 m (2 feet) wide and 3 m (10 feet) long; the alligator cracking was observed 4.572 m (15 feet) in each direction from the pothole. Moderate pumping was also observed in the pothole. This section also had patches applied in three places in November 1993.

The flexible base section F5 exhibited base failure, with rutting, severe alligator cracking, and raveling appearing on the outside wheel path for the right lane from station 1009+70 to 1008+90, which was located at the crest of a vertical curve. For the forensic analysis, seven cores were taken from the site and vacuum extraction was performed by the district. According to maintenance records available at the district, the AC base and surface seem to be a very porous mix, with air voids ranging from 8 to 10 percent. Because water was observed migrating through the ACP and along the coarse surface treatment, two samples of the flexible base (taken from the top and bottom of the layer) were checked for moisture content. The bottom sample presented a higher water content of 8.5 percent, while the top sample presented a water content of 7.5

percent. After confirming that the failure mode of the pavement structure was associated with base failure, the district, in conjunction with CTR staff, decided to remove the distressed area and replace it with a cement-treated patching material 33 cm (13 in.) thick, a commonly used corrective procedure for this type of failure. After subsequent rainfall, additional distressed areas were observed in the outside wheel path. The distressed areas underwent the same type of treatment described previously. To prevent further rapid deterioration, a seal coat was applied in March 1993 to the areas showing distress.



- F1 - SBS MODIFIED AC OVERLAY TYPE D
- F2 - SBS MODIFIED AC OVERLAY - TYPE C
- F3 - AC OVERLAY - TYPE C
- F4 - AC OVERLAY - TYPE C
- F5 - REMOVE STRIPPED LAYER - FLEXIBLE BASE
- F6 - REMOVE STRIPPED LAYER
- F0 - AC OVERLAY - TYPE D (CONTROL)

*1 inch = 2.54 cm

Figure 2.3 Construction of test section in flexible site



Figure 2.4 Example of failure in R2A



Figure 2.5 Example of failure in F5

Finally, we determined that heavily loaded timber trucks were causing much of the pavement distress observed on the test sections. Besides causing structural damage, these trucks leave many small pieces of wood on the pavement. During hot summers, these wood particles penetrate the soft pavement; later, as the wood decays, voids are created that lead to potholes.

CHAPTER 3. WEIGH IN MOTION INFORMATION

3.1. INTRODUCTION

The AASHO Road Test and other research efforts have determined that pavement performance is directly related to the number of load applications imposed on the pavement section. Precise information on traffic loads is essential for the study of pavement performance. Particularly relevant are the following: (1) effects of traffic loading on pavement performance, (2) selection of optimal rehabilitation strategies, and (3) development of a pavement rehabilitation design method. The effects of traffic loading on pavement performance, the selection of optimal rehabilitation strategies, and the development of a pavement rehabilitation design method will be discussed in a subsequent report.

Unlike previous test sections in several uncontrolled experiments (where precise information on traffic volumes and axle loads was not available), the test sections described in the previous chapter have a complete history of axle load applications, as recorded by a weigh-in-motion (WIM) station installed at the test site. A WIM station is an installation capable of, first, measuring the dynamic tire forces of a moving vehicle, and then estimating with great accuracy the corresponding axle loads of the vehicle; such information can then be used to calculate the equivalent single axle loads (ESALs) applied to the pavement test sections (Ref 6). The software and hardware combination included at the US 59 test site WIM station identifies traffic mix by estimating gross vehicle weights. In addition to collecting WIM data, the hardware and software set-up installed at the test site can report speed, axle spacing, lateral position of the vehicles passing through the test site, and pavement temperatures.

3.2. INSTALLATION OF THE WIM STATION

In March 1992, the weighpads of the WIM station were installed on the control section of the rigid test sections; after installation, the rigid test section was open to traffic. Unfortunately, the longitudinal traffic stripes were found to be misplaced on the rigid section during a routine survey carried out in July 1992 by CTR staff. Because this problem affected the data collected for lateral displacement, it will be discussed later in this report. After reviewing the longitudinal stripes after overlay, a contractor sandblasted the paint stripes off the pavement, about 6,096 m (20,000 feet) in length; the stripes were then relocated in June 1993. Figure 3.1 shows the improper location of the longitudinal stripes on the rigid section; the corrected positions of the longitudinal stripes are depicted in Figure 3.2. The WIM station for the flexible section was installed in July 1992; these sections were open to traffic once installation was completed.

The WIM station was calibrated using a TxDOT three-axle truck in November 1992; continuous traffic data collection started the following month. In addition to traffic load information, air and 2.54 cm (1 inch) deep pavement temperatures were accumulated during April 1993. Further calibration with a TxDOT five-axle truck was performed in August 1993; lateral position measurements were also calibrated using a test car on the same date.

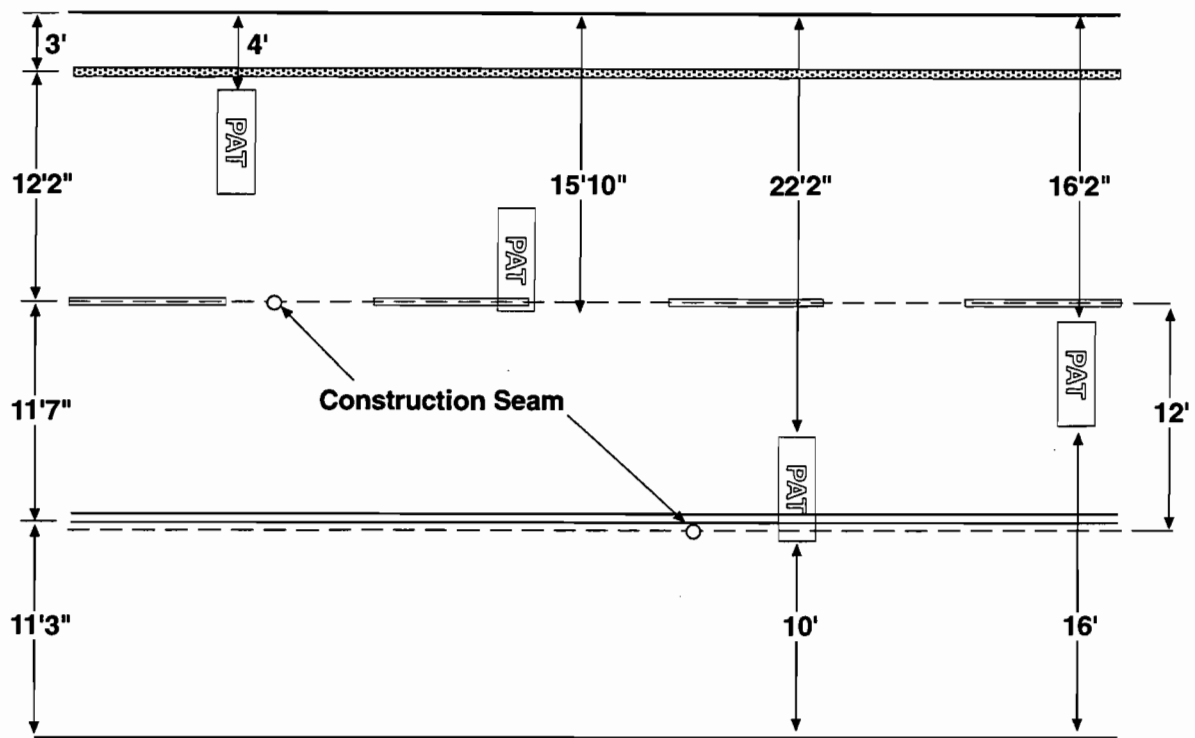


Figure 3.1 Incorrect lateral striping location (1 inch=2.54 cm; 1 foot=0.304 m)

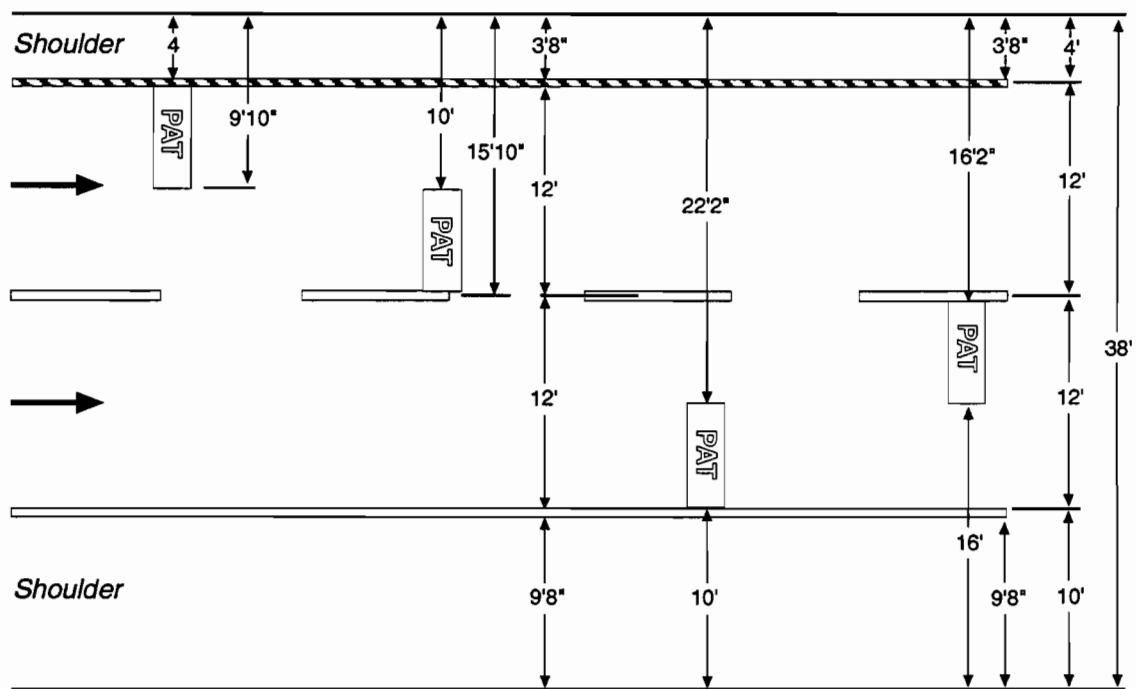


Figure 3.2 Current striping location (1 inch=2.54 cm; 1 foot=0.304 m)

The first version of the software developed for the traffic data acquisition of the WIM station considered only the truck traffic load data for both the rigid and flexible sections. Given the small amount of pavement damage caused by a passenger car (as translated into ESALs), we considered the missing WIM passenger car data in the early stages of the traffic monitoring unimportant.

3.3. DESCRIPTION OF THE WIM STATION

The WIM station consists of weigh-in-motion weighpads placed on each wheel path, an inductance loop detector placed before the weighpads, an infrared light beam transmitter, and a receiver in each lane. The infrared transmitter is connected to the corner of one of the weighpad frames, while the receiver is placed at the edge of the shoulder. The data processing units are located in a cabinet near the edge of the right-of-way line. The loop detector senses the presence of a vehicle, so that the weighpads can count the correct number of axles per vehicle. The two weighpads in each lane are staggered 4.5 m (15 feet) apart. This distance divided by the time interval for an axle to pass between the weighpads allows for the calculation of vehicle speed. The axle spacing is calculated by measuring the time interval between successive wheels crossing the same weighpad, and then multiplying the time by the speed.

The infrared light beams are located just above the pavement surface and at a sixty-degree angle (with respect to the direction of travel). The time interval between one front wheel crossing the weighpad threshold and breaking the infrared light beam is used to calculate the lateral position of the wheel with respect to the edge of the lane. The interruption time for each successive wheel on the vehicle is measured and compared with that of the front wheels. This interruption time multiplied by the speed can be used as a proxy for the tire width. The front axle of each vehicle is assumed to have single tires. The interruption times for wheels on the other axles can be compared with the front wheel to indicate whether they have single or dual tires.

The data collected for each vehicle include time of day, lane, wheel weights, speed, axle spacing, lateral position, and single or dual tires. All data collected in one day at each site are included in one computer file, which may be either downloaded directly to a computer on site, or downloaded by modem to a computer in Austin.

3.4. TRAFFIC DATA ANALYSIS

The traffic data analysis for this research project will be covered more fully in a subsequent report. Data made unavailable by calibration activity and unexpected operational errors were extrapolated. Average daily traffic volume (ADT), equivalent single axle load (ESAL), and the lateral distribution data summaries on the rigid section are discussed below.

3.4.1. Average Daily Traffic Statistics

The ADT for the test sections was calculated by dividing the accumulated traffic volume by the number of days for which traffic was counted. Since the continuous count of all vehicle classes started in December 1992, the traffic information for 1993 was used to calculate the ADT.

This ADT, summarized in Table 3.1, totaled 7,207 vehicles, of which 80 percent were two-axle vehicles. Report 987-2 includes detailed traffic flow summaries, including hourly and weekly traffic volumes, lane distribution by volume, traffic composition, and speed. (Ref 3). ADT volume variations are shown in Figures 3.3 and 3.4 for both the right and left lanes. The traffic volume for two-axle vehicles on weekdays is higher than that for weekends. However, the truck traffic for five-axle trucks is lower during the weekends. This indicates that the road is used by truck traffic during weekdays, and by smaller cars during weekends. Another conclusion drawn from Figures 3.3 and 3.4 is that there are significant vehicle volume differences between the right and left lanes, such that right lane volumes far exceed left lane volumes. This information will be used in subsequent reports to calculate the indirect costs (e.g., user delay costs and operating costs) of rehabilitation activities.

Table 3.1 Average daily traffic information for test sections in 1993

	Number of Axles				
	Two	Three	Four	Five	Six or more
Left Lane	1602	31	28	131	4
Right Lane	4138	137	134	982	21

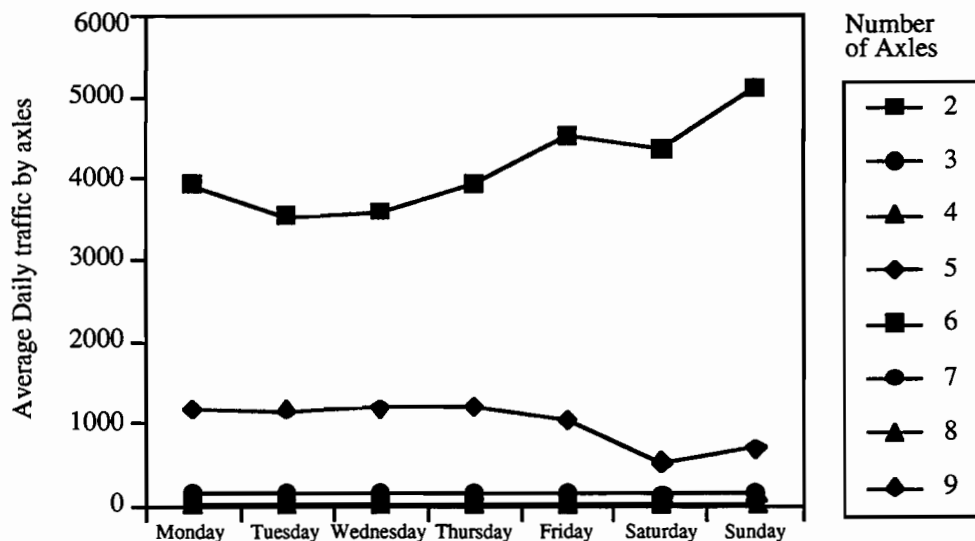


Figure 3.3 Average daily traffic volumes for the right lane

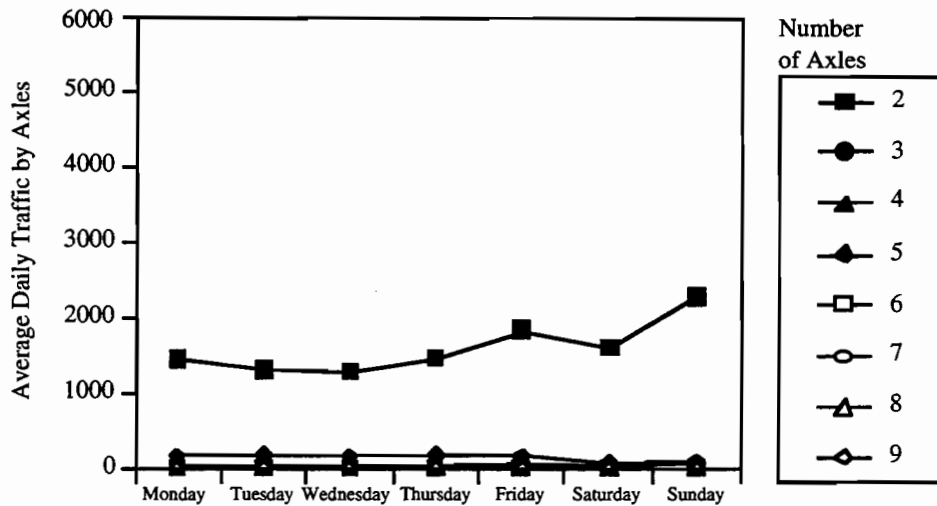


Figure 3.4 Average daily traffic volumes for the left lane

3.4.2. ESAL Summaries

One of the most important conclusions of the AASHO Road Test was that the axle-load-to-pavement-damage relationship follows a fourth power relationship, such that a wheel load twice as large as another will cause the equivalent of 16 times the pavement damage. Each test section of the AASHO Road Test was subjected to uniform traffic loading and, to convert the results to mixed traffic condition, the concept of equivalent single axle load (ESAL) was developed. The damage caused by one ESAL is defined as the pavement damage caused by an 80-kN (18-kip) single-axle load, which was the legal limit in the U.S. at that time. According to the AASHTO guide, the ESAL is a function of the pavement structure, as represented by the structural number (SN), axle type and weight, and terminal serviceability (Ref 7).

Based on the stiffness results obtained from the backcalculation procedures reported in Chapter 5, the structural number for each of the test sections was calculated. The terminal serviceability was set at 2.5, since this is considered the value that reflects TxDOT's policy for pavement management. The ESALs for the rigid sections were calculated using the data accumulated since the installation of the WIM station, a period of about 18 months. The detailed calculations for the ESALs are provided in Report 987-6; the relevant summaries are reported below.

The classification of traffic by number of axles for both lanes is presented in Figures 3.5 and 3.6 by ESAL and vehicle volumes on a yearly basis for 1993. The distribution by vehicle volumes shows that the light, two-axle vehicles, usually passenger cars, comprise 76 percent of the total volume on the right lane and 89 percent on the left lane. The standard truck, the regular five-axle 18-wheeler, comprises 19 percent of the total traffic volume on the right lane and 8 percent of the traffic volume on the left lane. The left lane has a higher percentage of passenger cars and less truck volume, as expected.

The traffic summaries based on the ESALs show dramatic differences in the statistics when compared with the summaries based solely on the traffic volumes for the different vehicle categories. Two-axle vehicles cause only 2 percent of the pavement damage, as represented by ESAL applications, while five-axle trucks caused 90 percent of the pavement damage in the right lane. The left lane also has 86 percent of the pavement damage caused by five-axle trucks, and only 4 percent of pavement damage caused by the two-axle vehicles. This means that two-axle cars are responsible for less than 5 percent of the total pavement damage, even though the two-axle cars account for over 80 percent of the traffic volume. Among the trucks, the five-axle truck accounts for most of the pavement damage, with such trucks responsible for over 85 percent of the damage. Moreover, five-axle trucks caused 90 percent of the pavement damage on the right lane, which is the design lane. This underscores the need for accurate traffic predictions for truck traffic volumes, since a small error in such predictions will lead to large errors in the pavement design.

These results suggest that the lane distribution calculated by traffic volume could represent unreliable information for the pavement thickness design, since 70 to 80 percent of the traffic volume consists of lightweight, two-axle cars. For example, the lane distribution by traffic volume presented in Table 3.2 was calculated in a previous report (Ref 3). This resulted in an overall lane distribution of 75:25. After continuously monitoring the traffic using the WIM station, we obtained the lane distribution by traffic volume shown in Figure 3.7. The total accumulated traffic volume on the right lane is about 3.2 million vehicles, and about 0.87 million vehicles for the left lane. The right lane carries about 75 percent of the total traffic volume, while the left lane carries 25 percent. This means that the lane distribution determined by sampling the traffic for a week (as described in Report 987-2) was correct, considering that the error margin was less than 1 percent.

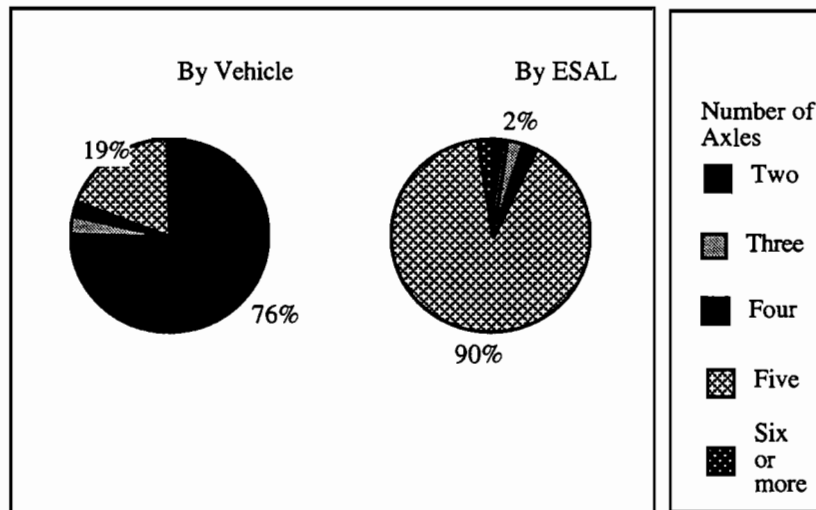


Figure 3.5 Vehicle classification in the right lane

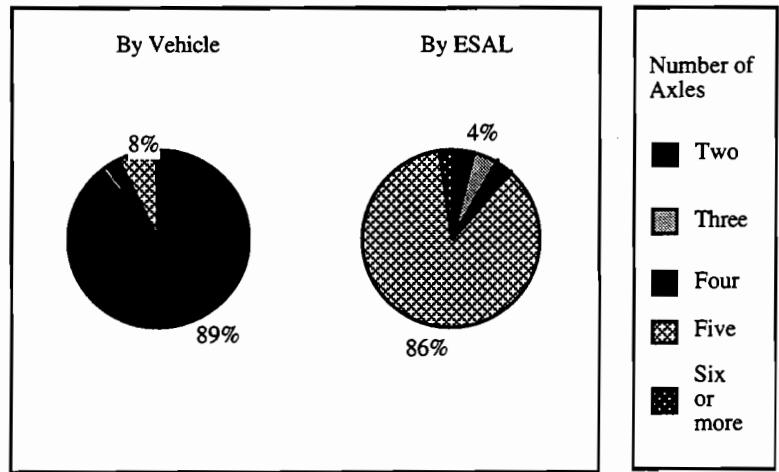


Figure 3.6 Vehicle classification in the left lane

Table 3.2 Lane distribution at rigid test section (after Ref 3)

Location	Single Tire (Veh. per hour)	Dual tire (Veh. per hour)	Total
Right Lane (Lane 1)	166	55	221
Left lane (Lane 2)	60	13	73
Total	226	68	294
Lane Distribution	73:27	81:19	75:25

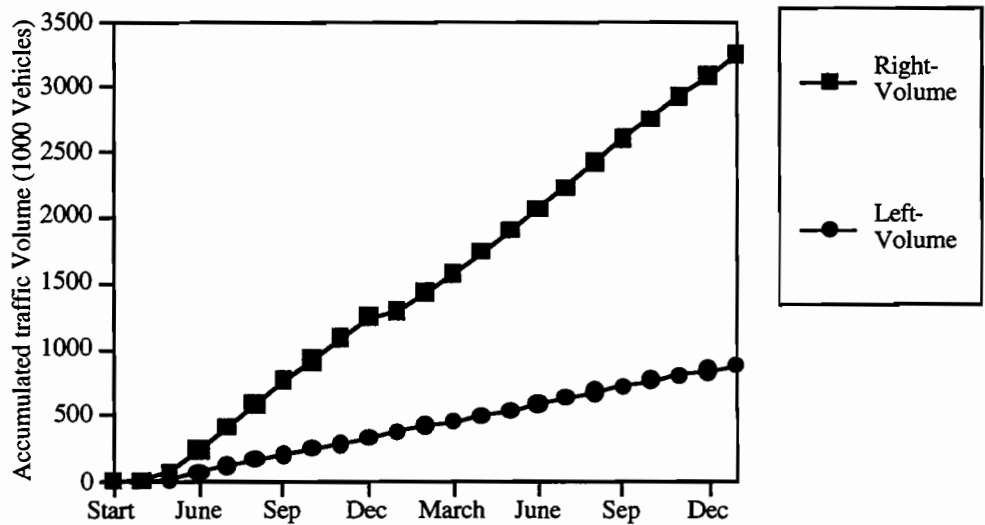


Figure 3.7 Accumulated traffic volume

The summaries of the calculations based on the ESALs and traffic volumes are reported in Table 3.3. The lane distribution calculated by ESALs is 89:11; this means that almost 90 percent of the pavement damage from traffic loading occurred on the right lane. In pavement design, the design traffic is obtained by multiplying the directional ADT by the lane distribution factor. Consequently, inadequate lane distribution factors based on ADT will translate into thinner layers, which over the long run will require more frequent maintenance and repair. However, if precise ESAL counts are not available, then lane distribution factors calculated by heavy vehicle traffic volume distributions could be an acceptable option. This may be observed in Table 3.3, where the results based on ESALs and traffic volumes are fairly similar.

Table 3.3 Lane distribution of the rigid section

Lane Distribution	All vehicles	Two-axle	Four-axle	Six or more axles
by Vehicle	75:25	72:28	83:17	86:14
by ESAL	89:11	83:17	85:15	88:12

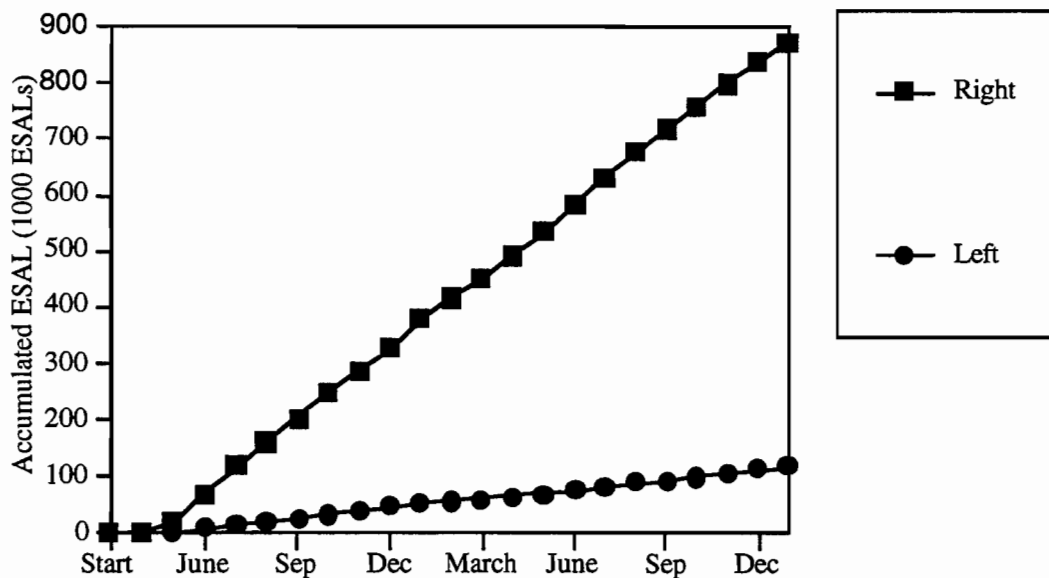


Figure 3.8 Accumulated ESALs of two lanes under SN = 4

Since the test sections consist of various layers, the structural number (SN) for each of the test sections is different, as explained in Chapter 5. The different SN affects the ESAL calculations, with such calculations more sensitive to changes in an SN range of between 6 and 7. Figure 3.9 shows that the accumulated ESAL difference between SN 6 and 7 is larger than the difference between SN 4 and 6. For about 20 months, the difference is about 100,000 ESALs, a number that suggests the importance of the structural number in calculating ESALs for pavement design.

Usually the pavement design process requires at least 20 years of traffic estimation obtained either by simple extrapolation of the available traffic data, or through more complex traffic modeling. Many pavement engineers rely on simple curve fitting to obtain design traffic information for a 20-year period.

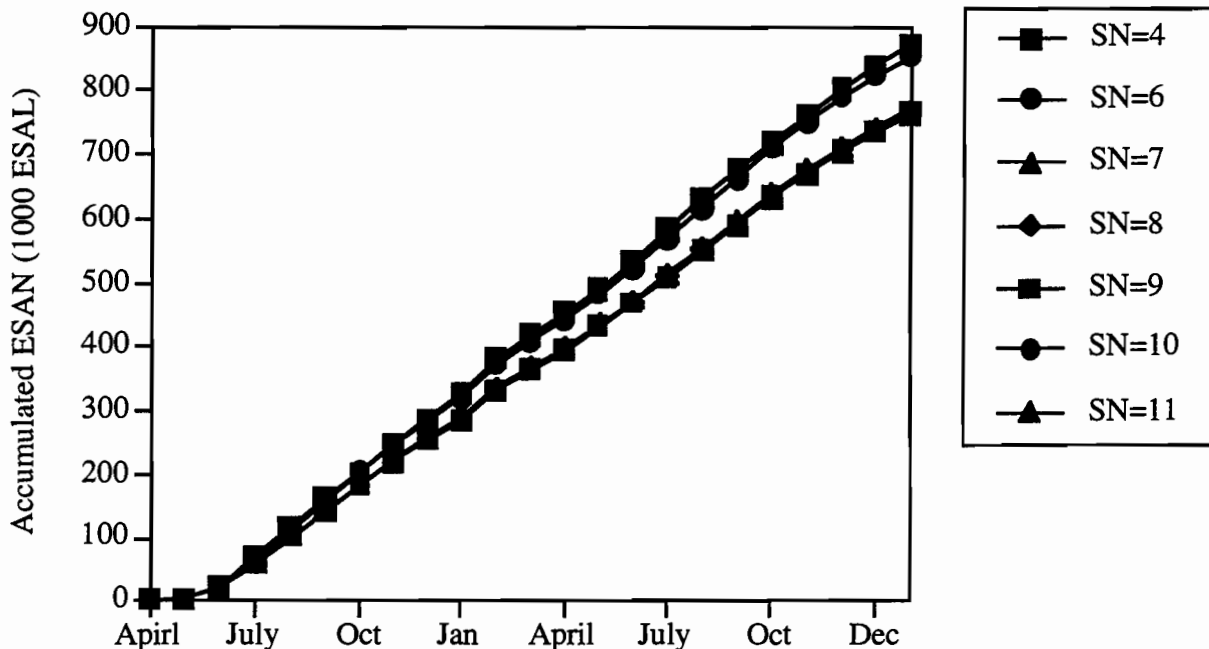


Figure 3.9 Accumulated ESAL variation under different SN

The test section design was also based on an extrapolation of ESALs (Ref 2). The comparison between observed ESALs obtained from the WIM station and the results of the prediction used in the design permits the study of the reliability of the ESAL predictions used in the design of the pavement test section. Figure 3.10 shows that the design-predicted ESALs were 2 times larger than the ESALs calculated using the WIM station information, meaning that the design led to a more conservative design thickness.

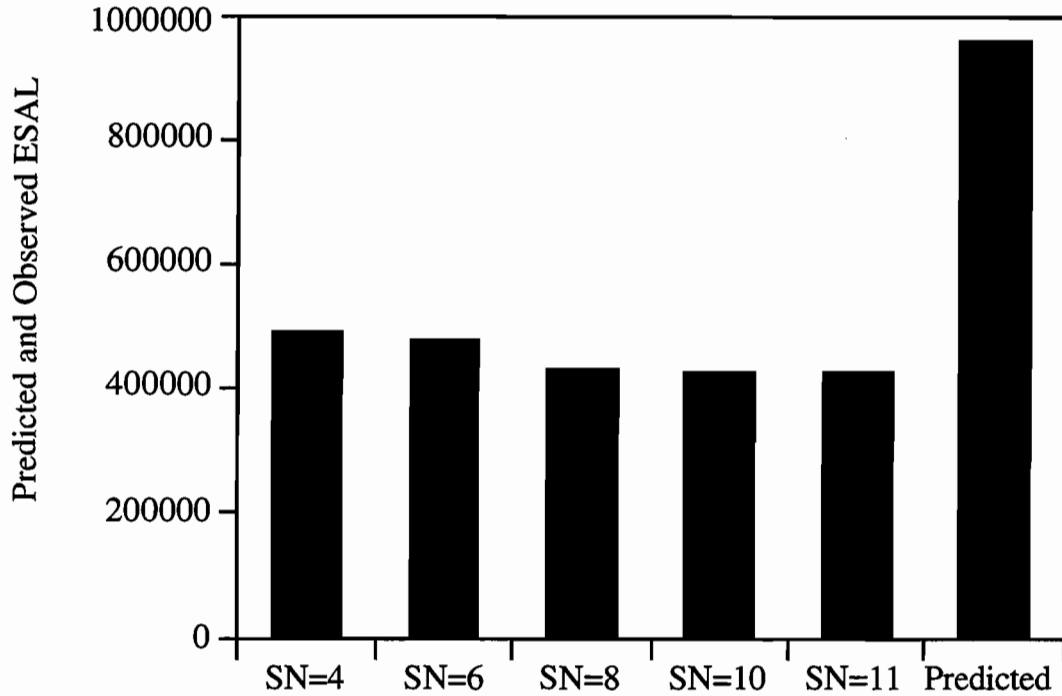


Figure 3.10 Comparison between predicted and observed ESALs in rigid section in 1993

3.4.3. Lateral Distribution

The lateral distribution of traffic loading is important in the estimation of test section pavement performance. Beginning with the plate theory of the 1930s, the importance of the traffic loading position on the pavement has been recognized. Using infrared sensors, the lateral distribution of each lane has been calculated. This will demonstrate the exact pavement behavior under traffic loading through three-dimensional pavement analysis, and will offer a possible explanation of distress growth in the test section. The distance from the outside wheel of a vehicle to the pavement shoulder was measured; Figure 3-10 shows the lateral distribution of two- and five-axle vehicles in the right lane of the test section. The mean value of two-axle vehicles was 1.31 m (4.3 feet) from the edge of the right shoulder, and .91 m (3.0 feet). The figure also shows that the vehicle loading position on the pavement varies from less than .30 m (1 foot), to more than 1.82 m (6 feet).

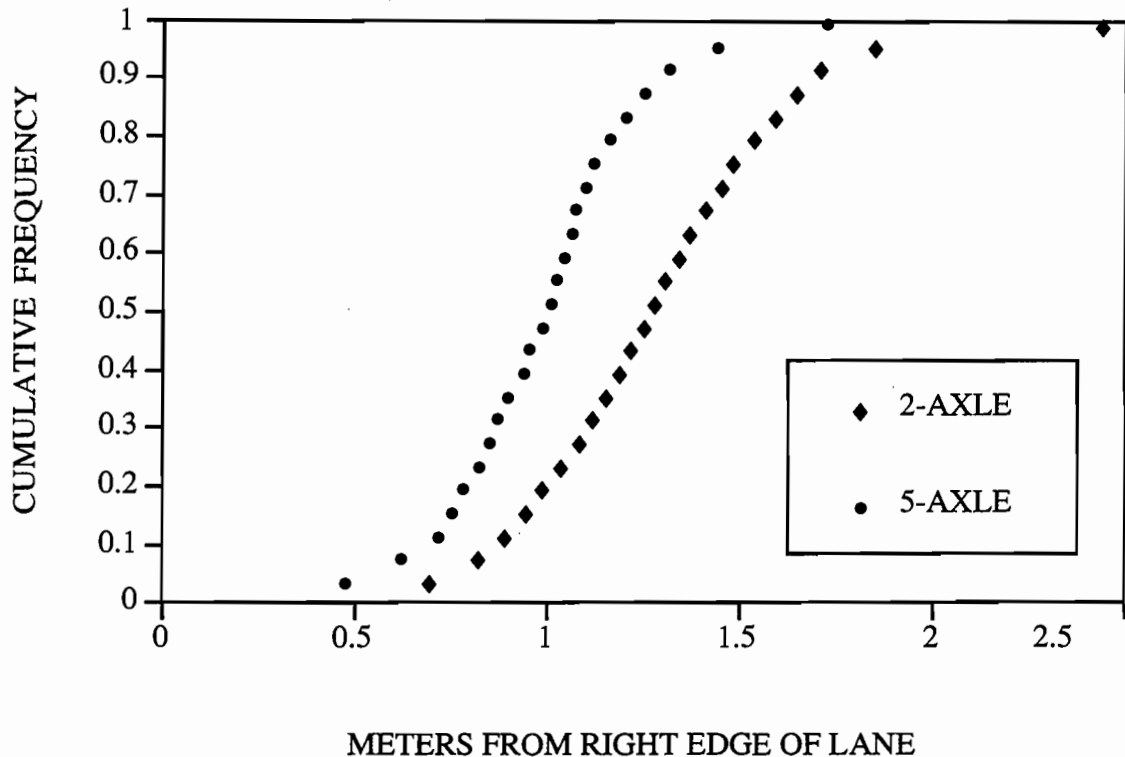


Figure 3.11 Accumulative lateral distribution of two- and five-axle vehicles (1 m=0.304 ft)

3.5. TEMPERATURE DISTRIBUTION IN THE TEST SECTION

Air temperatures and pavement temperatures were measured and stored by the WIM station installed at the site to correlate these to the thermal effects on the overlay. The probe used to measure pavement temperature was installed in flexible test section F0 and in the rigid test section R0. Air temperature was measured by the WIM station on the pavement shoulder. Pavement temperature was collected at a 2.54-cm (1-inch) depth in the outside shoulder. Seasonal and daily temperature distributions are reported below.

3.5.1. Hourly Temperature Variations

Hourly temperature distributions can determine the stresses caused by thermal gradient changes within the pavement structure. Additionally, asphalt stiffness is strongly related to temperature. While increases in air temperature will increase pavement temperature (as a result of solar energy absorption and interaction with the surrounding air), the pavement temperature will increase more slowly than the air temperature, because of the lower thermal conductivity of asphalt concrete. Throughout the day, the air temperature will decrease after a peak temperature is reached; the pavement temperature, on the other hand, will not decrease as rapidly. Consequently, the

temperature of the top layer of the pavement will be higher than the temperature of the bottom layer of the pavement in the afternoon, while at night the reverse will occur, with the top layer reaching a lower temperature than the bottom layer. Thermal stresses caused by these phenomena will occur differently, depending on the time of day and on the position within the pavement structure. In the afternoon, the pavement will be curled upward, with the bottom layer of the pavement tensed by the slab's weight. The situation is reversed during the night, with the bottom layer under compression and the top layer of the pavement in tension. This means that the most extreme condition for rigid pavements occurs in the afternoon, when there is a combination of thermal and traffic load effects. Thermal stresses caused by curling or warping depend on vertical temperature differentials if the material stiffness is considered to be the same vertically. Stress can also result from uniform temperature changes that cause the pavement to expand or contract. If pavement structures were in a free condition, no stress would develop; but because the pavement structure necessarily interacts with various types of base or subbase materials, friction develops; this can ultimately lead to tensional or compression stress development in the pavement. Stress variations caused by temperature changes are well documented (Ref 8).

The stiffness of the asphalt also depends on the temperature, such that the higher the temperature, the lower the stiffness (Refs 9, 10). Thus, in the summer, the stiffness of the asphalt will decrease. This is illustrated in Figure 3.12, a summary of indirect tensile tests of the asphalt mix in the laboratory (Ref 10). These test results verify that thermal cracks develop primarily during the winter, and that rutting develops primarily during the summer.

Beginning in April 1993, we monitored pavement temperature on an hourly basis at the test site. The temperature measurements for five consecutive days were averaged to represent the daily variation from spring to winter. Figure 3.13 shows the daily distribution of temperature during the spring. It shows that air temperature differed slightly between the rigid and flexible sections. Generally, the temperature of the pavement is higher than the air temperature, with both in equilibrium around noon. The average difference between the minimum and the maximum temperature was about 13.89°C (25°F). As shown in Figure 3.15, the fall temperature distribution also shows a similar pattern and range. The daily temperature distribution for the summer shows a different pattern than that for the spring condition. For the summer, until sunrise, the air temperature was lower than the temperature for the pavement, with the air temperature increasing rapidly after sunrise. The pavement temperature increases at a slower rate, with the air temperature higher than the pavement temperature during the day. The maximum pavement temperature for the rigid section was 50.56°C (123°F), while the minimum was 32.22°C (90°F), resulting in a difference of almost 18.33°C (35°F) for the day. The flexible section also exhibited a similar pattern — we observed a 22.22°C (40°F) differential for the day. A similar pattern was also observed during the winter, the main difference being the magnitude of temperature changes. The maximum for the winter was about 16.67°C (62°F) and the minimum 6.11°C (43°F), about a 11°C (20°F) differential, as observed in Table 3.4.

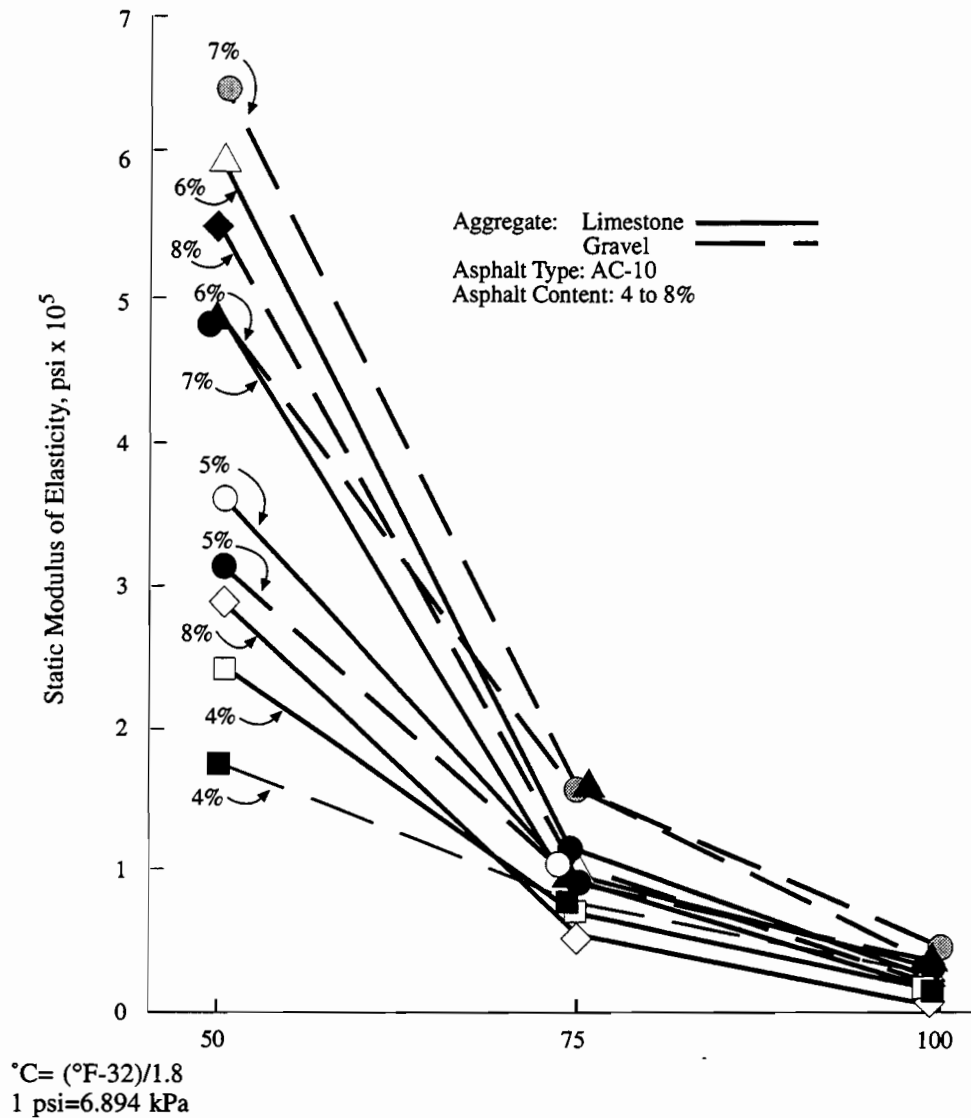


Figure 3.12 Asphalt stiffness variation on temperature

The daily pavement temperature distributions for the four different seasons show that the daily distribution follows a cosine-type function and may serve as a basis for the prediction of pavement temperatures using a simple cosine function to represent the temperature distribution throughout the day.

In summary, temperature is a significant factor in pavement distress development. The daily temperature differentials observed during the summer and the winter were about 18.33° C (35° F) and 13.89° C (25° F), respectively. The pattern of temperature for the four seasons shows a similar cosine pattern, with a similar range for the spring and fall. A similar pattern was observed for the summer and for the winter, though the magnitude of the lowest and highest

temperatures differed. The air temperature distribution for the winter does not appear to follow a cosine trend, with the pavement following the same air temperature pattern during the day.

Table 3.4 Average maximum and minimum temperature for the test sections

Class	Spring		Summer		Fall		Winter	
	min.	max.	min.	max.	min.	max.	min.	max.
Rigid, air	65	90	73	112	51	77	32	62
Rigid, pvm	76	96	90	123	64	83	43	62
Flexible, air	58	82	85	117	46	65	30	52
Flexible, pvm	66	92	94	134	56	79	40	63

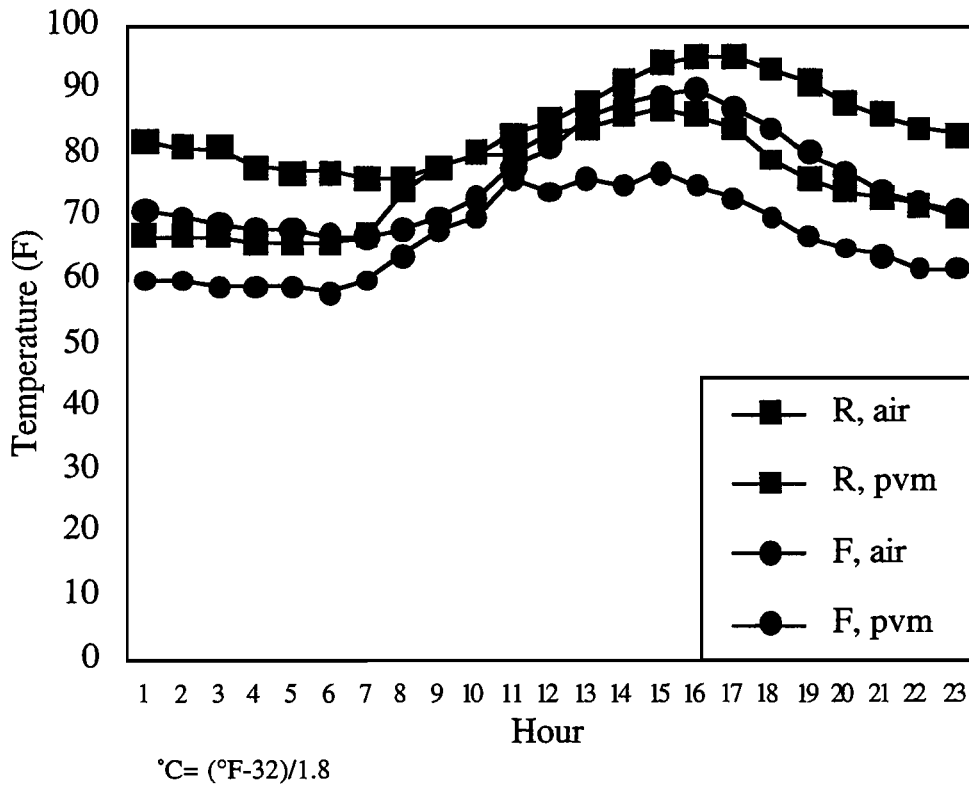


Figure 3.13 Hourly distribution of temperature in test section — Spring (May 1993)

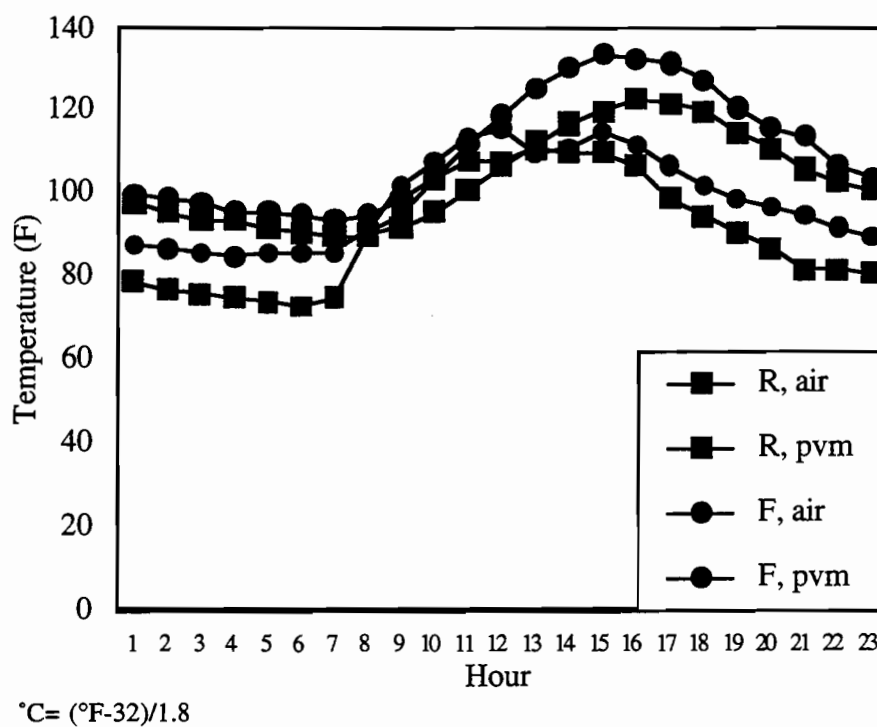


Figure 3.14 Hourly distribution of temperature in test section — Summer (July 1993)

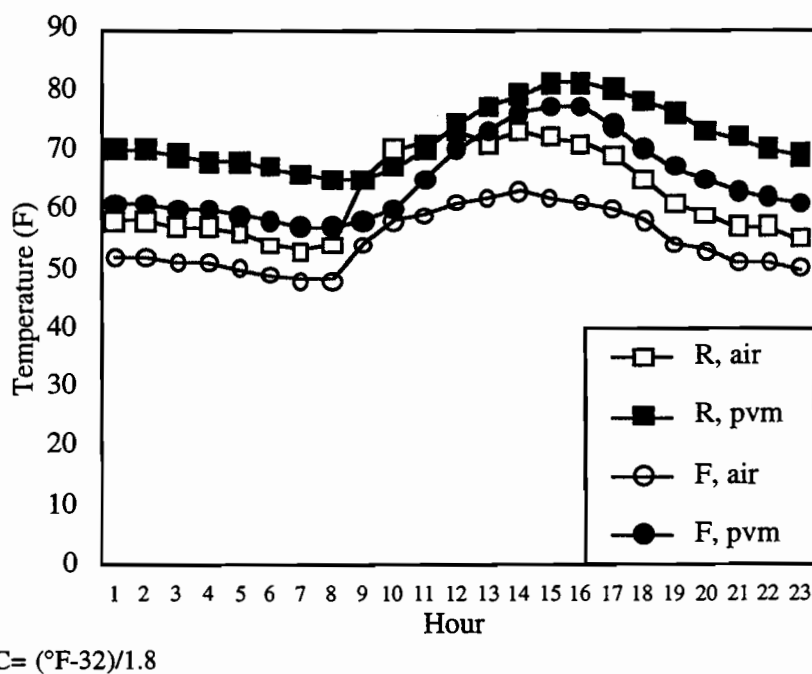


Figure 3.15 Hourly distribution of temperature in test section — Fall (October 1993)

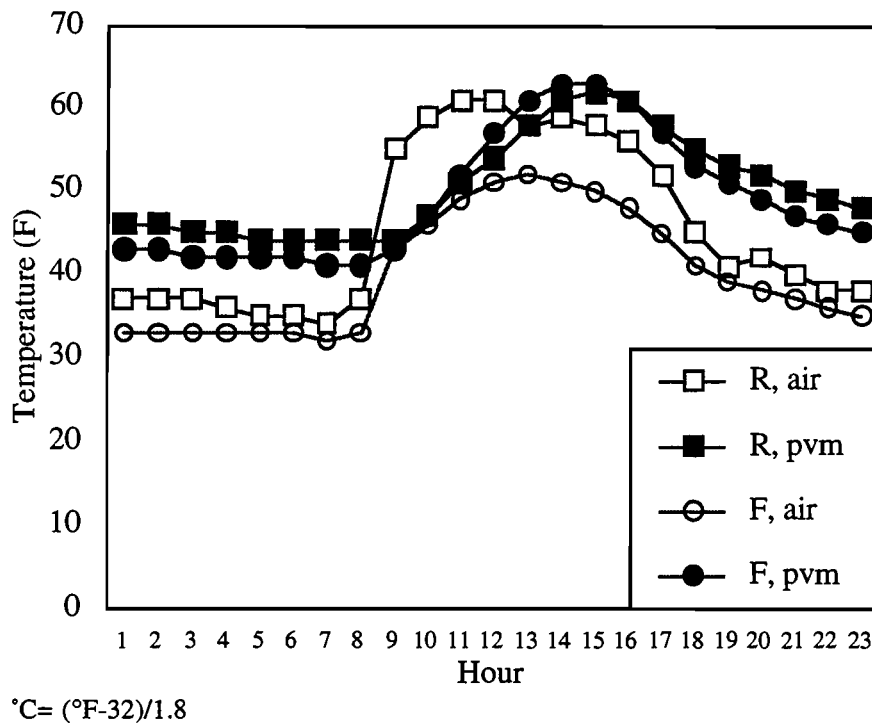


Figure 3.16 Hourly distribution of temperature in test section — Winter (December 1993)

3.5.2. Daily Temperature Variations

The daily variations of pavement temperatures were calculated using the minimum and maximum temperatures for the day. The rigid and flexible test sections showed little difference in the daily temperature variations, and almost the same pavement temperature pattern throughout the year. An observation that deserves discussion is the daily variation for the summer presented in Figure 3.18. Since the thermal conductivity of asphalt is higher than that of concrete, the pavement temperature of the flexible section exhibits a higher value than the rigid section. Figures 3.17, 3.19, and 3.20 show that the differences between the temperature distribution for the flexible and rigid sections are not so significant, making it possible to use the same temperature distribution in the analysis of thermal effects on the asphalt overlay for the flexible and rigid sections. These observations may have been a result of the installation of thermocouples on the asphalt shoulder.

The largest temperature differentials occurred during the summer — not during the winter, as would be expected. This finding is illustrated in Figures 3.18 through 3.21. This is not a problem, since it is generally believed that the stresses caused by temperature are not greater than the strength gained by the asphalt concrete during the summer. However, during the winter the thermal stresses may exceed the tensile strength of the asphalt concrete, which could ultimately lead to thermal-related cracking.

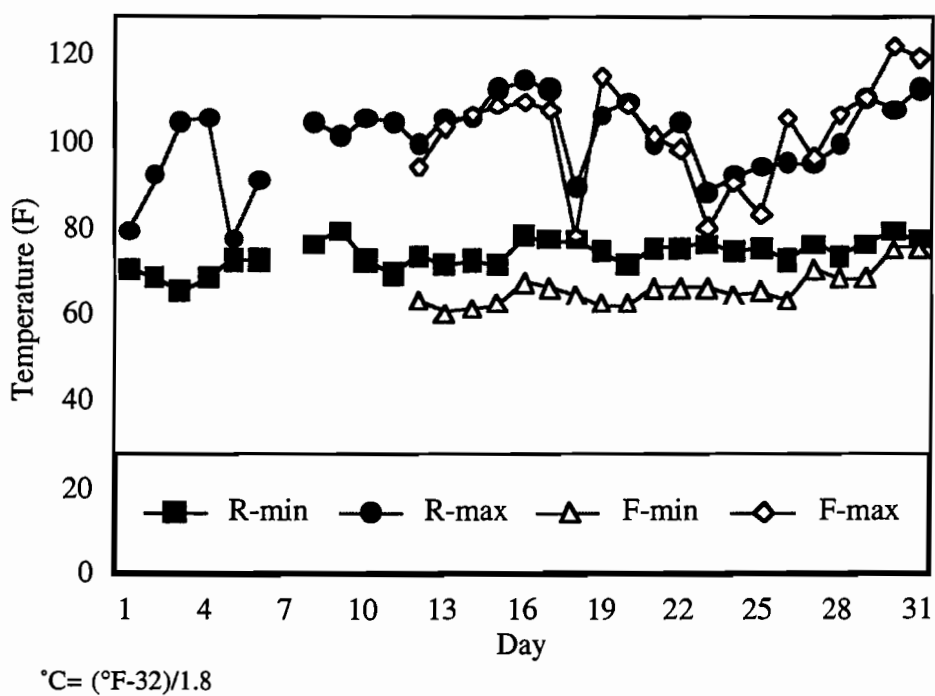


Figure 3.17 Daily variation of temperature in the test sections — Spring (May 1993)

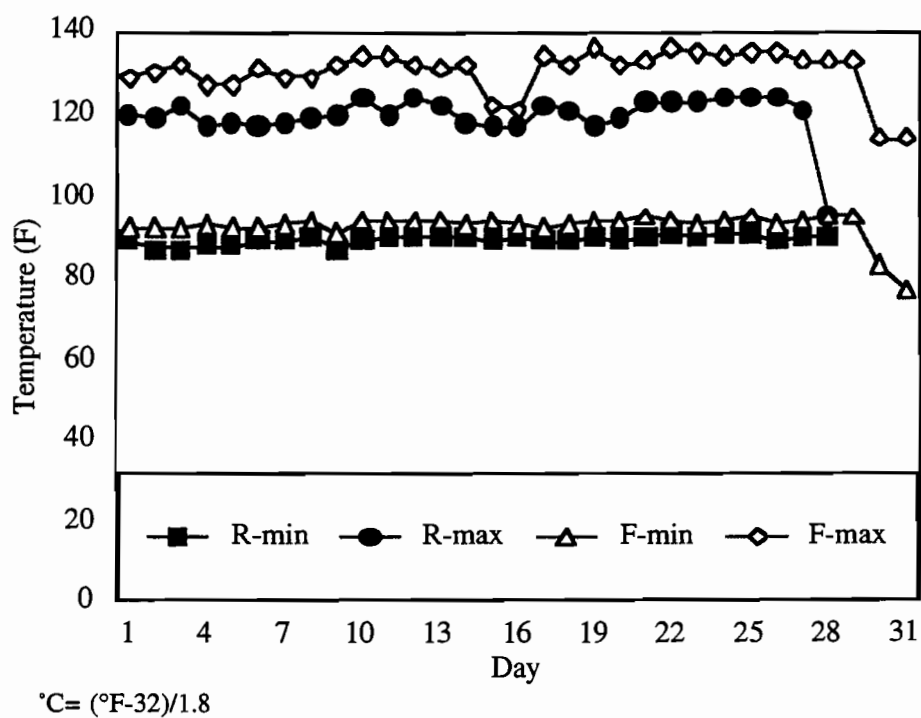


Figure 3.18 Daily variation of temperature in the test sections — Summer (July 1993)

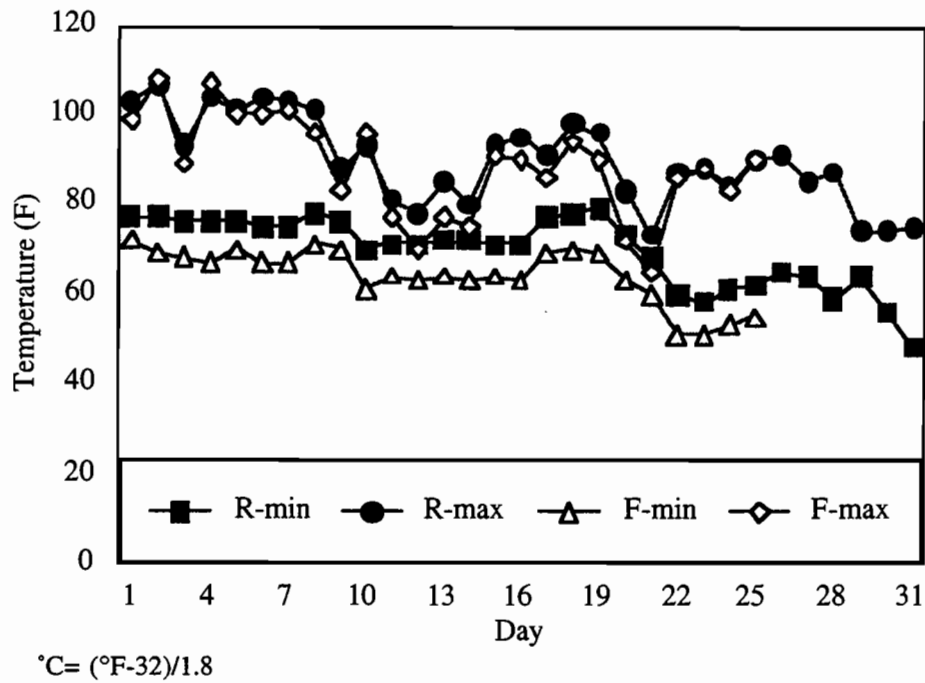


Figure 3.19 Daily variation of temperature in the test sections — Fall (October 1993)

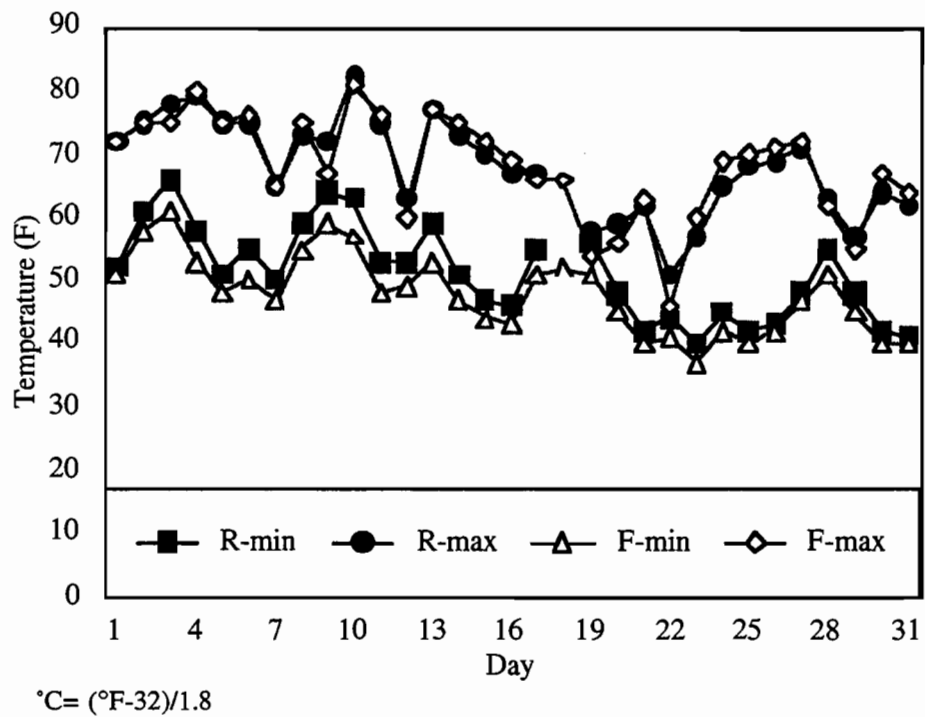


Figure 3.20 Daily variation of temperature in the test sections — Winter (December 1993)

3.5.3. Monthly Variation of Temperature

The monthly temperature variations for both the rigid and flexible test sections were also summarized. The average minimum and maximum temperatures of the month are depicted in Figures 3.21 and 3.22. The curves show a sinusoidal function form for the air and pavement temperature distributions. The maximum pavement temperature in the rigid section was 53.8° C (129° F) in July 1993, while the minimum was 2.78° C (37° F) in January 1994. The flexible section experienced a slightly higher pavement temperature; the maximum temperature was observed in July, while the minimum temperature was observed in December.

Both minimum and maximum temperatures for the test sections are usually above the air temperature, probably because both sections have a black asphalt overlay with a surface absorptivity of almost 0.90. The temperatures measured in the flexible section also show that the pavement temperature at 2.54 cm (1 inch) depth is always higher than the air temperature. The difference is 5.56° C (10° F) on average, suggesting that careful modeling is needed when calculating pavement temperatures based on air temperature.

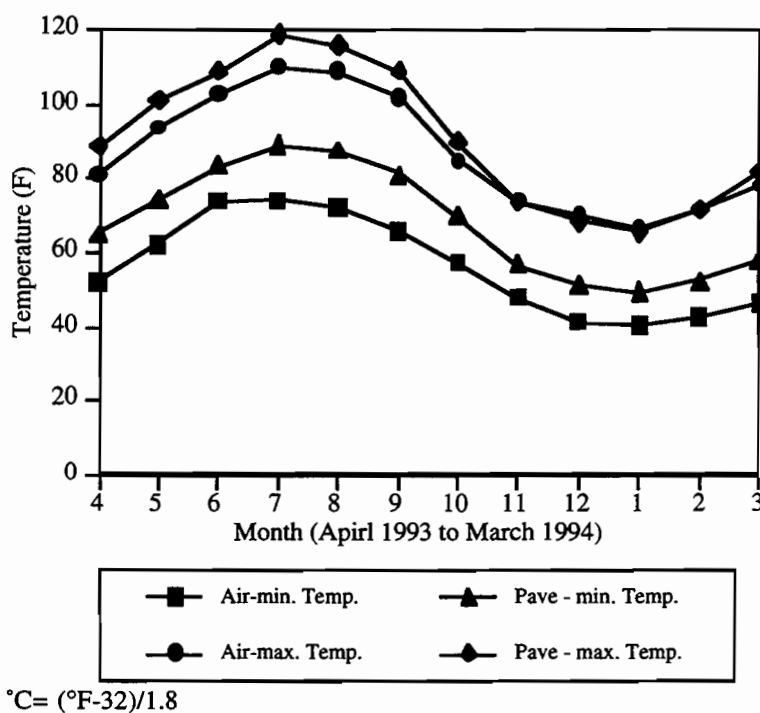


Figure 3.21 Monthly variation of average min. and max. temperature in the rigid section

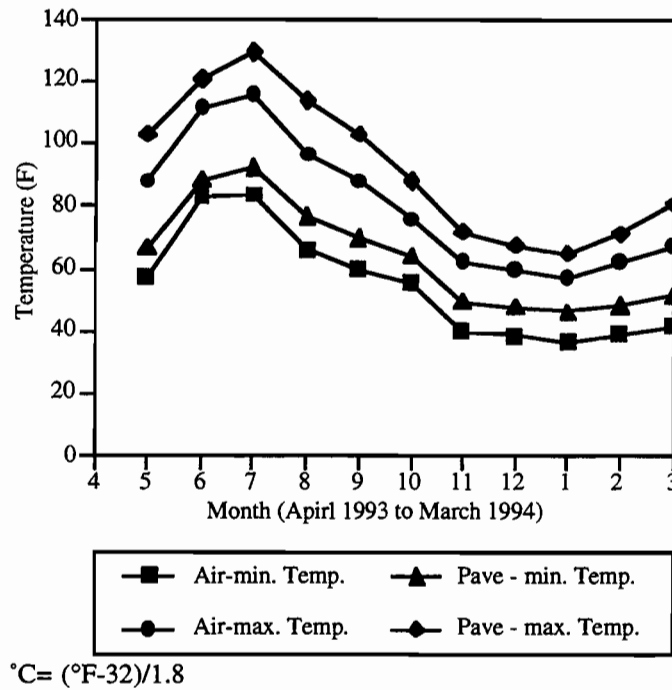


Figure 3.22 Monthly variation of average min. and max. temperature in the flexible section

The maximum daily temperature differential during a month is depicted in Figure 3.23. It shows that the maximum daily temperature differential of the pavement structure in the rigid section ranges from 16.7° C to 22.2° C (30 to 40° F). During the winter, the temperature range is slightly lower than that in the summer.

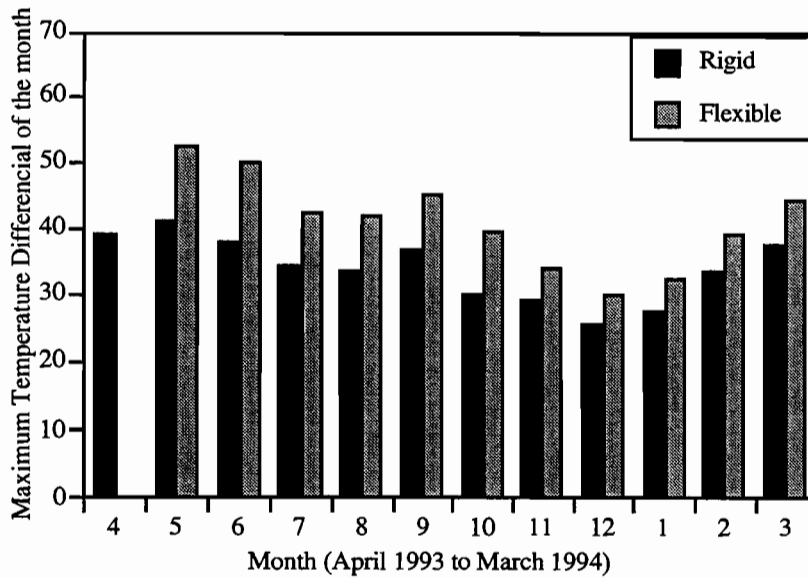


Figure 3.23 Maximum temperature differential by month

CHAPTER 4. PAVEMENT DEFLECTION MEASUREMENTS

4.1. BACKGROUND

Pavement deflections can indicate the capacity of a pavement structure to carry traffic loadings. While several devices are used to measure pavement deflections (Ref 11), those that provide a deflection basin are preferable to those devices that merely measure point deflections (e.g., the Benkelman beam). The most common deflection-basin devices include the falling weight deflectometer (FWD) and the Dynaflect. For these devices, a pavement deflection basin is recorded by sensors located at various distances from the load source. Usually, deflection basins with a small curvature radius indicate large pavement deflections. To quantitatively summarize the deflection basin, researchers developed the surface curvature index (SCI) (Refs 12, 13). Using this index, deflections can be used to explain distress progression through statistical methods. Another example of an application of the deflection results is the calculation of a load transfer efficiency (LTE) to evaluate the load transfer capability of a discontinuity in JCP or CRCP (e.g., a crack or a joint).

Other studies on overlay design based on deflection measurements have used the maximum deflection as a criterion to select overlay design thickness (Ref 14). Procedures to backcalculate pavement layer properties have also become increasingly common, a result primarily of the advance in computers and of developments in analytical pavement structure modeling. Since deflections can be directly related to pavement layer stiffness using a backcalculation process, pavement designers have increasingly used deflection measurements in mechanistic overlay designs.

Deflection measurements can also indicate pavement performance under traffic loadings. In controlled laboratory testing using an accelerated wheel load simulator, researchers have found that pavement deflections increase as the number of wheel load applications increase (Ref 15). The SCI was used to explain the performance of CRCP (Ref 16). And pavement deflections and rutting have a relationship such that the pavement does not experience rutting problems in the absence of large deflections.

In summary, the application of pavement deflections has been extended from a simple structural behavior indicator to a pavement performance indicator; accordingly, obtaining deflection information for overlay design and for pavement performance assessments has become essential.

4.2. TEST EQUIPMENT AND DATA COLLECTION

In this study, pavement deflections were measured using an FWD. Deflections were measured six times on the rigid test sections, as shown in Table 4.1. Instances of missing and inconsistent data (observed when compared with subsequent measurements) required that we make some assumptions in the analysis. The deflection near transverse cracks was also measured to obtain the load transfer efficiency (LTE) on the composite section in December 1993. A special pavement deflection measurement was performed in March 1994 to compare the deflections

between wheel paths and on the wheel path. Because the deflection measurements were taken at different places for the 1992 and 1993 measurements (see Table 4.1), it was necessary to take measurements for the 1994 set between wheel paths and on the wheel path to allow for comparisons. Another reason for taking measurements between wheel paths and on the wheel path was to determine if the effects of the traffic load applications had enough compacting energy to transform the overlay material into a plastic material (this will certainly lead to a rutting problem along the wheel path of the pavement, and the deflections measured on the wheel path will be larger than the deflections between the wheel paths). If the elastic properties of the overlay material are preserved in the wheel path, the measured deflections should be the same for the wheel path or between the wheel paths.

Table 4.1 History of deflection measurement (rigid section)

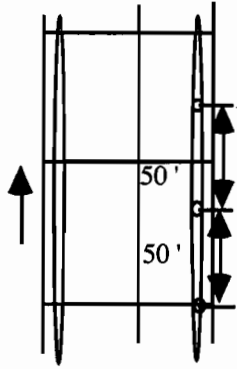
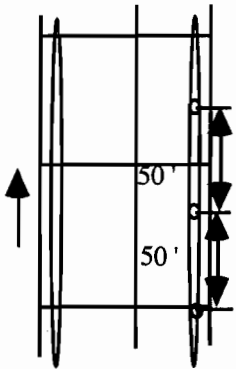
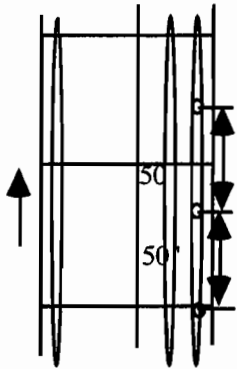
	Before Construction	During Construction	After Construction
	March 1992	March 1992	March 1992
Plane view of test position			
Measurement in Rigid	<ul style="list-style-type: none"> •Three times from second drop height (9000 lb target load) •Interior and corner deflection •Measurement at every 60' •Special arrangement of slab was used to take random effect 	<ul style="list-style-type: none"> •Three times from second drop height (9000 lb target load) •Interior and corner Deflection •Measurement every 60' •R1 & R2 Only 	<ul style="list-style-type: none"> •Three times from second drop height (9000 lb target load) •Outside wheel path deflection only •Measurement every 50" •No measurement at R0 due to WIM installation

1 foot=0.304 m

1 lb=4.45 N

1 inch=2.54 cm

Table 4.1 Continued — History of deflection measurement (rigid section)

	March 1993	December 1993	March 1994
Plane view of test position			
Rigid Measures	<ul style="list-style-type: none"> • Four times from second drop height (9000 lb target load) • Outside wheel path deflection only • Measurement at every 50' 	<ul style="list-style-type: none"> • First, second, second, and third drop height (6000,9000, 9000, 12000 lb target load) • Outside wheel path deflection only • Measurement every 50" • To check load transfer, R1, R2, and R6 were measured. 	<ul style="list-style-type: none"> • First, second, second, and third drop height (6000,9000, 9000, 12000 lb target load) • Outside wheel path and between wheel path • Measurement every 50"

1 foot=0.304 m
1 lb=4.45 N
1 inch=2.54 cm

For the flexible sections, the first set of deflections was measured to support the thickness design of test section overlays in June 1989, as shown in Table 4.2. When the construction was completed (June 1992), the second set of deflection measurements was taken; these unfortunately were lost as a result of a data processing error. The third set of pavement deflection measurements was performed in March 1993. All measurements were taken from the wheel path — with the exception of the last one, which was taken from both the wheel paths and between wheel paths for the same reasons discussed previously for the rigid sections.

4.3. PAVEMENT DEFLECTIONS BEFORE OVERLAY CONSTRUCTION

4.3.1. Rigid Section

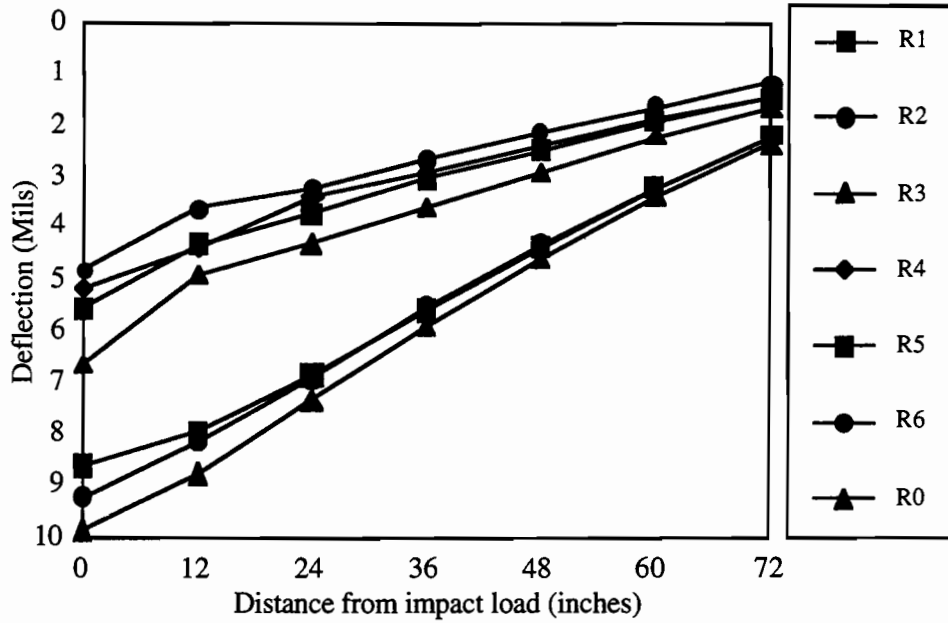
Measured deflections varied along the roadway before construction, as was documented in a previous research report (Ref 2). The average deflection was computed to estimate the structural

integrity before the new overlay was applied under 40 kN (9,000 lb) traffic loading. As presented in Figures 4.1 and 4.2, the average deflection shows that the test sections had a non-homogeneous bearing capacity under traffic loadings. Sections R1, R2, and R3 observed relatively large deflections, while the other sections experienced smaller deflections. The maximum deflection was about 0.254 mm (10 mil) for the left lane of test section R3. The left lane presented a slightly higher deflection than the right lane for the high deflection sections.

Table 4.2 History of deflection measurement (flexible section)

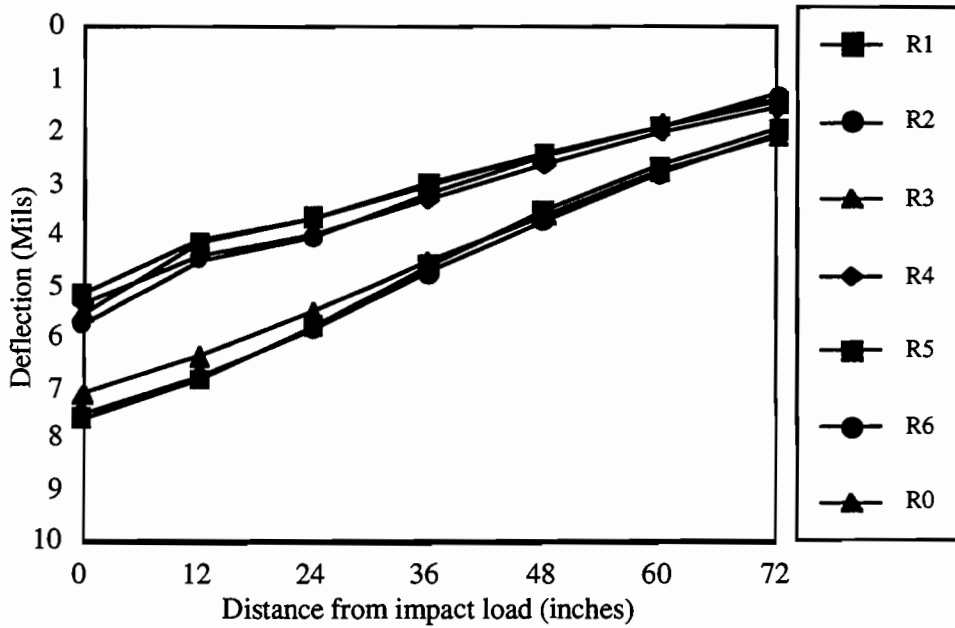
	Before Construction	During Construction	After Construction		
	June 1989	June 1992	March 1993	December 1993	March 1994
Plane view of test position					
Flexible Measures	<ul style="list-style-type: none"> • First, third, and fourth drop height • Outside wheel path on the right lane only 	<ul style="list-style-type: none"> • No recoverable data set 	<ul style="list-style-type: none"> • Four times from second drop height • Outside wheel path on both lanes • Measurement every 100" 	<ul style="list-style-type: none"> • Inside lane: first, second, and second drop • Outside lane: first, second, second, and third drop height • Outside wheel path on both lanes • Measurement every 50' 	<ul style="list-style-type: none"> • First, second, second, and third drop height (6000, 9000, 9000, 12000 lb target load) • Outside wheel path and between wheel path • Measurement every 50 "

1 foot=0.304 m
 1 lb=4.45 N
 1 inch=2.54 cm



1 mil=0.025 mm
 1 inch = 2.54 cm

Figure 4.1 Average deflection of left lane at the test section (March 1992)



1 mil=0.025 mm
 1 inch = 2.54 cm

Figure 4.2 Average deflection of right lane at the test section (March 1992)

One-way analysis of variance (ANOVA) was applied to the data to verify the existence of a statistically significant difference between the means for these sections. To represent the deflection basins, the Surface Curvature Index (SCI), area, and the seventh sensor readings (w7) were selected (Ref 13). The SCI, which is calculated based on the difference between the first and second sensors of the FWD, is known to be related to the structural condition of the surface layer in the pavement system. The area under the deflection basin is known to represent the overall pavement condition under traffic loadings. The seventh sensor reading is recognized as being representative of the subgrade condition. These three variables were used as dependent variables, while test section and lane were chosen as independent variables for the ANOVA procedure. As shown in Table 4.3, there exists a significant difference between lanes, based on SCI. However, it is difficult to assert that a significant difference exists between test sections under a 95 percent significance level. The ANOVA results for the area and w7 showed the same statistical results. These findings suggest that the bearing capacity of the test section may be uniform statistically, though the long-term performance results may be affected by previous structural conditions. However, the deflection plots presented in Figure 4.2 indicate that test sections R1, R2, and R3 were structurally weaker than the other test sections before the overlay.

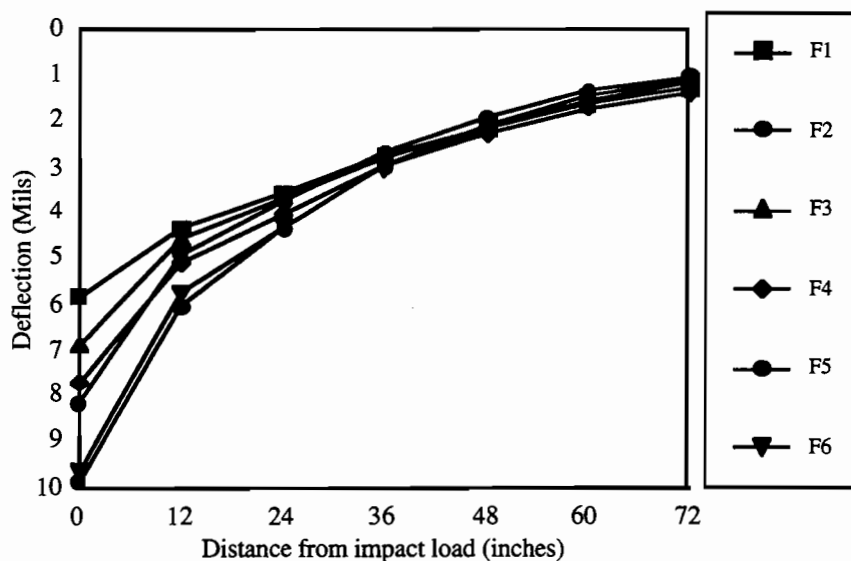
Table 4.3 ANOVA procedure to test for mean differences between test sections for the SCI

	SSM	DOF	MSM	F	Result
Lane	16.17	6	2.695	5.23	Sig.
Section	1.29	1	1.295	2.51	-
La .* Se.	2.63	6	0.439	0.85	-

4.3.2. Flexible Sections

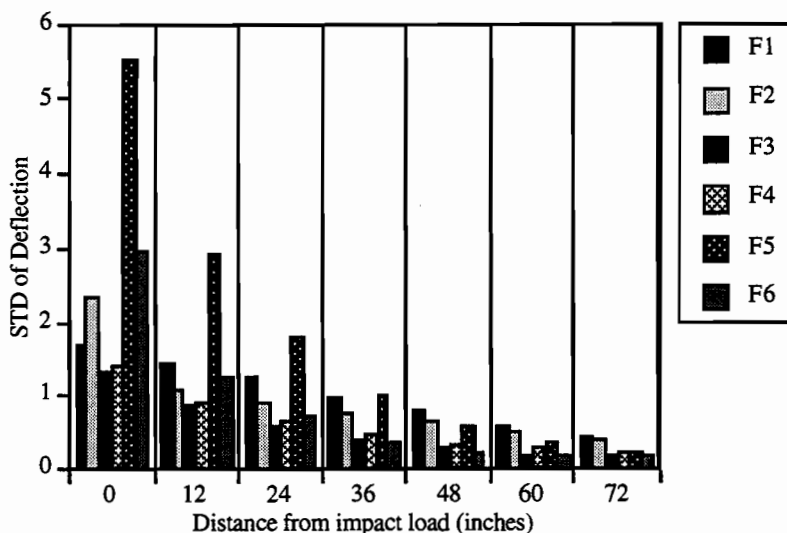
The flexible section deflection data were obtained at the beginning of the project, approximately 5 years ago. While the deflections may not represent the condition just before the new overlay, they can nonetheless show the comparative structural strength of each section before overlay, since the new overlay design thickness was based on this deflection set. The average deflections and standard deviations are presented in Figures 4.3 and 4.4. Deflections were measured only on the right lane on the outside wheel path; the third drop height was used to compute the average and to compare bearing capacities for each section. The deflection data were discussed in a previous report (Ref 2).

Based on mean deflections, section F1 had a better structural condition before the overlay was applied, while sections F5 and F6 exhibited poorer structural conditions. These sections also presented a large SCI. Like the rigid sections, the flexible sections also showed different structural conditions, a fact that will certainly affect the performance of the overlaid pavement (as will be discussed in subsequent chapters).



1 mil=0.025 mm
1 inch = 2.54 cm

Figure 4.3 Average deflection of right lane at the flexible section (June 1989)



1 inch = 2.54 cm

Figure 4.4 Standard deviation of deflection of right lane at the flexible section (June 1989)

4.4. DEFLECTIONS FOR THE RIGID TEST SECTIONS

Deflection measurements obtained with the FWD may vary, depending on position, temperature, and the magnitude of impact loading. Following completion of the new overlay (March 1992), deflections were measured every March, with one exception: The fifth set of

measurements, used to determine the effect of temperature on the deflection measurements, was undertaken in December 1993. If we assume that, for each successive March, the temperatures of the test sections are the same, it is possible to compare the deflections over the project period.

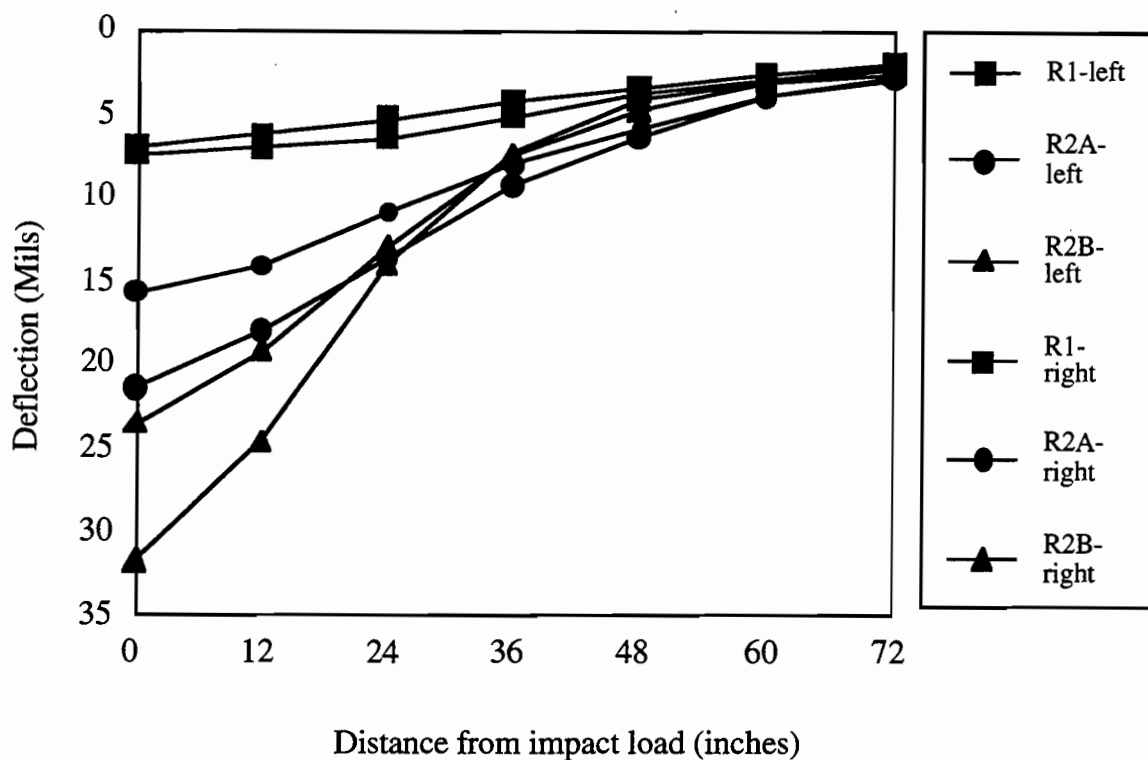
When reducing the deflection data, we detected an inconsistency among the impact loads used during the test period. This inconsistency made normalization impossible for the first two sets of deflection measurements (March 1992 and 1993). The second drop height, whose target load was 40 kN (9000 lb), was used to simulate the 80-kN (18-kip) standard wheel load. We estimated that, if the impact load follows a normal distribution throughout the measurements, and if the impact loading of the second drop height lies within the possible ranges suggested by SHRP (Ref 17), a deflection trend would emerge. The loading position, prior to overlay, was set between the wheel paths. To compare the position effect, the last set of deflection measurements (March 1994) was taken both on the wheel path and between the wheel paths.

4.4.1. Deflections during Construction

Different pavement structural configurations were available during the construction process. Deflections were measured on the new and old asphalt overlays and on the existing JCP. The average deflections were summarized for the different states of the pavement structure to determine the effects of the different asphalt overlays.

The asphalt overlays on test sections R1, R2A, and R2B were milled so that deflection measurements could be taken directly on the JCP. As shown in Figure 4.5, a significant difference in the deflection measurements was found among the test sections. In either the right or left lane, sections R2A and R2B presented larger deflections than section R1. Section R1 had previously been rehabilitated before the overlay was placed; thus, the crack repair most likely preserved the pavement's integrity and strength. However, sections R2A and R2B, which had undergone a break and seat procedure to protect the overlay from reflective cracking, could no longer be regarded as rigid pavement sections: The left lane of R2B showed over 0.75 mm (30 mil) of deflection, which could make it susceptible to distress caused by traffic loadings if a proper overlay method and thickness are not carefully designed and applied.

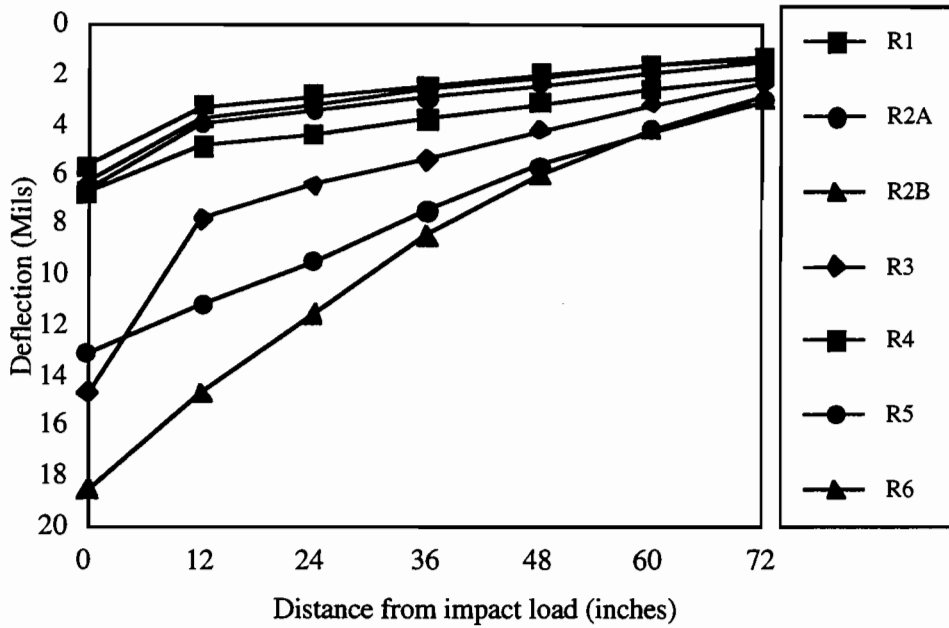
To verify the effect of the new overlay on the test section, deflections were measured right after construction — before the test section was opened to traffic. Section R0 was excluded owing to interference with the installation of the weigh in motion (WIM) station. After the overlay was applied, the sections that showed the maximum deflections were still R2A, R2B, and R3. However, the shapes of the deflection basins differed from the shapes observed before the overlay was applied. Deflection basin shapes may be classified into two categories, according to the load carrying capacity of the pavement structure. One category presents a bending action that has a smooth radius of curvature on the deflection basin. The second category displays a shear action that translates into a sharp slope between the first and second sensors. If the bending action is dominant in a pavement, the pavement will develop large tensile stresses at the bottom that will likely lead to related distresses. For the second category, where shear action is observed, shear-stress-related failures, such as rutting or shoving, will most likely be observed. The SCI may be used to characterize the two categories.



1 mil=0.025 mm
1 inch = 2.54 cm

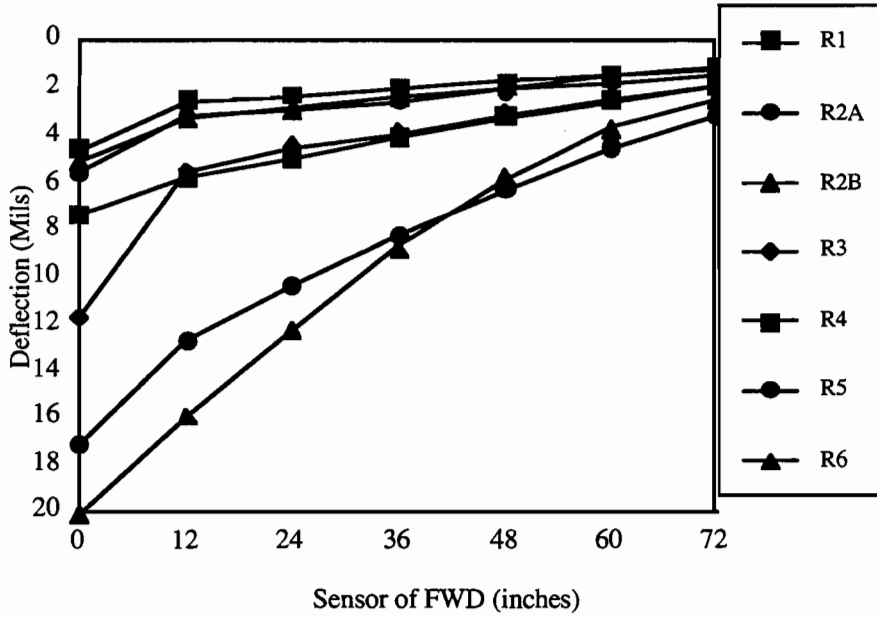
Figure 4.5 Average deflection for both lanes for the test sections (March 1992)

Based on the previous discussions, we can expect that the performance of two test sections, R2A and R2B, will differ from that of the other test sections. The milled sections display a smooth deflection basin associated with bending action and show a structurally weaker condition. These factors will lead to a distress that is related mainly to tensile failure (e.g., alligator cracking or reflective cracking). However, section R3, which has the largest SCI value among the test sections, will experience shear-failure-related distresses (e.g., rutting). This may be related to the flexible base layer, which, as a stress relief layer, prevents reflective cracking. The non-milled sections (R4, R5, and R6) showed fewer deflections, though they had a relatively larger SCI (which may be associated with the layers placed between the new overlay and the JCP). This finding suggests that, for these sections, any traffic load failure will likely be a shear mode failure (e.g., rutting).



1 mil=0.025 mm
1 inch = 2.54 cm

Figure 4.6 Average deflection of left lane for the rigid section (March 1992)



1 mil=0.025 mm
1 inch = 2.54 cm

Figure 4.7 Average deflection of right lane for the rigid section (March 1992)

In summary, deflections for the three stages of construction (before milling, after milling, and after construction) are shown in Figures 4.8 and 4.9. Comparing the new asphalt overlay and the existing JCP, the average deflection decreased after the application of the new overlay in section R2A, though these deflections still represented the highest value for the test sections. The right lane presented the highest decrease in deflections after the overlay was applied. The mean surface deflection of section R1 increased after the new overlay, a finding that may be ascribed to the greater flexibility of the asphalt overlay.

Comparisons of new and old overlay deflections can be used to predict performance. The first three sections R1, R2, and R3, which were structurally weaker, presented different structural capacities following overlay. Section R1 improved its overall stiffness, such that it may not pose pavement performance problems associated with traffic loadings during its design life. Section R2 experienced a significant decrease in its structural capacity, such that it might develop traffic-related performance problems (e.g., rutting and fatigue cracking). Section R3, which had the largest deflection after the new overlay with the flexible base, may have a higher susceptibility to rutting problems in the future (this will be discussed in Chapter 6, where the rutting survey results are summarized and discussed).

The remaining test sections, which were not milled, presented almost the same deflection basin after the new overlay was applied. Owing to interlayer effect, the slope between the first and second sensors observed after overlay was comparable to that observed before overlay.

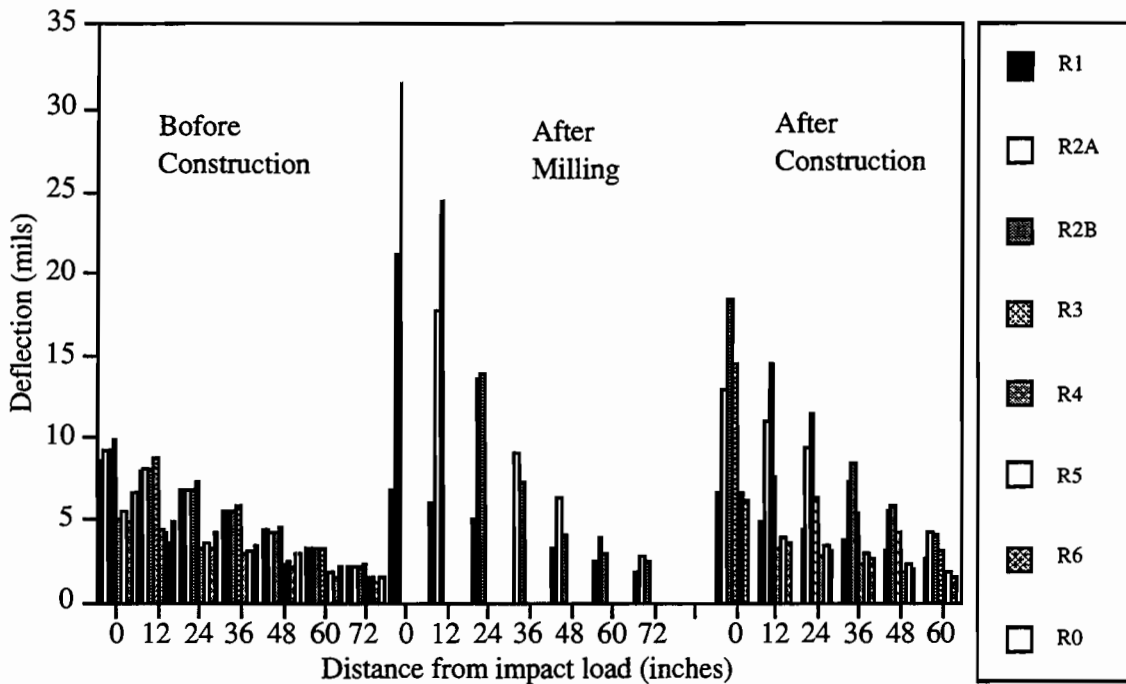


Figure 4.8 Deflection variation of three stage of construction, left lane (March 1992)
 (1 inch=2.54 cm, 1 mil=0.025 mm)

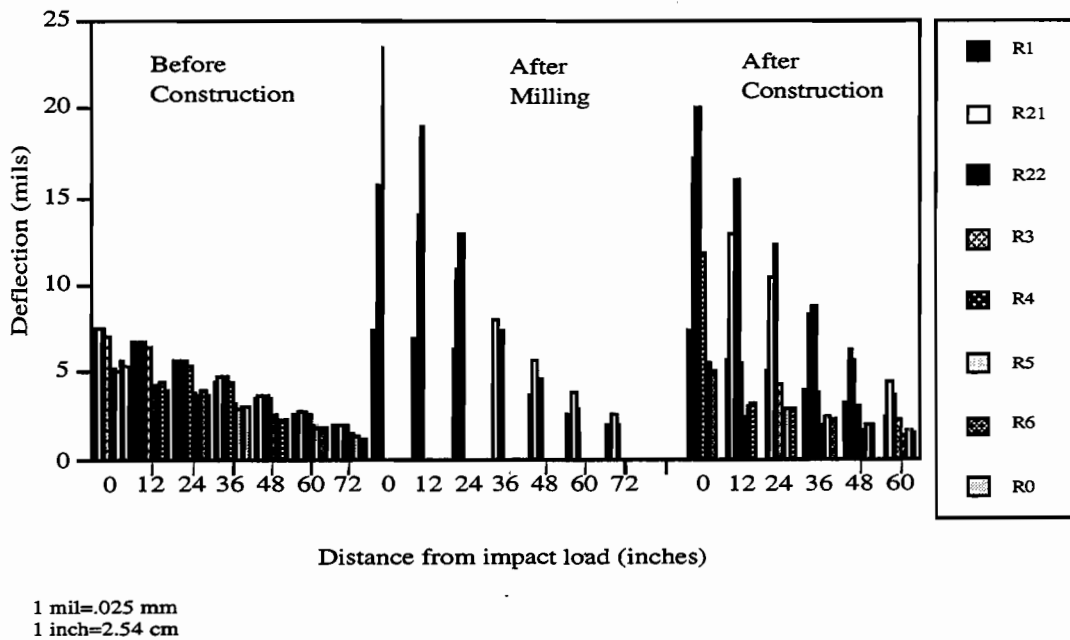


Figure 4.9 Deflection variation of three stage of construction, right lane (March 1992)

4.4.2. Deflections after Construction

As discussed previously, pavement deflections were measured every March to monitor the structural performance of the pavement overlay. Because the stiffness of the asphalt is strongly related to ambient temperature, direct comparison of the deflection results may lead to wrong conclusions; thus, the temperature effects must be discussed in combination with the deflection results. The March temperatures recorded were mild, with an average temperature of 23.89° C (75° F) for 1993.

Figures 4.10 and 4.11 show the deflection variation for both lanes over 3 years. The deflections measured in December 1993 were also included to study temperature effects. The third and fourth charts in Figures 4.10 and 4.11 show these temperature effects on the average deflection on the composite pavement. We also see that the deflections of the milled sections differ from those of the unmilled sections: The milled sections show consistency among the deflections, while the unmilled test sections present large differences. The difference in the surface curvature index was predominant in sections R4, R5, R6, and R0 — a finding that could be ascribed to the differences in ambient temperatures between the deflection measurements. Because the stiffness of the asphalt overlay increases during the winter (owing to lower average temperatures), the sections that have an old asphalt overlay (non-milled), with a thickness of at least 25.4 cm (10 inches) of ACP overlay, provide a stiffer pavement surface during the winter. The sections that had the existing overlay removed have a thinner asphalt overlay; and because they are less sensitive to temperature variations, they provide more consistent deflection results.

The first three charts in Figures 4.10 and 4.11 show the trend of the deflections over time for both lanes. These charts show that the average deflection has generally increased for almost all sections since the beginning of construction (sections R2A, R2B, and the left lane of section R3 showed decreasing deflections). These results contradict the commonly held assumption (Ref 15) that pavement deflections will increase over time and traffic loadings. A possible explanation for the conflicting results observed in the evolution of the deflections over time is the densification of the sublayer owing to the application of traffic loadings. Construction compacting is designed to achieve minimum air percentage in the asphalt concrete, with such design meant to ensure the kind of elastic material behavior that protects the pavement from rutting problems. However, if substandard compacting occurs during construction on a weaker flexible base section, the remaining compaction will occur as a result of the application of the traffic loadings. While this action translates into an increase in deflections during the early life of the overlay, the deflections will stabilize once the layers reach maximum compaction. On the other hand, the discrepancies may be a result of AC layer aging, or of ambient temperature.

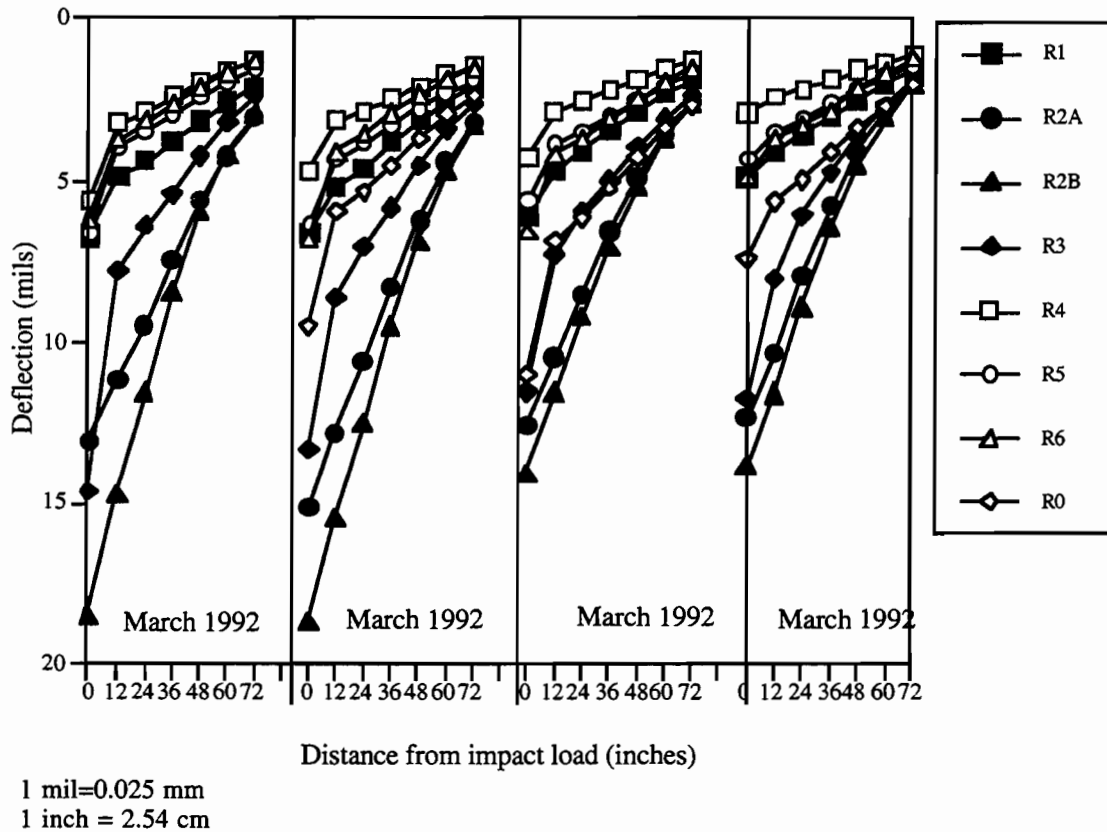
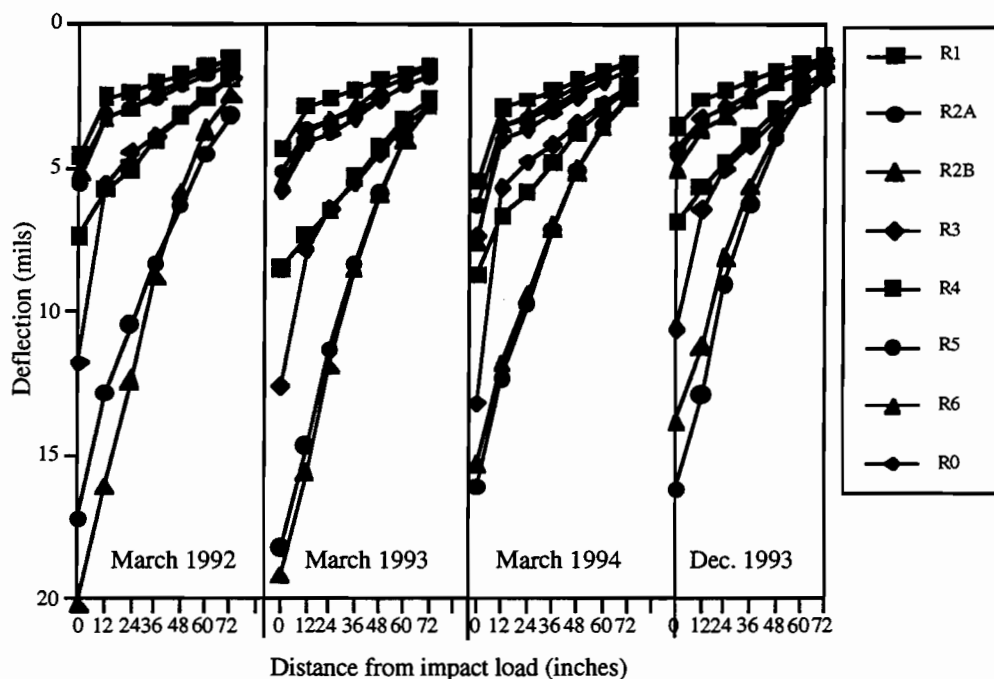


Figure 4.10 Variation of average deflection of the left lane of the rigid section



1 mil=0.025 mm
1 inch = 2.54 cm

Figure 4.11 Variation of average deflection of the outside lane of the rigid section

4.4.3. Load Transfer for the Composite Pavement

Load transfer at cracks in a composite pavement — asphalt overlay on JCP — is defined as the ability of the pavement structure to transfer loads across transverse cracks. The loss of load transfer in composite pavements is known to be one of the main causes of reflective cracking (Ref 18). Among the researchers investigating load transfer across joints in JRCP or CRCP (Ref 19), Teller has provided a particularly relevant procedure, one that evaluates load transfer across joints using a deflection ratio. Figure 4.12, an illustration of Teller's procedure, shows that, if load transfer efficiency (LTE) is zero, then no load is transferred from the loaded slab to the adjacent unloaded slab. If a perfect load transfer is present, then the procedure should result in a value of 100 percent.

$$\text{LTE} = \frac{2 W_u}{W_u + W_l}$$

where:

- LTE = load transfer efficiency (percentage),
- W_u = deflection on the unloaded slab, and
- W_l = deflection on the adjacent loaded slab.

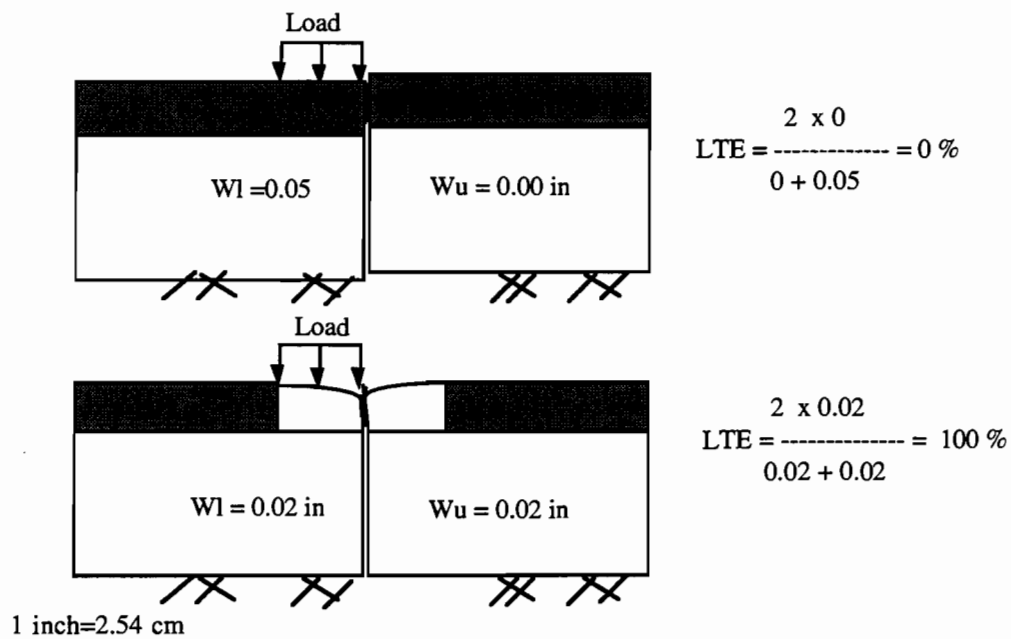


Figure 4.12 Illustration of the Teller Procedure for assessment of load transfer

Another procedure included in the literature was suggested by Ricci (Ref 20). In his scheme, one end of which is shown in Figure 4.13, deflection was measured by an upstream and downstream loading arrangement. Load transfer efficiency for each loading position is evaluated as follows:

$$\text{LTE}_d = \frac{W_2}{W_3} \times 100$$

$$\text{LTE}_u = \frac{W_3}{W_2} \times 100$$

where:

LTE_d = Load transfer efficiency for downstream loading,

LTE_u = Load transfer efficiency for upstream loading,

w_2 = deflection measurement at sensor 2, and

w_3 = deflection measurement at sensor 3.

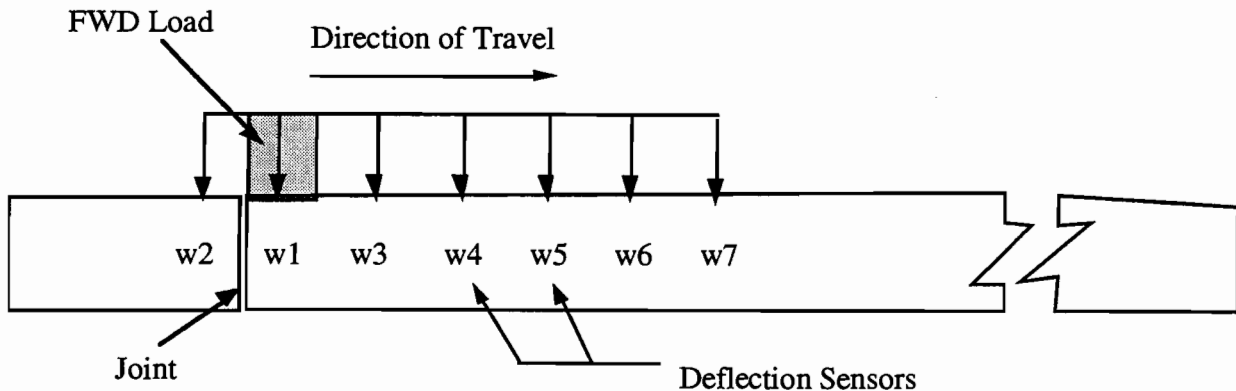


Figure 4.13 FWD deflection sensor locations — downstream position

A recent study on load transfer for asphalt overlays on CRCP concluded that the loading position effect, either interior or edge, on the load transfer efficiency (LTE) is not significant (Ref 21). The study also showed that the LTE is not strongly related to the magnitude of the impact loading (which depends on the drop height). Consequently, the third drop height loading was selected to calculate the load transfer efficiency for the asphalt overlay on JCP applied at the test site.

Figures 4.14 and 4.15 present the December 1993 results of LTE for the rigid test sections. Three test sections — R1, R2, and control section R0 — were selected. Within section R1, the subsection that had sawcuts was segregated and referred to as “R1S” for identification purposes. The LTE, using the Teller method, gives a slightly higher value than the LTE calculated using the Ricci method, as was also noted by previous CTR studies (Ref 19). The charts also show that there is no significant difference between downstream and upstream LTE results. All the test sections show over 95 percent LTE either upstream or downstream. Among the test sections, sections R1 and R0 have better LTE than R2. The R2 test section, which was built using a break and seat method, presented the lowest value for LTE, a situation that may lead to reflective cracking through traffic loadings. Test section R1S, which had the highest LTE among the test sections, will consequently not be prone to reflective cracking caused by traffic loadings.

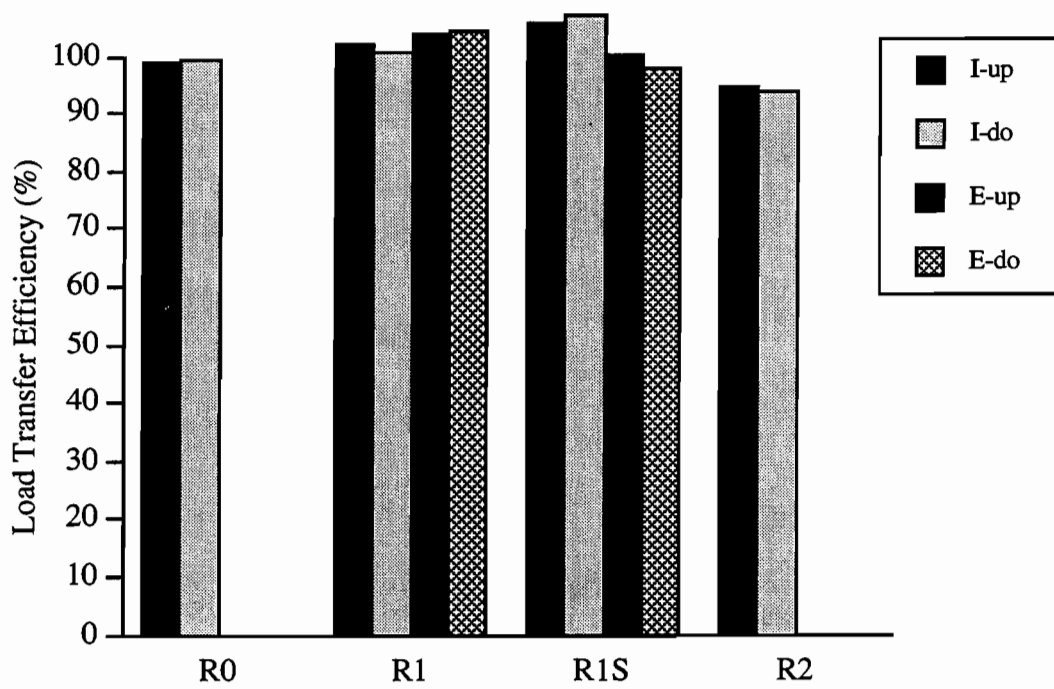


Figure 4.14 Load transfer efficiency at transverse cracks using the Ricci procedure

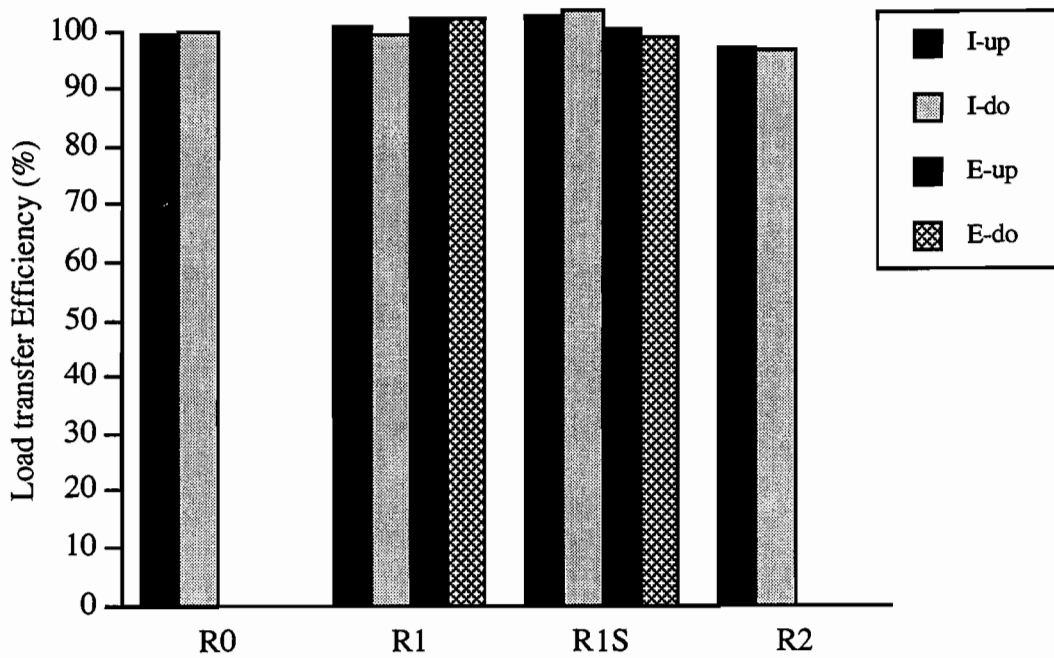


Figure 4.15 Load transfer efficiency at transverse cracks using the Teller procedure

4.4.4. Deflection Variation within the Lane

The last set of deflection measurements was taken in March 1994. The right lane generated two sets of data: One set of measurements was taken for the outside wheel path and the second set of measurements was taken between the wheel paths; the results are summarized in Figure 4.16.

A comparison of the deflections between these conditions shows the effect of the traffic loadings applied on the pavement structure after construction. Even though some variation is observed for each section, the general trend shows that the deflection between the wheel paths is smaller than the deflections on the wheel path. The sections that had the largest deflection on the wheel path were R3 and R2A, while the smallest deflections on the wheel path were observed for sections R0, R5, and R6. Only sections R3 and R2A experienced severe failures (discussed in Chapter 7) and low stiffness sections. Between these failed sections, the R3 section presented the largest variation between measurements taken on the wheel path and between wheel paths.

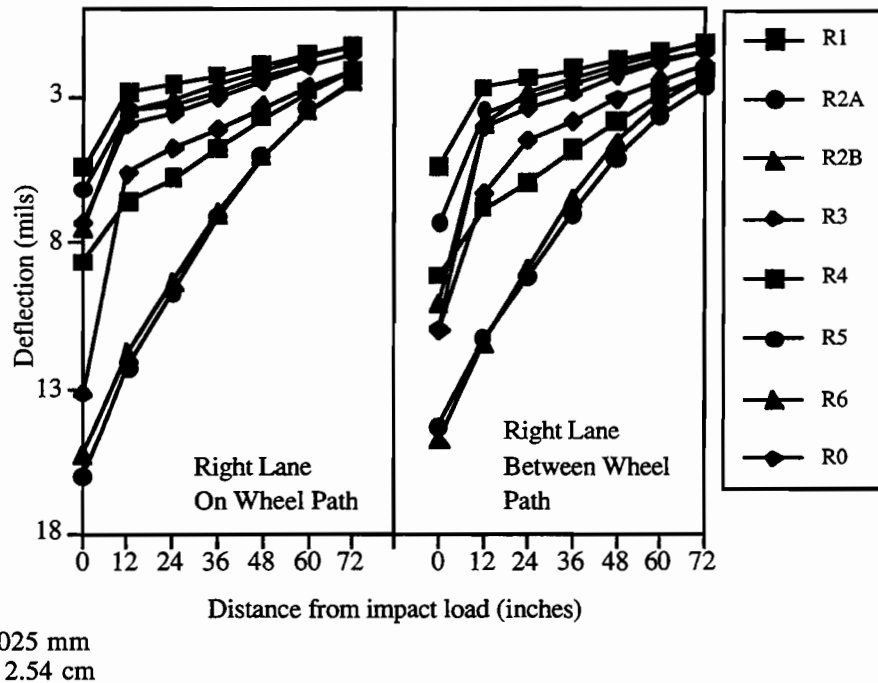


Figure 4.16 Deflection variations at rigid section — March 1994

4.5. DEFLECTIONS FOR THE FLEXIBLE TEST SECTIONS

4.5.1. Deflection Variation after Construction

Average deflection variations over the 2 years of deflection monitoring of the flexible test sections are shown in Figures 4.17 and 4.18 for the left and right lanes, respectively. The effect of

traffic was analyzed by comparing the first two charts in Figures 4.18 and 4.19, which summarize the available deflection information for March 1993 and March 1994. The effect of temperature was analyzed by comparing the deflection measurements for two different seasons, which are represented by the summaries of the deflection measurements taken in December 1993 (winter) and March 1994 (spring). As expected, the deflection generally increases as the number of traffic loading applications increases. Two test sections presented relatively larger deflections than the other sections; section F5, which has a flexible base, had the largest deflections and the largest SCI values. This section also experienced significant rutting problems, showing that SCI is a good indicator of rutting problems. Section F6 also presented a large SCI, indicating a possible susceptibility to rutting. Structurally, the remaining sections are relatively stable, considering the deflection results. Deflections between the left and right lane for test sections F5 and F6 differ significantly. The right lane for test section F5 presented in March 1994 about 0.375 mm (15 mil) while 0.25 mm (10 mil) were observed for the left lane. This was also observed for test section F6, which had higher values for the deflections being monitored on the right lane. These findings could be the result of traffic loadings, swelling, or insufficient drainage. Among these causes, the heavier traffic may be the main reason for the difference in structural-bearing capacity between the left and the right lanes.

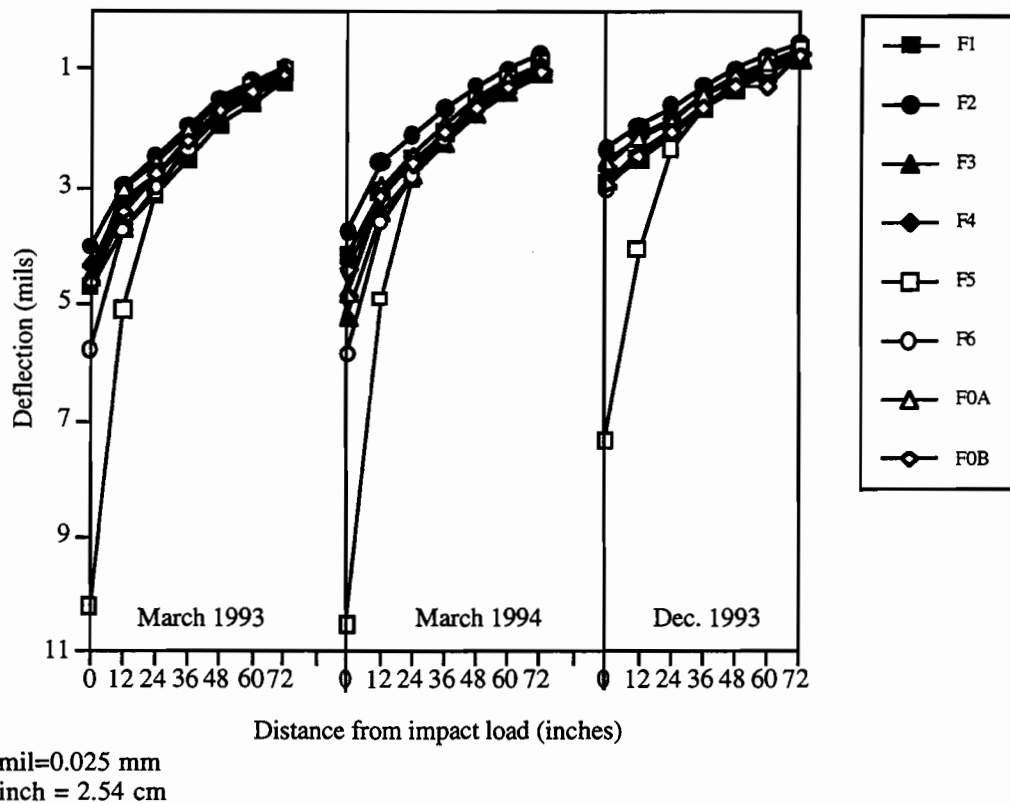


Figure 4.17 Variation of average deflection of the left lane of the flexible section

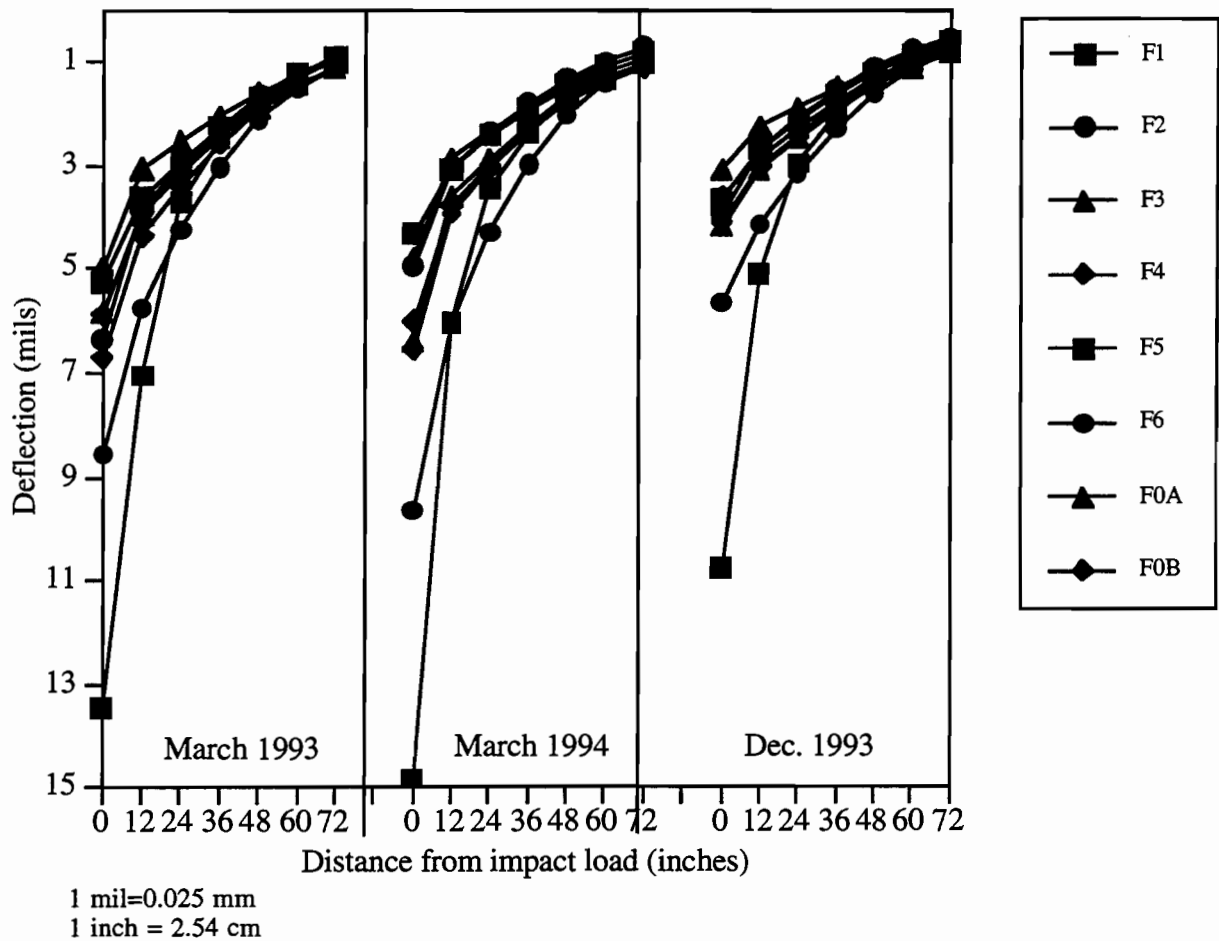
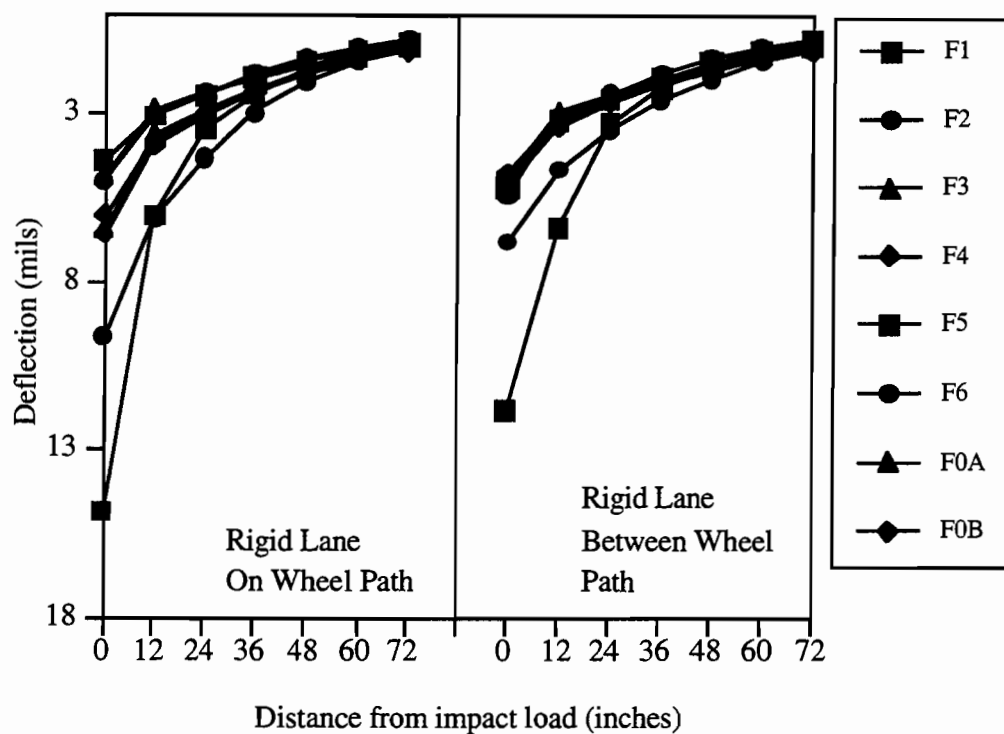


Figure 4.18 Variation of average deflection of the right lane of the flexible section

4.5.2. Deflection Variations within Lanes

Figure 4.20 presents the deflection variations within a lane. Unlike the rigid sections, the flexible sections that had the old asphalt overlay milled show less difference between the deflection measurements between the wheel paths and on the wheel path, while the sections that were not milled show a larger difference. These differences between the two wheel paths in section F6 and F5 are significant. Generally, the deflection results show that the deflections on the wheel path are larger than the deflections measured between the wheel path. This may indicate that the stiffness of the pavement structure is being progressively reduced by microfatigue cracking.



1 mil=0.025 mm
1 inch = 2.54 cm

Figure 4.19 Deflection variation between lanes for the flexible section — March 1994

4.6. SUMMARY

We employed deflection measurements to test pavement structures. Three stages of construction summarized the structural status of the different pavement test sections. Section R1 had its structural integrity increased after repair of cracks and joints. Deflections for sections R2A and R2B increased following a crack and seat procedure. The other rigid sections did not show large differences between before and after construction. The load transfer after overlay in the rigid sections showed higher load transfer efficiency, a finding that suggests that the main cause of reflective cracking (as discussed in Chapter 7) is not unequal displacement under traffic loadings, but probably slab movement caused by temperature loadings. During the 2 years of deflection monitoring, the deflection variation for some of the rigid sections contradicted the common assumption that deflections increase as traffic applications accumulate on the pavement, though there is good agreement with this assumption for the flexible sections. Further research must define temperature effects on the deflections of composite pavements. The deflections between wheel path and on wheel path do not generally differ, except for the sections that presented severe rutting problems on the wheel path, such as R3 and F5 (as will be discussed in Chapter 6). The deflections taken on the wheel path were larger than those taken between the wheel paths on these sections.

CHAPTER 5. BACKCALCULATION OF PAVEMENT PROPERTIES USING DEFLECTION DATA

5.1. BACKGROUND

Backcalculation procedures determine the elasticity modules of existing pavement layers using deflection results measured by such devices as the falling weight deflectometer (FWD) and the Dynaflect. Backcalculating layer stiffness of existing pavements involves: (1) measuring pavement deflections, (2) performing the backcalculation procedure, and (3) verifying the accuracy of the results by comparing them with core testing results.

The literature describes three basic approaches for backcalculating pavement properties based on deflections. The first method, known as an iterative backcalculation process, makes repeat calls to an elastic layer analysis subroutine in order to match measured deflections with predicted deflections. The method is successful when the measured and predicted deflections match within a tolerance level set by the user, or when a maximum number of iterations are met. Examples of this method include RPEDD1, BISDEF, CHEVDEF, WESDEF, ELSDEF, and BOUSDEF (Ref 22). The major limitation of this approach is the time required to process the algorithm, especially when the pavement structure being analyzed has many layers.

The second method described in the literature uses the pavement stiffness data associated with deflection basins obtained in previous backcalculation procedures, which are matched to possible deflection basins and layer stiffness using a search algorithm. While the processing time of this method type is faster than that of iterative programs, the method applies only to situations comparable to those for which the database of deflections and layer stiffnesses was generated. Examples of this method include the COMDEF and MODULUS computerized routines. COMDEF is a program developed specifically for the AC/PCC pavement, while MODULUS was developed originally for flexible pavements (Refs 23, 24).

The last approach described in the literature is the closed-form backcalculation approach. ILLIBACK, an example of this procedure, was developed for PCC pavements only.

After evaluating these different backcalculation routines, we selected COMDEF and MODULUS to perform the backcalculation procedures for the deflection data. COMDEF was developed by the Waterway Experimental Station (WES) to perform backcalculation of pavement layer properties for composite pavements. COMDEF uses a layer analysis program to match deflection basins with optimal layer stiffness using a numerical searching routine (making it faster than the iterative method). However, COMDEF can handle only three layers of pavement (e.g., asphalt, concrete, and soil) and requires no fewer than seven sensors spaced at fixed intervals of 30.48 cm (12 inches) (Ref 23).

MODULUS, developed originally for flexible pavements, is one of the most widely used programs for backcalculation procedures. Hall (Ref 22) showed that MODULUS can be used for composite pavements (i.e., those included in the test sections studied in this project).

COMDEF and MODULUS differ in their maximum number of backcalculated layers and in their temperature considerations for estimating the stiffness of the asphalt layer. MODULUS does not consider temperature effects on the asphalt layer, while COMDEF includes a subroutine to estimate a reasonable AC modulus based on previous research (Ref 25). In addition, MODULUS requires a seed value for soil properties and a possible range of values for the layer stiffness, while COMDEF does not require any of these additional inputs.

5.2. DATA REQUIREMENTS

Backcalculation routines generally require information regarding the FWD device used for the deflection measurements, the type of pavement system, impact loading, and possible range of layer modules. This information is also needed for running COMDEF and MODULUS, the only difference being the temperature information required by COMDEF if the user desires to estimate stiffness of the ACP layer from previous research directly. The output of the two programs includes an estimated and observed deflection and average stiffness for the pavement section layers.

Because both backcalculation routines are designed to handle no more than four layers, test sections having more than four layers must be consolidated into three or four idealized pavement layers (Ref 26). While WESDEF and MODCOMP3 have been recently developed to handle up to five layers, these programs are still being evaluated (Ref 29).

Among the rigid sections, R1 does not require consolidating to run both backcalculation routines, since it is possible to represent R1 accurately using three layers. However, for the other sections, consolidation of some of the layers is needed to run the backcalculation procedures. Section R3 could not be modeled using the COMDEF routine because it has one more flexible pavement layer between the new ACP overlay and the existing JCP and was modeled using the MODULUS routine only. The other non-milled sections, which have old and new asphalt overlays, were modeled by treating them as one homogeneous layer using the COMDEF routine (this was not a problem with the MODULUS routine, which can handle four layers). In the MODULUS routine, the new overlay was considered a surface layer, while the old overlay was treated as an asphalt base.

For the flexible sections, MODULUS was chosen to perform the backcalculation procedures. The fact that the flexible test sections consisted of multiple layers added to the imprecision involved in the backcalculation process. Four idealized layers were chosen to represent the existing layers. In section F5, which has more than five layers, flexible base and black base were considered one layer — a consolidation that may lead to unreliable results.

5.3. BACKCALCULATION PROCEDURE

The backcalculation of pavement properties for PCC pavements with an asphalt overlay is a complex engineering task, as discussed in a similar study using a relatively thin asphalt overlay on CRCP (Ref 21). Simple, yet reasonable, approaches were adapted to solve this complex problem for the deflection data available for the US 59 study. Because deflection data for three pavement conditions were available (before construction, after milling, and after the overlay), and

because laboratory test results on cores extracted from the pavement at the different stages were also available, the procedure summarized by Figure 5.1 was developed to implement the backcalculation procedure.

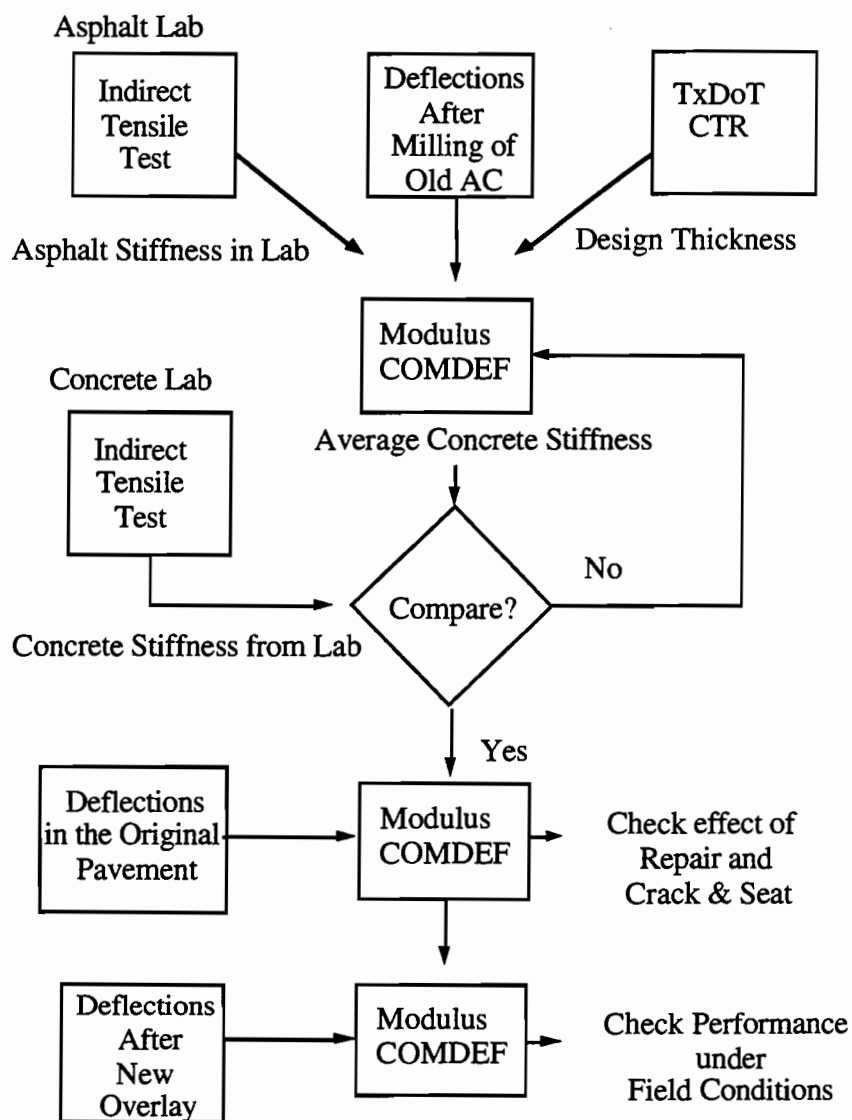


Figure 5.1 Backcalculation procedure adopted in the research

First, concrete pavement stiffness for test sections R1 and R2 were estimated using the milled deflection data and the MODULUS program. Because section R1 was already repaired and R2 was cracked and seated when deflections were measured, the backcalculated stiffnesses thus represent the stiffnesses for both the repaired and cracked JCP.

To perform a sensitivity analysis of the effect of the seed values for the subgrade moduli on MODULUS-backcalculated stiffnesses for section R1, results were compared using 137.8,

206.8, and 275.7 MPa (20, 30, and 40 ksi) for the subgrade modulus of elasticity. These results are summarized by Table 5.1; as shown in this table, the different subgrade moduli of elasticity did not significantly affect the calculated elasticity moduli for the concrete.

Table 5.1 Sensitivity analysis for the MODULUS program using different seed values of subgrade stiffness (unit=ksi)

Seed*	R1 - Right Lane				R1- Left Lane			
	JCP	COV	Soil	COV	JCP	COV	Soil	COV**
10	4669	32	17.2	26.5	4544	21	21.7	27.4
20	4628	35	17.3	21	4544	21	21.7	27.4
30	4668	35	17.3	21	4544	21	21.7	27.4

*Seed modules in the Modulus Program (ksi)

**Coefficient of Variation (%)

The next step was to estimate existing concrete stiffness from the deflection data before milling based on the ACP stiffness from the laboratory results using the backcalculation program. The basic assumption was that the stiffness from the laboratory was equivalent to that of the backcalculation. As previous research has pointed out, moduli of elasticity obtained through laboratory tests seldom agree with results obtained from backcalculation procedures (Ref 28). These discrepancies occur because field conditions cannot be well-replicated in the laboratory, and because such distresses as cracks and rut depth development can affect the deflection measurements. Another problem associated with backcalculation procedures is that the loading of the FWD is associated with impact, while most of the existing backcalculation programs use a static loading analysis program. However, Lundy has shown that the mean value resulting from backcalculation procedures can represent the pavement stiffness and, thus, may be suitable for mechanistic overlay design, even though the moduli of elasticity resulting from backcalculation procedures are usually lower than the mean value obtained in laboratory tests. Laboratory data for the existing asphalt moduli of elasticity from indirect tensile tests were available (Ref 29).

Another practical problem associated with the backcalculation procedures for the test sections is that the old asphalt overlay consists of four asphalt layers that have accumulated since the first overlay was applied. Laboratory test results showed, as expected, that the moduli of elasticity varied across the different asphalt layers. To address this variation in the backcalculation procedure, an equivalent stiffness was assumed to represent the old ACP overlay stiffness, based on the laboratory results. This equivalent stiffness was used to predict material property of the old

JCP. This step involved three layers — the asphalt, the JCP, and the soil — where the asphalt layer stiffness was fixed, as discussed previously, and the stiffness of the soil and the concrete was backcalculated. The resulting value was compared with the concrete stiffness obtained from the laboratory tests. If the resulting stiffness of the concrete was within a reasonable range, all other inputs were fixed for the next step of the backcalculation procedure. The deflection data obtained from the new overlay were then introduced using the same procedure described above. The analysis of the results will show a trend of the stiffnesses under field conditions. The backcalculation of the flexible section was straightforward, compared with that for the rigid section.

5.4. BACKCALCULATION RESULTS FOR THE RIGID SECTIONS

5.4.1. Stiffness before Overlay

The asphalt modulus of elasticity of the old overlay was estimated as being 3100 MPa (450,000 psi), based on the results from indirect tensile tests; concrete and soil moduli were backcalculated using the computerized routines, as discussed previously. Tables 4.4 through 4.8 summarize the moduli for the JCP and soil. Looking at the deflections reported in the previous chapter, we see that sections R1 and R2 have, as expected, relatively lower moduli for the concrete, while sections R4 and R5 show the higher values that denote a better condition. This may be explained by the fact that sections R1 and R2 presented severe cracking and some punch-out failures prior to the new overlay. The backcalculated moduli for sections R4 and R5 show that the jointed concrete pavement was in relatively good condition after about 50 years in service, suggesting that the ACP overlay did a good job in protecting the JCP from further deterioration.

Stiffness variation between lanes is also reported in Tables 5.2 through 5.5; it can be observed that the backcalculated stiffness for the concrete layers in the left lane is greater than the concrete stiffness for the right lane, though the soil layer does not show a similar trend. The soil backcalculated moduli show large differences for the pavement that has the lower concrete modulus, while no large differences are observed for the section that has the higher concrete modulus. These results are consistent with the fact that the right lane deteriorates faster than the left lane as a result of more intense traffic loading, as was discussed in Chapter 3.

Figures 5.2 and 5.3 compare the results of the MODULUS and COMDEF routines; in these figures, it may be observed that backcalculated concrete moduli were consistent for both programs, while the moduli results for the soil did not present a good match. MODULUS gives higher moduli results for the soil than does COMDEF. This is consistent with the results reported in previous research that compared the MODULUS and RPEDD1 programs for asphalt overlays on CRCP (Ref 21). This may be caused by approaches used in the MODULUS routine that have a strong dependency on subgrade modulus to calculate the modulus of other layers. Since both programs provide reasonable results, and because MODULUS is more applicable to new overlays (according to the literature), MODULUS was selected for further analysis.

Table 5.2 Backcalculated moduli of concrete — Left lane of rigid section

Program	Section	R1	R2A	R2B	R3	R4	R5	R6	R0
Modulus	Mean	1724	1810	1587	1569	5825	6162	5055	3118
	STD	848.6	972.2	535.3	551.2	1995	2033	1700	1423
	COV	49.2	53.7	33.7	35.2	34.3	33	33.6	45.6
COMDEF	Mean	1291	1991	1799	1929	6137	6343	4469	4345

Unit: ksi (1 ksi=6.894 MPa)

Table 5.3 Backcalculated moduli of concrete — Right lane of rigid section

Program	Section	R1	R2A	R2B	R3	R4	R5	R6	R0
Modulus	Mean	1952	1963	1583	2526	3953	4422	2960	2963
	STD	536.1	44.4	182.7	1150	1503	1757	1516	585.3
	COV	27.5	21.1	11.5	45.5	38	39.7	51.2	19.8
COMDEF	Mean	1999	2370	1799	2959	4370	5129	3052	3600

Unit: ksi (1 ksi=6.894 MPa)

Table 5.4 Backcalculated moduli of soil — Left lane of rigid section

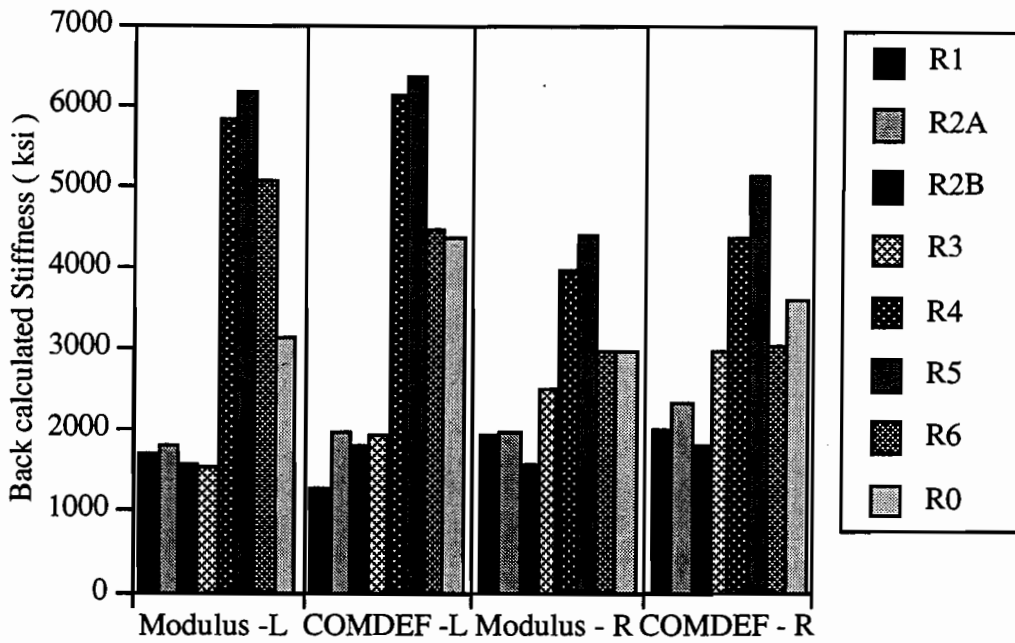
Program	Section	R1	R2A	R2B	R3	R4	R5	R6	R0
Modulus	Mean	14200	12500	13000	12900	25100	25300	29000	21900
	STD	4700	1800	2300	2900	4600	7200	5800	5300
	COV	32.9	14.1	17.9	22.9	18.5	28.2	20	24.4
COMDEF	Mean	11200	9580	11000	10200	17960	17600	21700	15700

Unit: psi (1 psi=6.894 kPa)

Table 5.5 Backcalculated moduli of soil — Right lane of rigid section

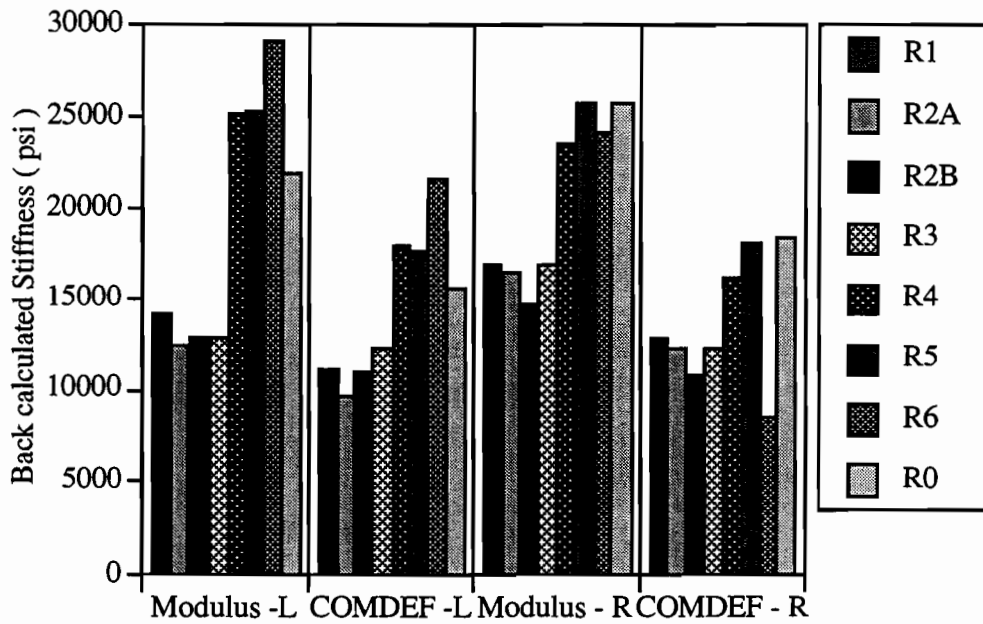
Program	Section	R1	R2A	R2B	R3	R4	R5	R6	R0
Modulus	Mean	17000	16600	14700	17000	23500	25700	24200	25600
	STD	4100	1700	1300	3600	5100	6100	4900	5100
	COV	24.3	10.3	9.1	21.2	21.6	23.7	20.2	19.8
COMDEF	Mean	12980	12200	10800	12300	16300	18100	8500	18500

Unit: psi (1 psi=6.894 kPa)



(1 ksi=6.894 MPa)

Figure 5.2 Comparison of the results between COMDEF and MODULUS for the JCP layer



(1 psi=6.894 kPa)

Figure 5.3 Comparison of the results between COMDEF and MODULUS for the soil layer

5.4.2. After Milling

Deflections were measured after milling to compare the effects of repairs applied with some of the test sections and the effect of cracking and seating of the existing JCP applied to other test sections. After milling the old asphalt overlay on test section R1, the existing JCP in the test section was repaired before the new overlay was applied. Section R2, on which a crack and seat method was applied to prevent reflective cracking, also had deflections measured after the seating process was completed. The backcalculation results for the deflections measured after repairing section R1 show that the concrete moduli increased to 31,000 MPa (45,00 ksi), which is comparable to a new concrete condition (and which underscores the importance of repairing cracked concrete before overlay procedures). Test sections R2A and R2B, which received the crack and seat treatment before the overlay, exhibited a dramatic decrease in concrete modulus — to under 6,894 MPa (1,000 ksi), except for the right lane of section R2B — which is not surprising considering that the crack and seat method destroys the structural integrity of the concrete pavement. In addition, the coefficient of variation of concrete modulus for section R1 is lower than the coefficients of variation calculated for sections R2A and R2B, suggesting that the crack repair procedure leads to less structural variability, while the crack and seat procedure leads to a higher variability of concrete modulus and, ultimately, pavement stiffness.

Table 5.6 Concrete modulus results from backcalculation — After repair for R1 and crack and seat for R2

Section	R1	R2A	R2B	R1	R2-1	R2-2
Lane	L	L	L	R	R	R
Mean	4628	762	258	4544	1437	467
STD	1603	227	212	961	546	303
COV	35	30	82	21	38	65

Unit: ksi (1 ksi=6.894 MPa)

L: left lane, R: right lane

Table 5.7 Soil stiffness from backcalculation — After repair for R1 and crack and seat for R2

Section	R1	R2A	R2B	R1	R2-1	R2-2
Lane	L	L	L	R	R	R
Mean	17300	9800	8900	21700	12200	10000
STD	3700	1600	700	1760	3900	1100
COV	21.4	16.5	8.3	42.49	32.0	10.6

Unit: psi (1 psi=6.894 kPa)

L: left lane, R: right lane

5.4.3. Results after Construction

The assumption that the stiffness of the old asphalt could be used as a fixed value in the backcalculation procedure was also adopted. New asphalt overlay stiffness was estimated to be from 1,172 to 3,447 MPa (170 to 500 ksi). The lane effect does not show any significant influence on backcalculated stiffnesses. However, the variability of asphalt stiffness for the new asphalt overlay was relatively high. For example, in section R1, the right and left lane show almost the same value of approximately 2,344 MPa (340 ksi) for the stiffness on both lanes, though the coefficients of variation are up to 70 percent. This is a surprisingly high coefficient of variation, considering that the surface layer on most of the sections had type C asphalt concrete, and considering that the stiffness for the asphalt layer of the different test sections should be rather uniform. Sections R1 and R2 have similar range values for the stiffness of the asphalt layer. However, the other sections, which had old asphalt overlays or an interlayer, did not fall into the same mean range. This may be explained by the limitations of the backcalculation program, which can only model a maximum of four layers. This forced the representation of various layers into one layer, as was the case for section R4. The results for section R4 revealed the structural weakness of the stress relief interlayer located between the new and old asphalt overlays. Because the stiffnesses of the new overlay and the interlayer were combined into one layer during the backcalculation procedure, the stiffness of the ideal layer resulted in relatively low values when compared with expected values for AC overlays. The backcalculated asphalt stiffness was lower than that calculated for the old asphalt overlays, which was assumed to be 3.10 E+09 Pa (450,000 psi). Taking into account the aging effect and further densification, it is reasonable to suggest that the stiffness for the new overlay should be around 2,068 to 2,757 MPa (300 to 400 ksi) for type C asphalt.

Table 5.8 Backcalculated modulus of new asphalt — Left lane of rigid section

Program	Section	R1	R2A	R2B	R3	R4	R5	R6
Modulus	Mean	330	322	390	484	217	171	208
	STD	228	194	279	236	40	61	123
	COV	69.00	60.00	72.00	49.00	18.00	35.00	59.00

Unit: ksi (1 ksi=6.894 MPa)

L: left lane, R: right lane

Table 5.9 Backcalculated moduli for the new asphalt overlay — Right lane of rigid section

Program	Section	R1	R2A	R2B	R3	R4	R5	R6
Modulus	Mean	340	394	313	508	312	245	271
	STD	174	92	179	179	69	97	132
	COV	51.00	23.00	57.00	35.00	22.00	39.00	49.00

Unit: ksi (1 ksi=6.894 MPa)

L: left lane, R: right lane

After the new overlay was placed, the concrete stiffness ranged from 17,235 to 39,985 MPa (2,500 to 5,800 ksi), except for sections R2A and R2B, as shown in Tables 5.10 and 5.11. The coefficient of variation was approximately 30 percent, which is similar to that of the deflections previously discussed. However, sections R2A and R2B presented a larger variability. The crack and seat section had almost the same stiffness as that of the flexible pavements, that is, between 2,068 and 5,515 MPa (300 to 800 ksi). The backcalculated stiffness between lanes is also shown in Tables 5.10 and 5.11, which indicate that the right lane had a larger stiffness than the left lane (except for section R1).

Table 5.10 Backcalculated modules of concrete — Left lane of rigid section

Program	Section	R1	R2A	R2B	R3	R4	R5	R6
Modulus	Mean	5804	775.3	311.5	1659	2577	3660	2693
	STD	1290	538.9	313	635.2	901.8	1048	1028
	COV	21.00	69.50	100.50	38.30	35.00	28.60	38.20

Unit: ksi (1 ksi=6.894 MPa)

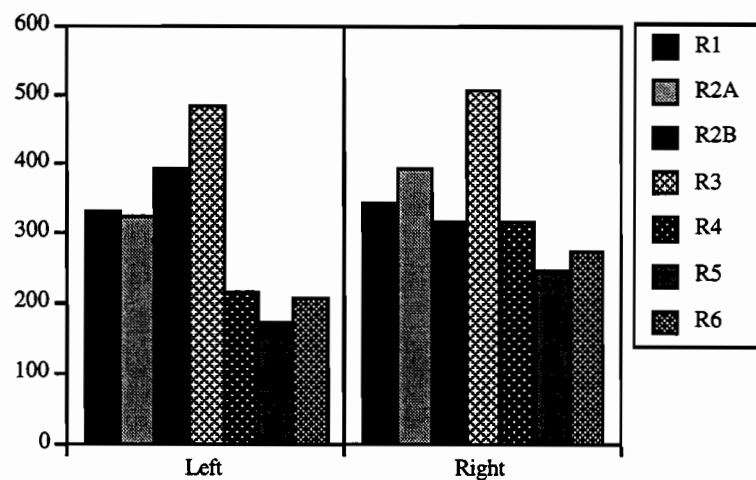
L: left lane, R: right lane

Table 5.11 Backcalculated modules of concrete — Right lane of rigid section

Program	Section	R1	R2A	R2B	R3	R4	R5	R6
Modulus	Mean	3912	794	612.3	2584	4524	4888	3402
	STD	1274	256.2	604.8	758.8	1190	1173	1045
	COV	32.60	32.30	98.80	29.40	26.30	24.00	30.70

Unit: ksi (1 ksi=6.894 MPa)

L: left lane, R: right lane



Unit: ksi (1 ksi=6.894 MPa)

Figure 5.4 Backcalculated asphalt stiffness in rigid section

The stiffness variation of concrete within the three stages of construction is shown in Figures 5.5 and 5.6. After repair of the rigid concrete pavement, the average stiffness of concrete increased over 50 percent on section R1. However, after the crack and seat method, the stiffness decreased significantly. This result contradicts the findings of Hossain et al., who showed that there is no large stiffness decrease associated with the break and seat method (Ref 30). The right lane on section R2 decreased close to 500 percent in concrete stiffness. These results show that the concrete stiffness dramatically decreased after the crack and seat; such a decrease will certainly cause problems related to a poorly supported pavement — even if the procedure provides safeguards against reflective cracking.

Table 5.12 Stiffness increase ratio due to the maintenance (%)

Section	R1	R2A	R2B	R1	R2A	R2B
Lane	L	L	L	R	R	R
Concrete	62.05%	-138%	-515%	57.81%	-36.6%	-239%

Figures 5.5 and 5.6 show the trend of the backcalculated stiffness of the concrete. Sections R1, R2, and R3 show a reasonable stiffness trend. However, there was a problem with the results for sections R4, R5, and R6 — sections that did not have the old asphalt overlay milled and which required that several asphalt layers be represented by one asphalt layer. These problems resulted in decreasing stiffness for the concrete for some of the test sections, a finding that contradicts conventional wisdom.

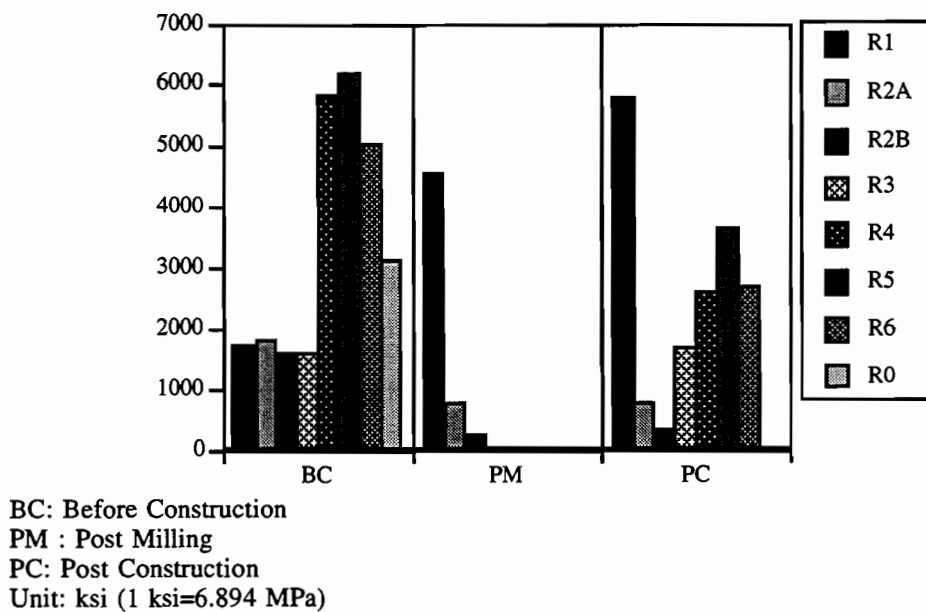


Figure 5.5 Backcalculated stiffness variation of left lane in rigid section

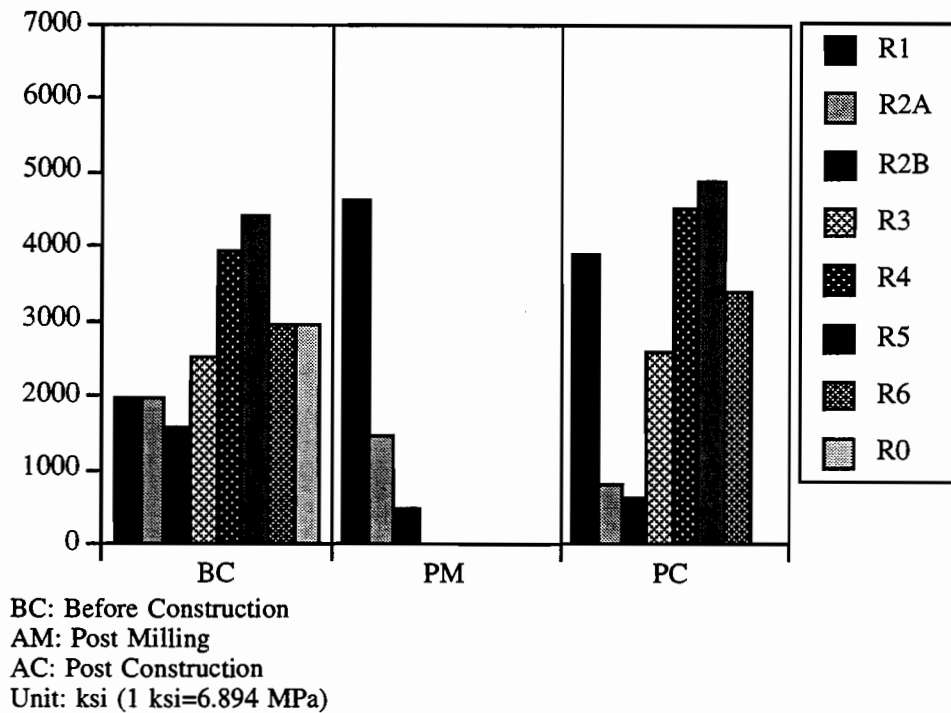


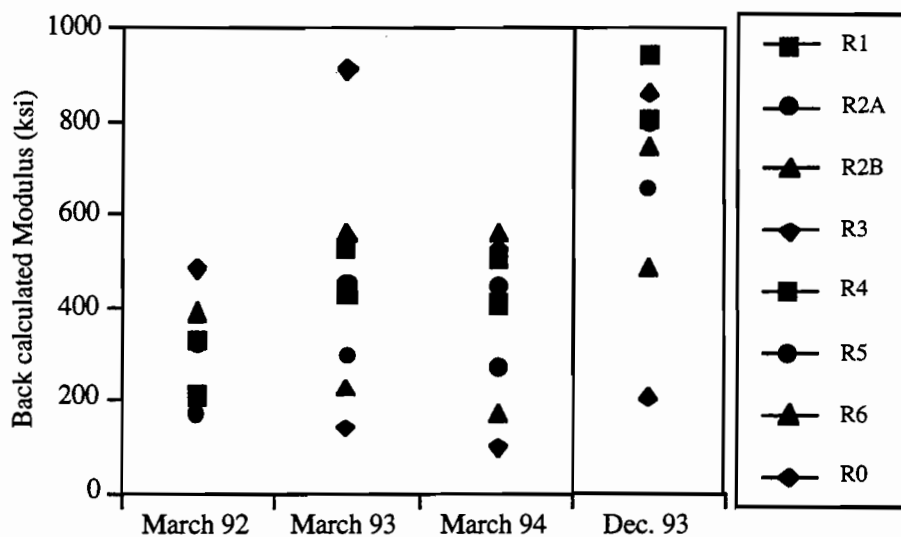
Figure 5.6 Backcalculated stiffness variation of right lane in rigid section

5.4.4. Results of 2 Years of Traffic Load Applications

It is generally accepted that pavement stiffness will decrease with time as the pavement structure accumulates traffic loadings and as it experiences climatic cycles. A cumulative history of pavement stiffness variations in time or cumulative traffic can serve as a basis for the development of a mechanistic design method, based on such fatigue concepts as the CTR-developed Pavement Rehabilitation and Design System (PRDS) (Ref 31). These methods assume that the pavement load carrying capacity will decrease as it approaches failure. In addition, a historical study of pavement stiffness for a given pavement section can show the quantitative benefit of asphalt overlays (which protect the overlaid JCP from further failures and consequent loss of stiffness). This can be demonstrated by showing that the stiffness of the JCP remains fairly constant with the accumulation of traffic loads, without a significant decrease in value.

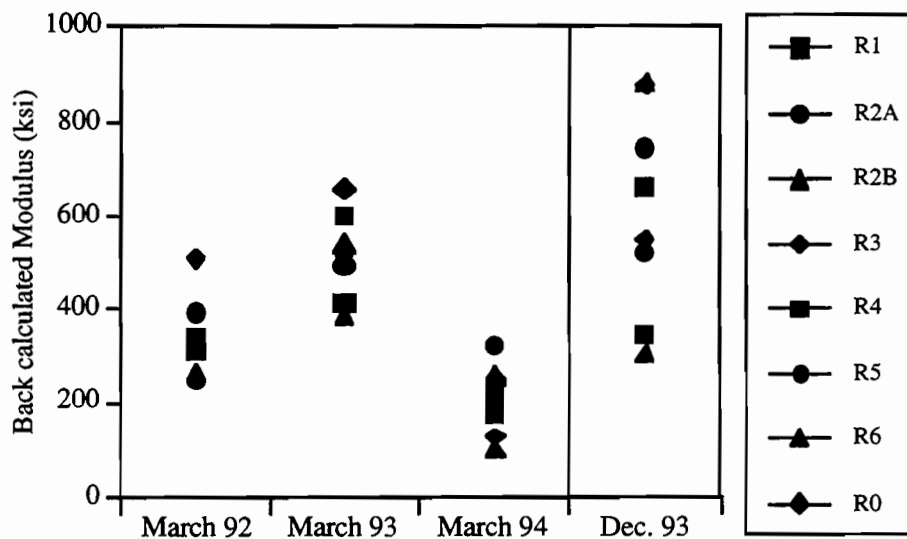
The stiffness variations over a 2-year period for the new asphalt overlay placed on existing JCP are shown in Figures 5.7 and 5.8. The stiffness for this layer varies continuously with time and associated traffic load applications. Interestingly, the stiffness of each lane behaves differently during this time, with the stiffness of the left lane not changing as much as the stiffness of the right lane. The stiffness of the right lane increases after 1 year of its serviceable life, and then decreases dramatically after 2 years, a phenomenon that can be ascribed to two important mechanisms for the asphalt layer: aging and fatigue. Under low traffic load applications, the stiffness of the asphalt overlay increases slightly, as occurred for both lanes. However, as traffic loading accumulations

continue, microcracking may develop in the asphalt concrete, with a consequent decrease in stiffness, as shown by the results for the right lane. In addition, for both the left and right lanes, the stiffness is higher in the winter than in the spring, as explained in Chapter 3. For example, section R2A's effective moduli were about 60 percent higher during winter.



1 ksi=6.894 MPa

Figure 5.7 The stiffness variation of asphalt in the left lane



1 ksi=6.894 MPa

Figure 5.8 The stiffness variation of asphalt in the right lane

Figures 5.9 and 5.10 show the stiffness variation for the concrete for both lanes. The stiffness of concrete did not experience major variations during the 2 years, confirming the hypothesis that the asphalt overlay protected the existing JCP from further loss of carrying capacity. A comparison of the results for the right and left lanes shows that for the left lane the stiffness remained fairly constant, while the right lanes experienced some deterioration. Temperature effects are not significant when comparing the results for winter and spring.

The stiffness results for the right lane in December 1993 show a relatively low stiffness for some sections (e.g., R4, R5, and R6) that have thicker asphalt overlays (including old asphalt overlays). Considering the stiffness of the next measurement, taken in March 1994, the backcalculation value of the concrete stiffness could be affected either by a large thickness of asphalt overlay, which was stiffer during winter, or by limitations in the backcalculation process, which had to assume a fixed stiffness for the old asphalt overlay.

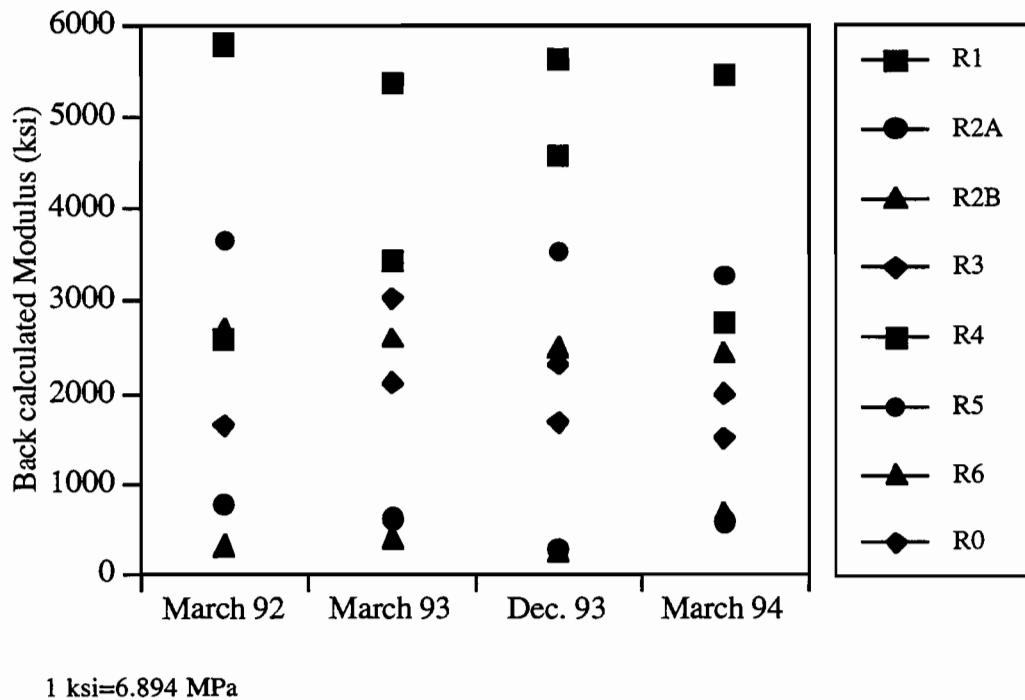


Figure 5.9 Stiffness variation of concrete in the left lane

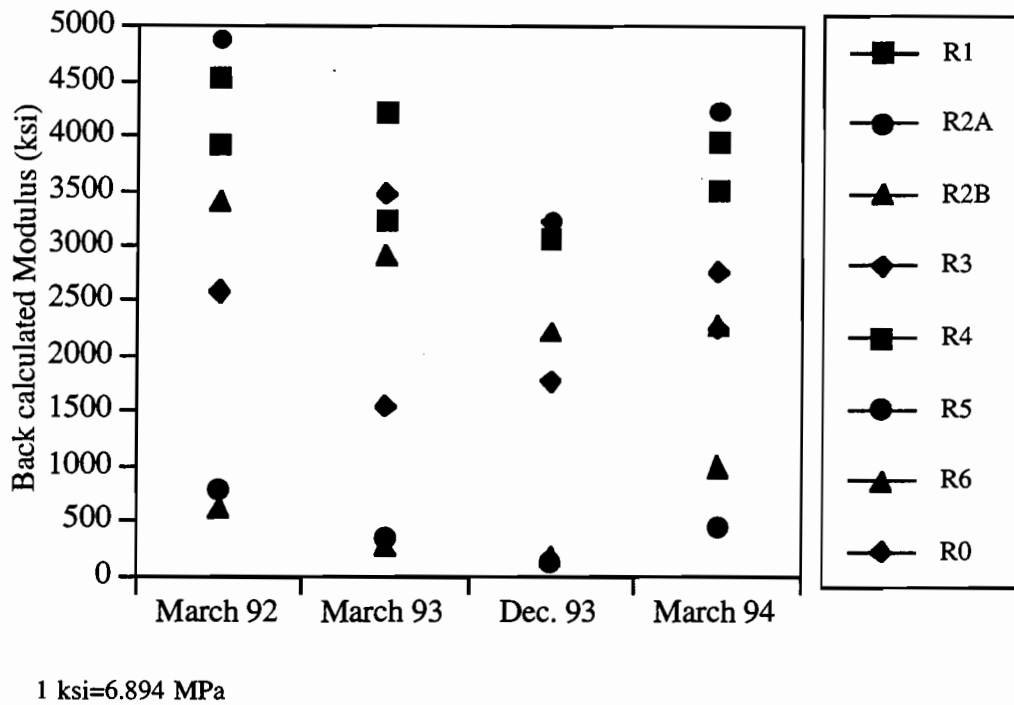


Figure 5.10 Stiffness variation of concrete in the right lane

5.4.5. Structural Numbers for the Rigid Sections

To support the calculations for 80-kN (18-kip) equivalent single-axle loads (ESALs) based on the 1986 AASHTO Design Guide, we calculated the SNs for the test sections, with the results summarized in Table 5.13. The structural number that represents the structural capacity of the different layers of the pavement was calculated based on the procedures recommended in the AASHTO Guide. The maximum structural number was 11 for section R4, while the minimum structural number for section R2A was 4.

Table 5.13 Structural number of each section

Layer	R1	R2A	R2B	R3	R4	R5	R6	R0
Surface	1.44	1.2	1.65	1.32	2.325	1.215	0.87	0.66
Inter layer	0	0	0	1.56	3.08	3.08	3.08	3.08
Concrete	5.6	2.8	2.8	5.6	5.6	5.6	5.6	5.6
Total	7.04	4	4.45	8.48	11.01	9.895	9.55	9.34
Suggested SN	7	4	4	8	11	10	10	9

5.5. BACKCALCULATION RESULTS FOR THE FLEXIBLE SECTION

Stiffnesses for the flexible test sections were also backcalculated using the MODULUS program. However, the time variation of the stiffness of the different layers of the flexible sections was not determined owing to the limitations inherent in the available backcalculation programs discussed previously in this chapter.

Since the post-construction deflection data were unavailable, the data set obtained in March 1993 was used in the backcalculation procedure. The initial set of deflection data, which was taken in June 1989, was excluded because it was already reported during the overlay design process. The average stiffness of 18.42 cm (7 and 1/4 inches) of the asphalt layer was backcalculated as being 2590 MPa (375,000 psi), 2070 MPa (300,000 psi) for the black base, 4830 MPa (700,000 psi) for the cement-treated base (CTB), and 172 MPa (25,000 psi) for the subgrade, using the RPEDD1 program.

Section F5 was excluded from the analysis because it did not lead to results within a reasonable range for its stiffness, which was probably due to the flexible base. This problem was circumvented by using the results for the flexible base stiffness obtained in the backcalculation process carried out for test section R3. Because of the limitations of the backcalculation routines available, the various layers were, as discussed previously, reduced to four layers, namely, the asphalt layer, black base, CTB, and lime-treated subgrade. The possible ranges for each layer for the modulus of elasticity were set to 689 to 3450 MPa (100,000–500,000 psi) for asphalt and black base, and 3450 to 6890 MPa (500,000–1,000,000 psi) for the CTB. The new and old asphalt layer could not be considered separately, owing to the limitations of the MODULUS program, as previously mentioned.

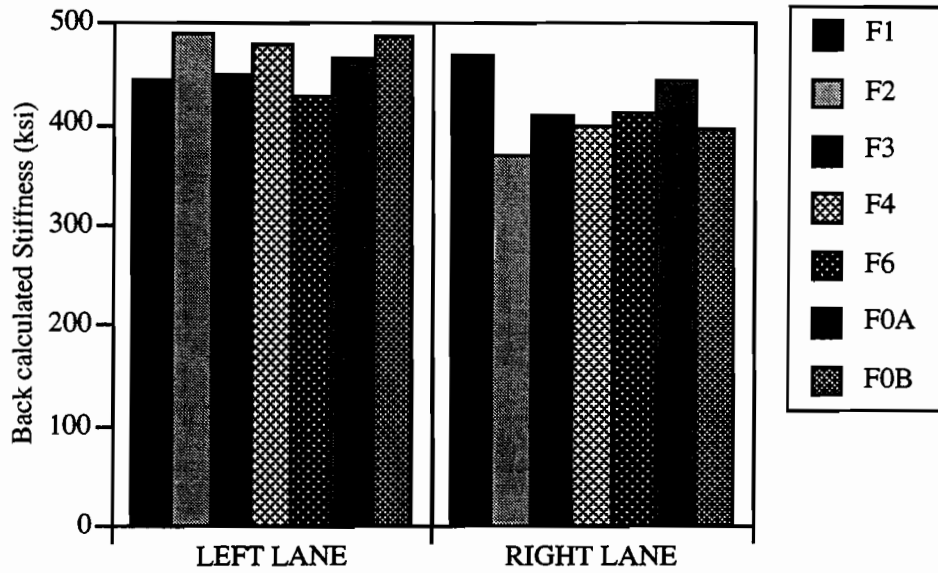
5.5.1. Stiffness Variation for Flexible Sections

The stiffness of most asphalt layers was in the 2760 to 3450 MPa (400 to 500 ksi) range within each section. The left lane stiffness shows a slightly higher value, as compared with the results for the right lane.

The black base layer has much more variability between sections than does the asphalt layer. It presented results from 1030 to 3450 MPa (150 to 500 ksi), which are less than what was estimated from the 1989 deflection data set. This discrepancy may be a result of either deterioration of the black base during the 2- year monitoring period, or simply of the difference between the two backcalculation programs. The black base layer also has larger stiffnesses in the left lane (except for section F3). The deterioration of the black base was presumably a result of the higher traffic volumes in the right lane.

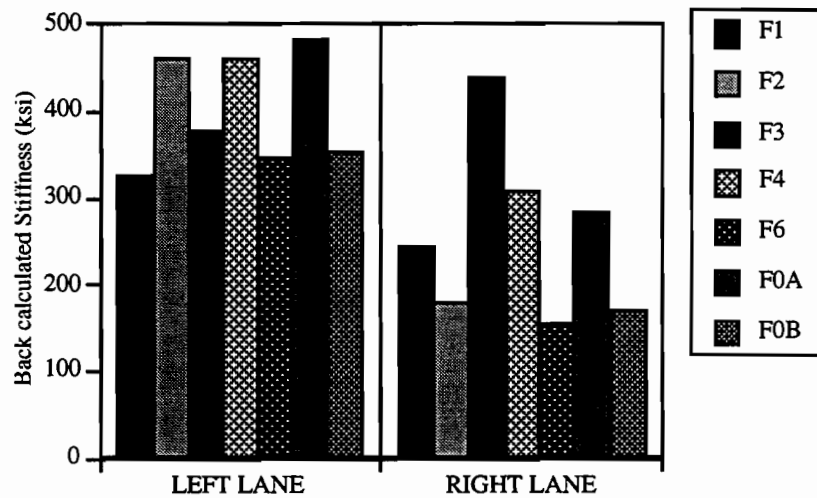
The modulus of elasticity for CTB is shown in Figure 5.12. The range of stiffnesses was from 4140 to 6204 MPa (600 to 900 ksi), which agrees well with results obtained by previous research in this project related to the design of the test sections. As against previous findings for the asphalt and black base, the stiffness difference between the two lanes was not significant for the

CTB. If we assume that the only difference between the two lanes is the traffic loadings, then it could be that the stiffness of the CTB layer is not as sensitive to traffic as the black base or the asphalt layer.



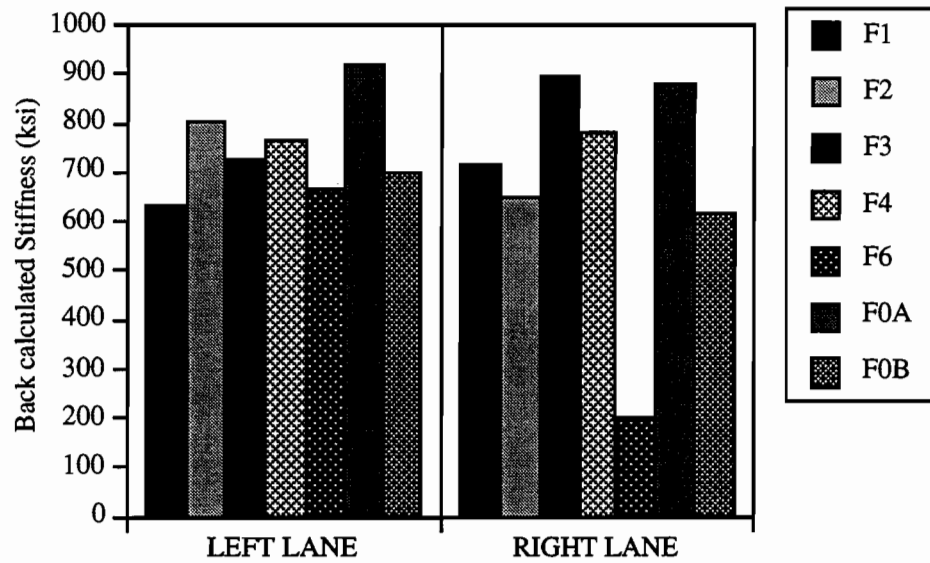
1 ksi=6.894 MPa

Figure 5.11 Backcalculated stiffness of asphalt layer — Flexible section



1 ksi=6.894 MPa

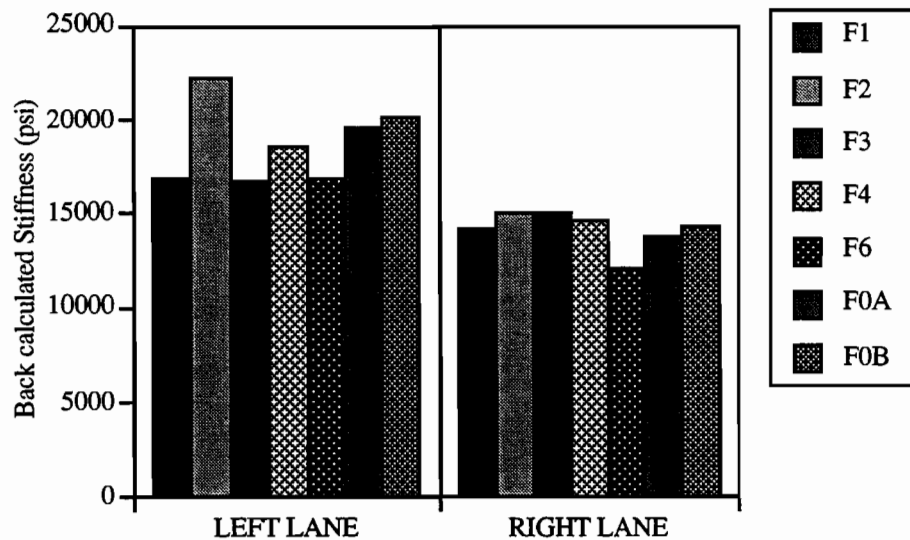
Figure 5.12 Backcalculated stiffness for the black base layer — Flexible section



1 ksi=6.894 MPa

Figure 5.13 Backcalculated stiffness for the CTB layer — Flexible section

The lime-treated subgrade shows homogeneous stiffness results between sections. It also shows a slightly higher stiffness in the left lane when compared with the right lane results, though the difference is not significant, as shown in Figure 5.14. The MODULUS calculations also result in slightly lower stiffnesses when compared with the results of the RPEDD1 program.



1 psi=6.894 kPa

Figure 5.14 Backcalculated stiffness for the soil layer — Flexible section

5.5.2. Structural Number Calculation

As with the rigid section, the structural number was estimated by the procedure suggested in the AASHTO Guide. Thickness information came from core and design plan sheets, as shown in Table 5.14. Based on the backcalculated stiffnesses, the structural number was calculated as shown in Table 5.15 by the procedure given in the AASHTO Guide (Ref 7). Unlike the rigid section, some variation existed within the range of 6 to 8. This value will be used to calculate the ESAL applications based on the WIM data.

Table 5.14 Thickness of each layer in every flexible section

Layer	F1	F2	F3	F4	F5	F6	F0A	FOB
Surface	10.3	10.3	11.8	10.3	3	9	9.8	10.3
Flexible	0	0	0	0	10	0	0	0
Black base	4.5	4.5	4.5	4.5	4.5	4.5	4.5	4.5
Subbase	6	6	6	6	6	6	6	6
Soil	INF.	INF.		INF.	INF.	INF.	INF.	INF.

Table 5.15 Structural number of each section

Layer	F1	F2	F3	F4	F5	F6	F0A	FOB
Surface	4.532	4.12	4.838	4.223	1.26	3.69	4.312	4.223
Flexible	0	0	0	0	1.95	0	0	0
Black base	1.35	1.35	1.35	1.35	1.35	1.35	1.35	1.35
Subbase	1.68	1.68	1.68	1.68	1.68	1.68	1.68	1.68
Total	7.562	7.15	7.868	7.253	6.24	6.72	7.342	7.253
SN	8	7	8	7	6	7	7	7

5.6. SUMMARY

Backcalculation was performed using two available programs for composite pavement and flexible pavements. The variation of effective stiffness was high, requiring additional support from laboratory results. However, the following general trends were identified: The backcalculated stiffness from the two programs resulted in similar trends, such that the backcalculated stiffnesses can be, at least, used to show the trends of stiffness under traffic. Stiffness recovery in repaired concrete pavements was shown in section R1, and a stiffness decrease on the break and seat section was shown in section R2. The other sections maintained similar stiffness trends for the concrete. The backcalculation procedure for the flexible section was

limited by the inherent constraints of the two programs. The structural number was estimated from the backcalculated stiffnesses for both sets of test sections. The structural number results provide basic data for calculating ESALs and can be used to develop overlay design models.

CHAPTER 6. RUTTING OF THE TESTS SECTIONS

6.1. BACKGROUND

Rutting is a traffic-induced, permanent deformation that can affect an asphalt pavement's subgrade, subbase, base, or pavement surface. In evaluating various solutions to the problem of rigid-section reflective cracking in the test sections used in this study, we discovered that such solutions can lead to rutting between layers. In the pavement rehabilitation literature, rutting is also known to be a principal cause of rapid failure in asphalt-overlaid sections (Ref 32). For all these reasons, we monitored the test sections for signs of rutting. This chapter describes this monitoring effort.

6.2. MECHANISM OF RUTTING

The mechanism by which rutting develops has been investigated by various researchers (Refs 1, 33, 34). The primary mechanism, as reported in the literature, is the densification or consolidation of each pavement layer by heavy traffic loadings. Pavement design methods, which mainly rely on the compressive strain on the subgrade of the pavement structure, recognize densification as the main factor in rutting development.

The AASHO Road Test discusses other possible mechanisms for pavement rutting. For these tests, trenches were dug to observe the rutting pattern in different layers. The observations suggested that rutting could occur not only in the subgrade, but also on the surface itself through shear stresses caused by traffic loadings. In other laboratory tests using wheel-tracking-test facilities, Eisenmann and Hilmer showed that three stages exist in the development of rutting (Ref 33), with such deformation developing initially as a result of the densification of the asphalt layer after fewer than 2,000 load cycles. They explained that the irreversible volume change below the tire is far greater than the volume change of vaults beside the tire. However, as traffic applications accumulate, the volume changes between two bounds are almost the same, as shown in Figure 6.1. Thus, the main cause of rutting is not the densification of asphalt, but the displacement through constancy of volume owing to shear stress. Rutting failure accelerates during the final stages of pavement failure.

In summary, rutting can be caused by permanent deformations in all layers of the pavement structure, as shown in Figure 6.2. However, rutting generally occurs on the surface layer as a result of a shear mechanism (Ref 35). Rutting can also be accelerated by a tender mix, extreme high temperatures, heavy loads, high tire pressure, and by the consolidation of the subgrade through the post-compacting of the soil.

6.3. FACTORS AFFECTING RUTTING PROGRESSION

There are various factors that promote rutting. The structural-related factors include traffic wheel loads, high temperature, and existing pavement structural strength. The wheel load and tire pressure effect on rutting has been studied by several researchers (Refs 36, 37, 38). Higher tire pressures on the top pavement layers lead to higher compressive stresses, which lead to accelerated

rutting of the pavement. Axle force, tire type, and speed of vehicle also contribute to rutting development. The asphalt concrete stiffness decreases with high temperatures, such that the rut depths will increase mainly in the summer. Ramon et al. showed that the temperature effect is even larger than the tire pressure effect, based on ELSYM5 analysis and field results (Ref 39).

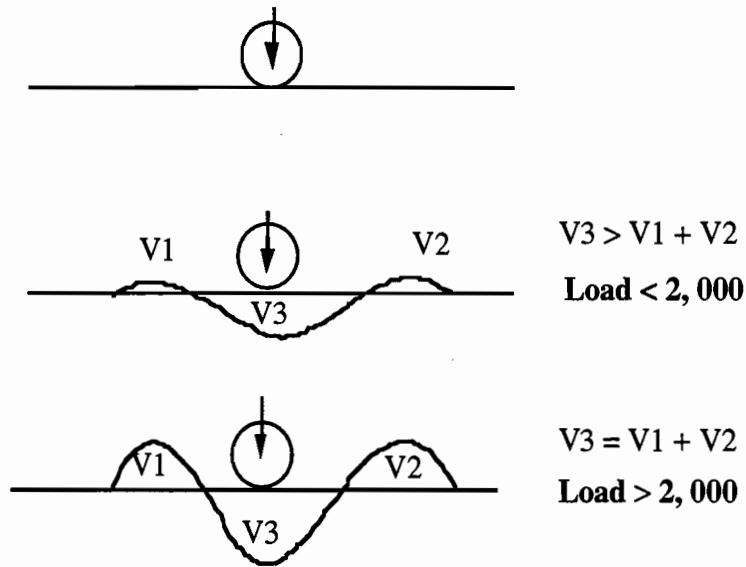


Figure 6.1 Rut depth development during laboratory testing (Ref 34)

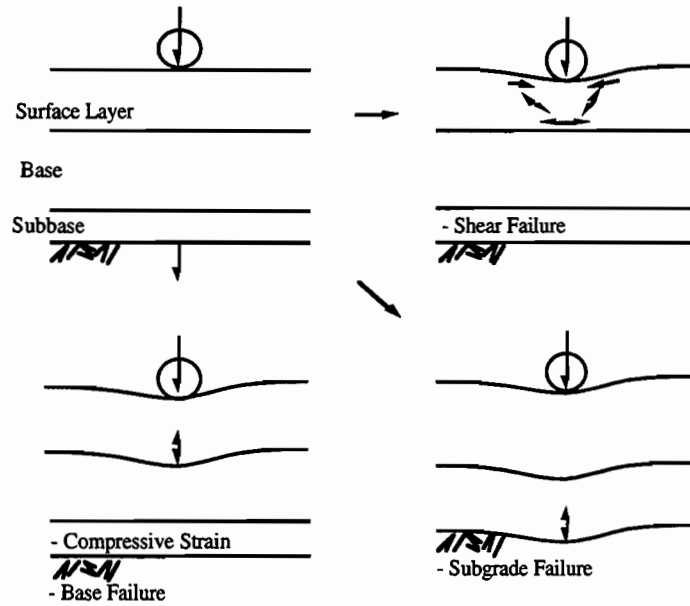


Figure 6.2 Rutting development in the pavement structure

Another set of factors affecting rutting progression is associated with the mix design of the asphalt concrete (Refs 40, 41, 42). The aggregate, which accounts for over 80 percent of the asphalt concrete by weight, strongly influences rutting development. For example, incorrect gradation of the aggregate (i.e., too much middle-sized sand) can increase the susceptibility to rutting. The shape of the aggregates also effects the progression of pavement rutting. A coarse aggregate will provide more aggregate interlock and, hence, more resistance to rutting progression than will a round aggregate.

The AC binder also plays a significant role in rutting development. Because high temperatures render the AC binder susceptible to rutting, the mix must be made sufficiently stiff to offset such effects. However, the increase in stiffness may not resolve the thermal cracking problem (and may even exacerbate the problem in some instances). Classical mix design approaches (e.g., the Marshall or Hveem design methods) do not properly account for rutting development. The recently completed Strategic Highway Research Program (SHRP) will provide valuable information on performance-related mix design methods. According to Kennedy,* rutting is strongly related to the AC binder in 80 percent of the cases. Consequently, the mix design factors, including AC percent, voids of mineral aggregate (VMA), air void, and poor mix design will affect rutting for the same structural design. For example, a higher content of AC binder will lead to low air voids, a condition that is highly correlated with rutting problems (Ref 35). The VMA associated with the aggregate also has a large impact on the rutting problem; it was observed that the rut depth will decrease as VMA increases (Ref 42). However, Cooper et al. and the Asphalt Institute discussed a minimum VMA level that would ensure satisfactory aggregate-binder compacting without the mixture becoming overfilled (Ref 43).

6.4. RUTTING MEASUREMENT EQUIPMENT

Rut depths can be measured using various devices. The simplest and most practical way of measuring rut depths is to measure vertical permanent deformation along the wheel path by ruler and straight edge. This method was used at the US 59 test site to measure test section rut depths before the new asphalt overlay was constructed. Another device available for rut depth measurement is the ARAN unit, which has been recently updated by TxDOT. The ARAN unit can also monitor pavement condition by video tape recording.

An electronic rut depth device was used to measure the rut depth development for the test sections over long-term monitoring. Developed by CTR, this device has been adapted from previous research (Ref 44). It consists of a 1.83-m (6-foot) straight edge and straight bar to measure the depth up to a precision of .00254 cm (1/1000 of an inch). The device, which is relatively simple, measures rut depths at the center of the straight bar (it cannot measure total transverse curvature along the wheel path). The results are point rut depth measurements that represent the maximum rut depth.

* Thomas W. Kennedy, in course lecture for CE 397 (Summer 1994), The University of Texas at Austin.

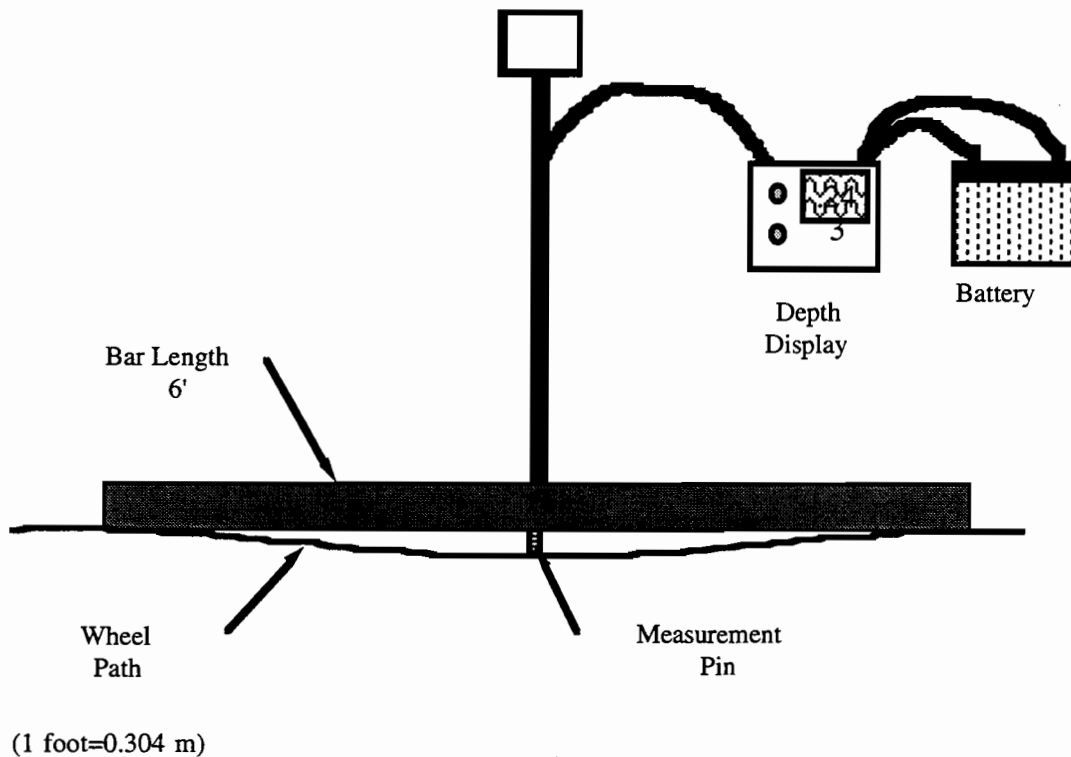
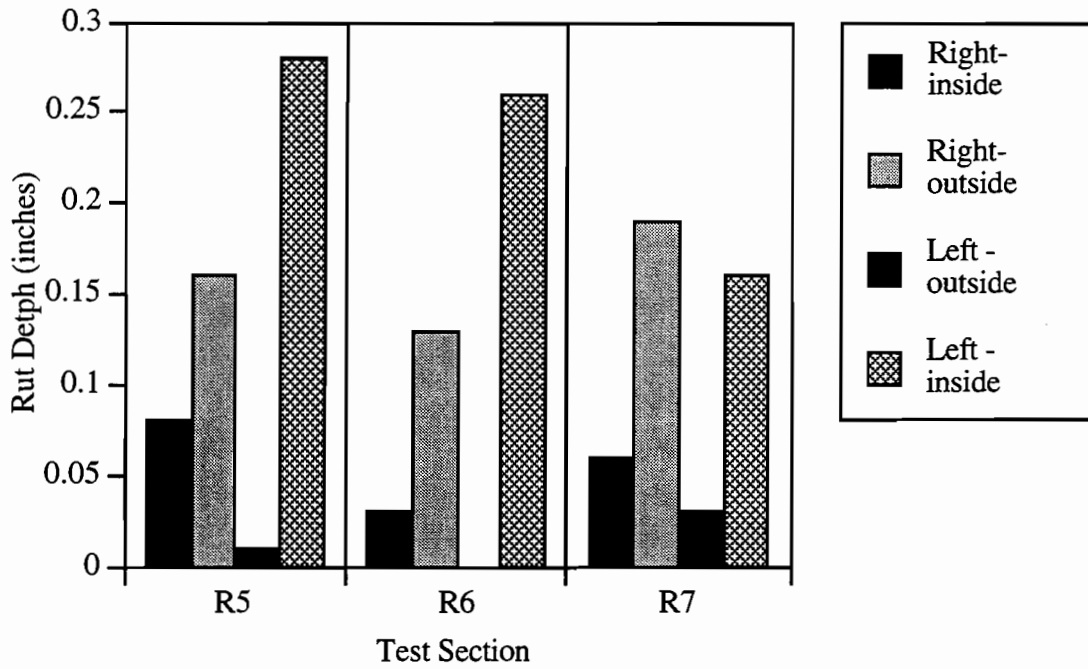


Figure 6.3 Rut depth measurement equipment

6.5. RUTTING MEASUREMENTS BEFORE OVERLAY

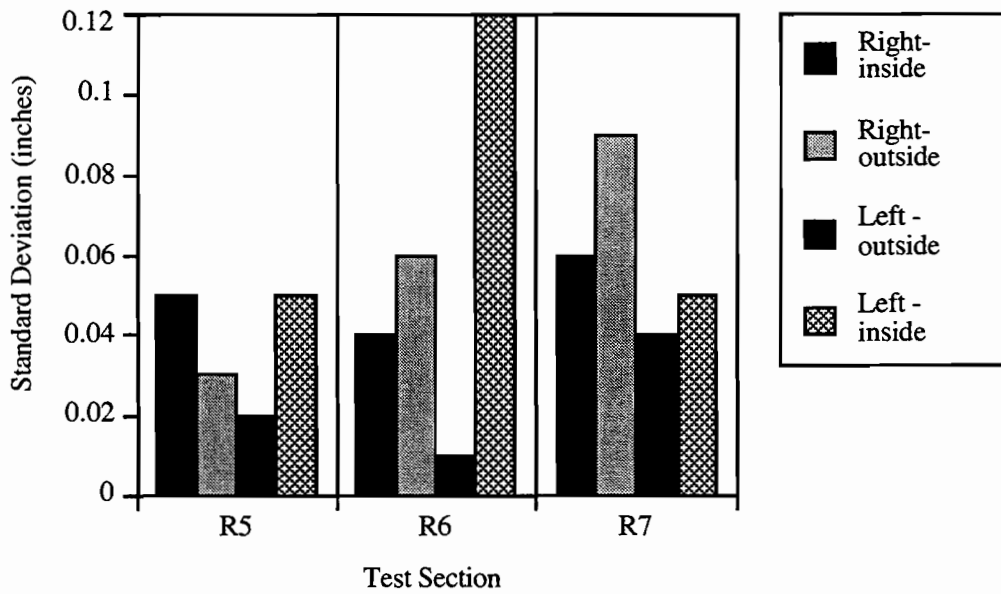
6.5.1. Rut Depths for the Rigid Section

Figures 6.4 and 6.5 show the results of the rut depth measurements taken on September 30, 1991, for test sections R5, R6, and R0. Measurements for the other rigid test sections were not taken because the overlay construction was in progress at that time. For the rigid test sections, measurements were taken every 15.24 m (50 feet) in each wheel path. The measurements were taken with a 1.82-m (6-foot) long straight edge and ruler that measured to .079 cm (1/32 of an inch), a simpler method than that used for the long-term performance monitoring. While the results cannot be directly compared with those obtained during the long-term performance measurements shown in Figure 6.3, they can certainly show the rutting condition before the overlay was applied. In general, there was little rutting in the rigid section with the exception of the left lane for the inside wheel path. The average maximum rut depth was 0.635 cm (0.25 in.), with a 0.305-cm (0.12-inch) standard deviation for the inside wheel path on the left lane. Although precise conclusions cannot be drawn from these results (owing to the imprecision of the device and to the lack of data for the other sections), there are clearly different rutting behaviors for the different lanes and wheel paths.



1 inch=2.54 cm

Figure 6.4 Average rut depth variation in the rigid sections — Before construction

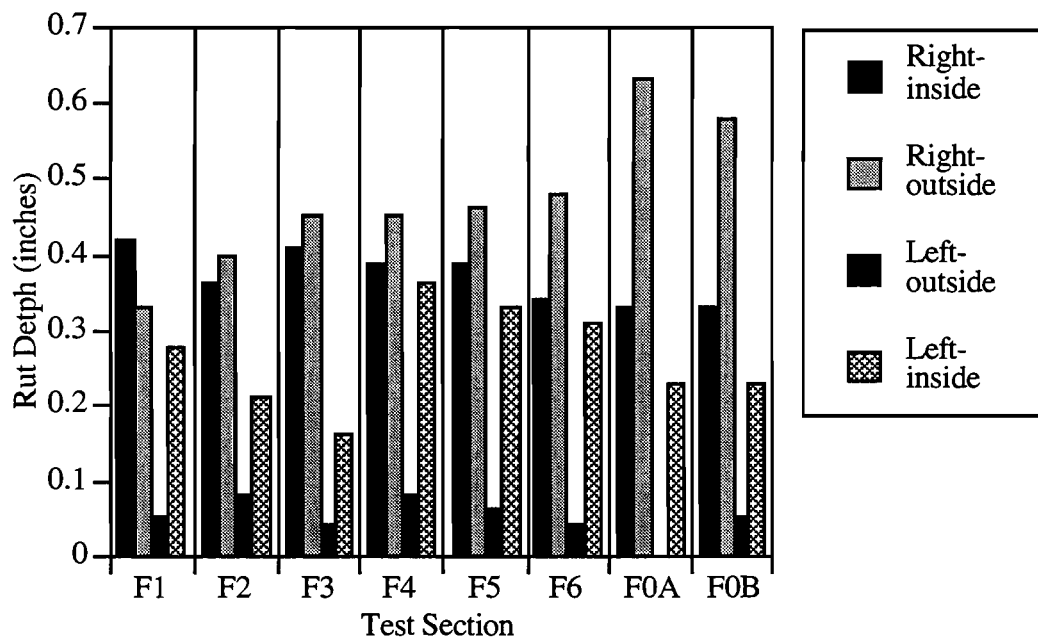


1 inch=2.54 cm

Figure 6.5 Standard deviation of rut depth in the rigid sections — Before construction

6.5.2. Rut Depth for the Flexible Section

Rut depth measurements were taken for the flexible test section on April 13, 1992. Measurements were taken every 15.24 m (50 feet) across the entire 2130 m (7,000 feet) of the flexible test sections, using the same procedure described for the rigid section. The flexible sections presented much more rutting than the rigid sections, though the rutting seemed to be fairly uniform for each wheel path (except for the left lane outside wheel path). The rut depth on the outside wheel path for the left lane showed rut depths significantly lower than those for the rest of the wheel paths. As with the rigid section, the inside wheel path of the left lane presented rutting that was deeper than that measured for the outside wheel path. As shown in Figure 6.6, the measured rut depths for the right lane were higher than the rut depths measured for the left lane, and the outside wheel path presented slightly higher rutting than the inside wheel path. The worst rutting condition was observed in test sections F0A and F0B, with average rut depths about 1.524 cm (0.6 in.), with a 0.254 cm (0.1 in.) standard deviation. This shows that the flexible section already had a rutting problem before the new overlay was applied. Possible causes of the rutting include heavy traffic- and moisture-induced stripping of the asphalt layers; this was confirmed by both core analysis and by the ARAN (Ref 2).



1 inch=2.54 cm

Figure 6.6 Average rut depth variation for the flexible test sections — Before construction

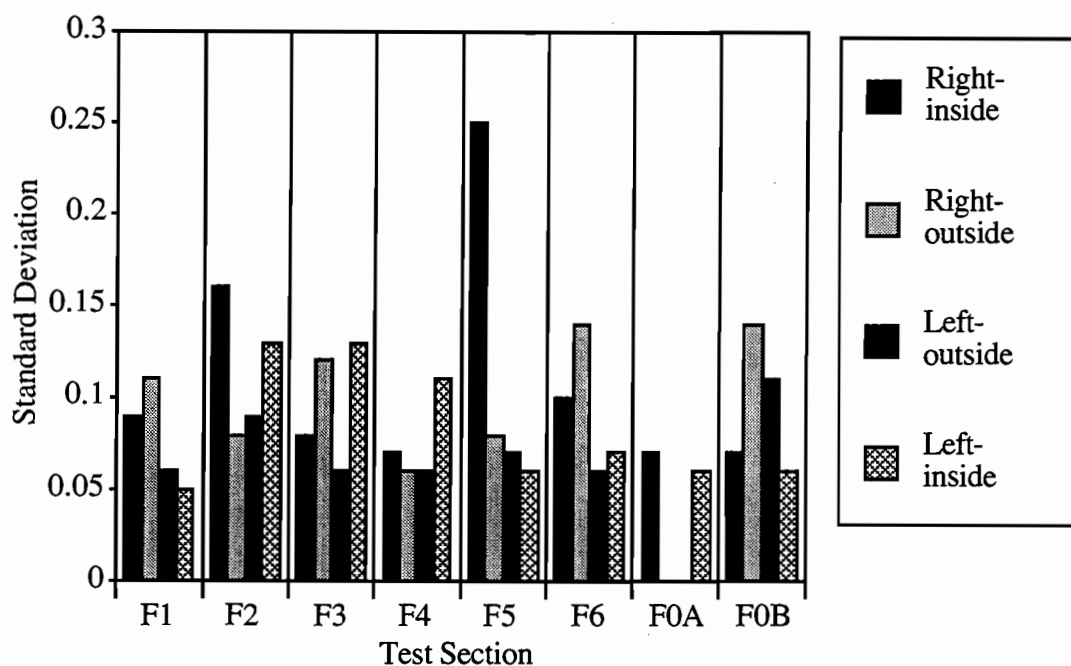


Figure 6.7 Standard deviation of rut depth for the flexible test sections — Before construction

6.6. RUT DEPTHS AFTER NEW OVERLAY

Rut depth data were collected from the test sections every 3 months following new overlay construction, with a total of seven sets of rutting measurements ultimately obtained. These results are summarized below.

6.6.1. Rigid Section

As expected, the test sections developed rutting. Figures 6.8 to 6.11 show the average rut depth development for the rigid test sections. Test section R3, composed of an asphalt overlay on a flexible base (applied to prevent reflective cracking), failed as a result of severe rutting. Section R2A and R2B also experienced rutting (a likely result of the crack and seat process, which led to lower bearing capacity). No rutting was detected on the other sections until the most recent available measurement (March 1994).

Figures 6.8 to 6.11 resolve many questions regarding the rutting performance of the different test sections: For example, is there a different rutting pattern between lanes? Does rutting performance differ between wheel paths? As shown in Chapter 3, the traffic volumes for the right lane are much larger than those for the left lane, a situation that will definitely lead to different pavement performance patterns between lanes. Because the rutting problem is strongly related to traffic volumes, it is expected that the right lane will present larger rut depths than the left lane. In addition, plate theory and nonrestrictive deflection tests show that the edge loading conditions for a slab will present higher deflections than interior loading conditions for a rigid pavement. Higher

deflections mean higher stresses, such that the chances of stress development are greater at edge or corner locations than at interior locations. In addition, moisture damage is more likely to occur on the outside wheel path than on the inside wheel path.

As shown in Figures 6.8 to 6.11, the difference between the right and left lane is significant in those sections — especially sections R2A, R2B, and R3 — that have large rut depths. The remaining test sections do not show large differences between lanes. For example, the average rut depth of the right lane of section R3 in the first measurement was 1.02 cm (0.4 in.), while the average rut depth for the left lanes was 0.203 cm (0.08 in.). Also, the wheel path difference is dependent on the lane. The average rut depth for the outside wheel paths is significantly larger than the average rut depths for the inside in the right lane wheel paths, while the results for the left lane show no apparent difference.

Based on the long-term monitoring, the development of rut depths can be divided into three phases: The first phase is a rapidly increasing rate of rutting caused by initial densification; the second phase is a steady rate of rutting development caused by traffic loads (this phase can also be characterized by no further increase in rutting); the third phase is marked by a rapid progression towards failure.

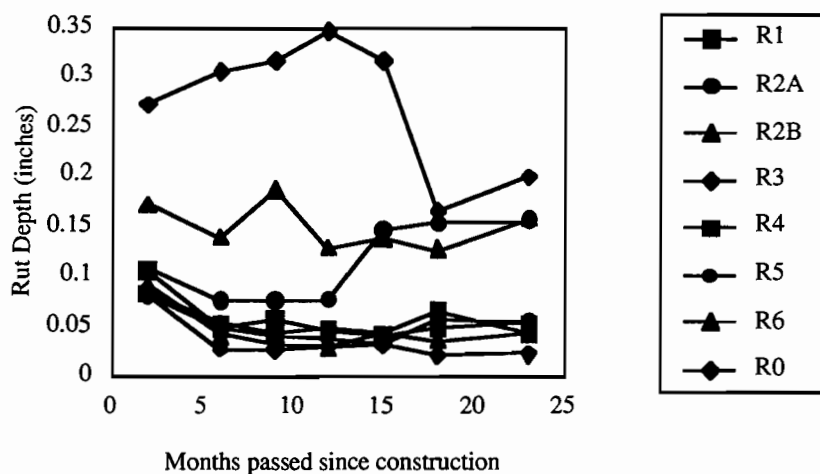
Rutting caused by initial densification was observed on some of the rigid sections. After only 3 months, average rut depth on the outside wheel path in the right lane of section R3 was over 0.635 cm (0.25 in.), though still less than the maximum acceptable rut depth of 1.067 cm (0.42 in.). The remaining rigid test sections were also rutted, with such distresses averaging 0.35 cm (0.14 in.) in R2 and 0.254 cm (0.10 in.) in R1. After the initial stages of rut development, almost all the test sections maintained their rut depths, even decreasing in some cases (this is excepting R3, which increased continuously until the lane markings were changed in June 1993). As was discussed in Chapter 3, changing the lane markings affected the traffic's lateral distributions, which consequently affected rut depth development. In addition, the rut depth measurements were taken using the pavement markings as a reference; accordingly, the measurements taken after the pavement markings were changed came from a pavement section that did not experience a high number of traffic loadings and, consequently, had minor rut depth development.

Some of the decreasing rut depths of the test sections may be related to the lateral distribution of the wheel path. Because wheel paths are stochastic (rather than deterministic) in nature, initial rut depths may be reduced as the traffic compacts the pavement surrounding the rutting area; such action may lead to an equilibrium throughout the section, translating into decreasing rut depths.

When rutting increases, the small cracks that appear on the surface of the pavement allow water to infiltrate the subgrade, a situation that can lead to rapid degradation of the soil support, severe rutting, and, ultimately, to pavement failure. Figures 6.8 through 6.11 suggest that this is not a problem for the rigid test sections, with the exception of test section R3, which during the last condition survey presented fatigue-type alligator cracking (meaning that R3 is at the final stages of rutting development and will probably deteriorate faster from this stage on).

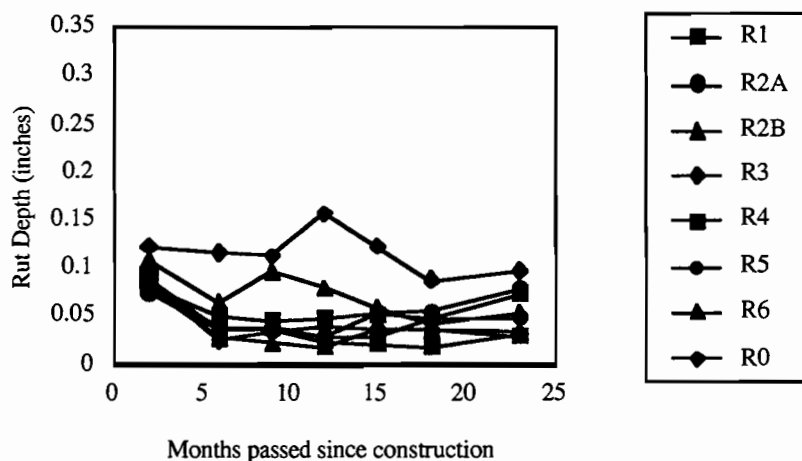
Because the stiffness of the asphalt pavement used for the overlays is strongly related to

ambient temperature, rutting may be more severe during the summer than during the winter. However, the effect of the hot climates may not be as critical as the literature suggests, since the long-term rutting performance measures taken at the test site showed mostly an average rut depth decrease during the summer. The only exception was test section R3, which experienced a continuous rut depth increase throughout the monitoring period, suggesting that the rutting mechanism for test section R3 differs from that of the other test sections, with rutting increasing rapidly in the final stages.



1 inch=2.54 cm

Figure 6.8 Rut depth versus time at outside wheel path in right lane — Rigid section



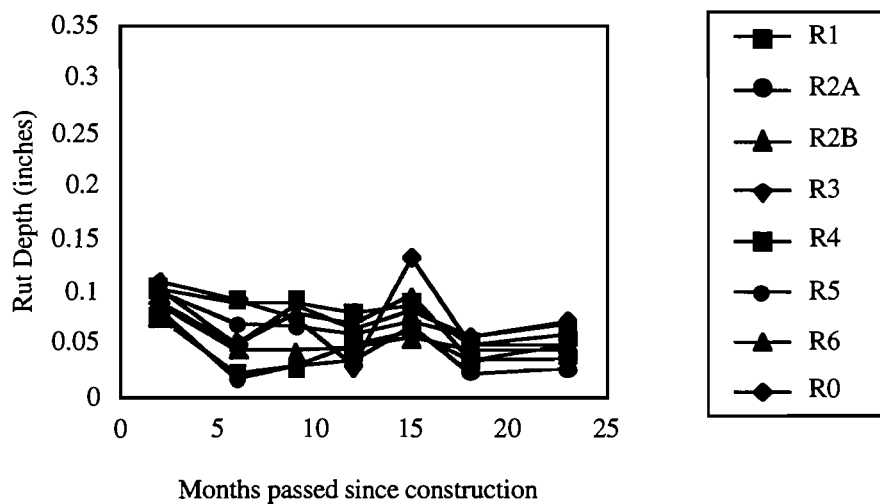
1 inch=2.54 cm

Figure 6.9 Rut depth versus time at inside wheel path in right lane — Rigid section



1 inch=2.54 cm

Figure 6.10 Rut depth versus time at inside wheel path in left lane - Rigid section



1 inch=2.54 cm

Figure 6.11 Rut depth versus time at outside wheel path in left lane — Rigid section

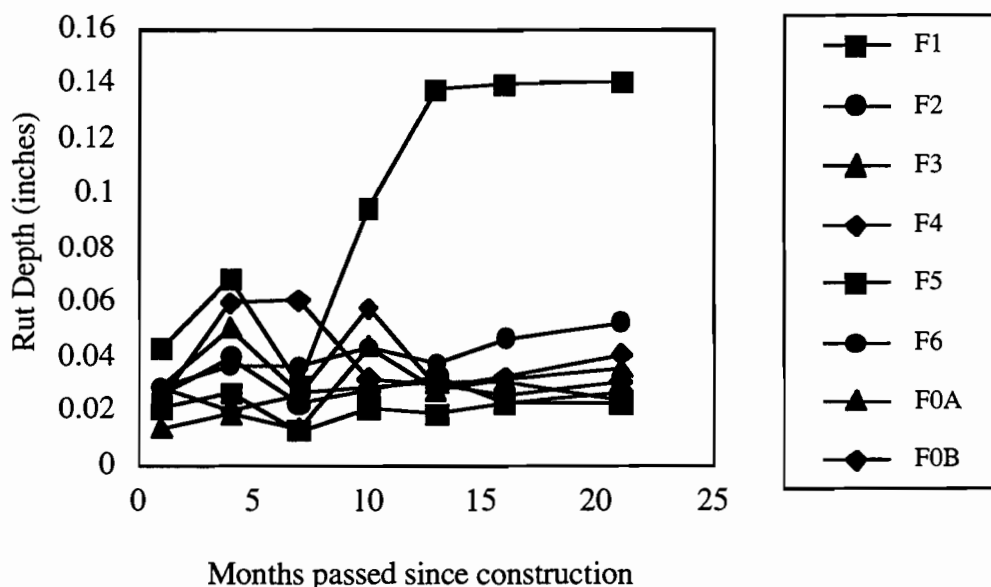
6.6.2. Flexible Section

We were concerned with the rutting development on the flexible sections even before the overlays for the test sections were placed. Test sections FOA and FOB had severe rutting problems

before the overlay, with the inside wheel path of the left lane showing more rutting development than the outside wheel path.

Rut depth measurements taken periodically from the flexible test sections are summarized in Figures 6.12 through 6.15; these also show the rutting trend for each wheel path in a lane. The rut depth increase pattern for the flexible sections differs somewhat from that observed for the rigid sections. The flexible sections follow the same rutting trend that was observed before the new overlay, with the right lane showing slightly more rutting. However, the inside wheel path has greater rut depths than those for the outside wheel path for both lanes. These rutting developments for the inside wheel path may be attributed to such construction problems as improper compacting. In addition, the fact that the two inside wheel paths developed deeper rut depths suggests the problem may be related to the previous pavement condition, which presented deeper rutting for the inside wheel path. These deeper ruts on the inside lane may also be related to a drainage problem that, in weakening the subgrade, led to rutting on the inside wheel path.

The flexible base section, F5, also developed a rutting problem similar to that observed on the rigid sections. The maximum rut depth developed in the inside wheel path of the right lane. The average rut depth measured in March 1994 was 0.406 cm (0.16 in.), while the maximum rut depth was 1.549 cm (0.61 in.). The standard deviation for the rut depths calculated for the section is 0.356 cm (0.14 in.); the calculated coefficient of variation was close to 85 percent. Up until the most recent survey, the other test sections presented rut depths of less than 0.254 cm (0.1 in.). Sections F0A and F0B, which had severe rutting problems before the new overlay, will probably develop further rutting problems in the future.



1 inch=2.54 cm

Figure 6.12 Rut depth versus time at outside wheel path in right lane — Flexible section



Figure 6.13 Rut depth versus time at inside wheel path in right lane — Flexible section

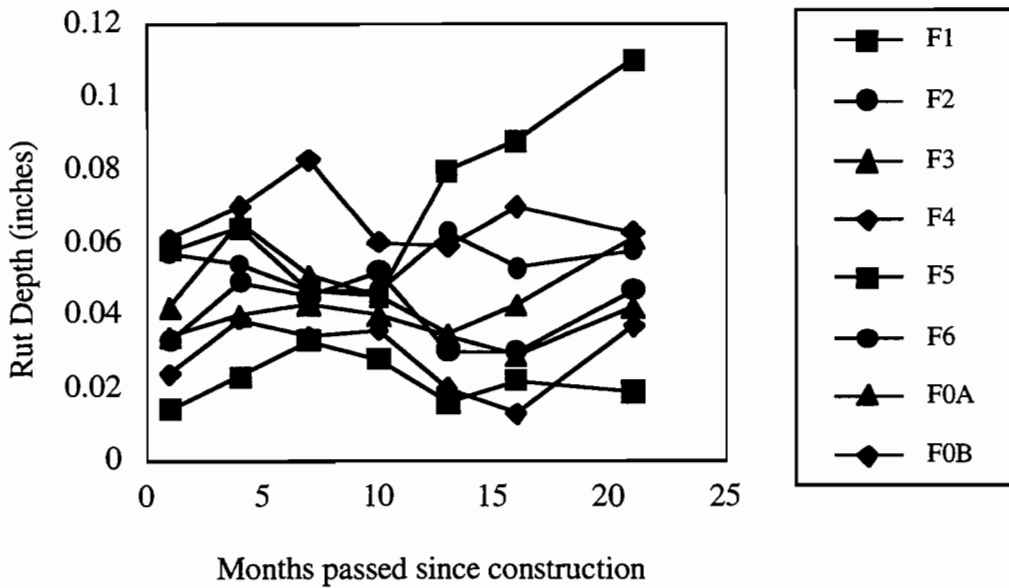
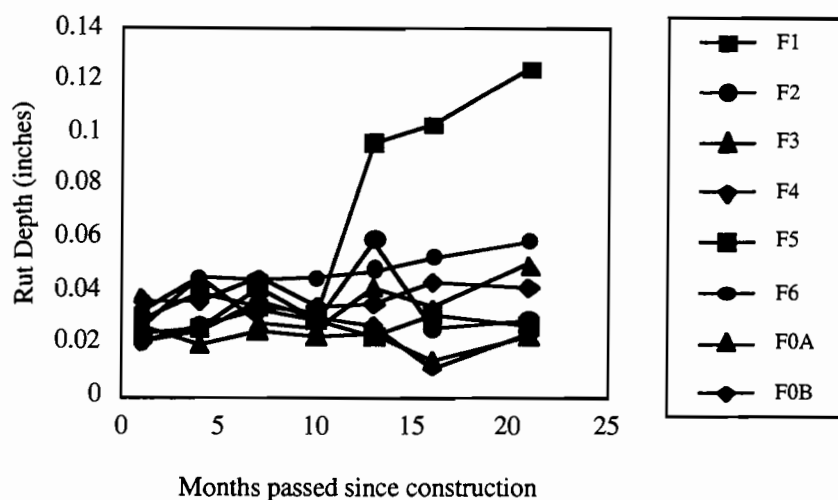


Figure 6.14 Rut depth versus time at inside wheel path in left lane — Flexible section



1 inch=2.54 cm

Figure 6.15 Average rut depth versus time at outside wheel path in left lane — Flexible section

6.7. RELATIONSHIP BETWEEN RUT DEPTHS VERSUS DEFLECTIONS

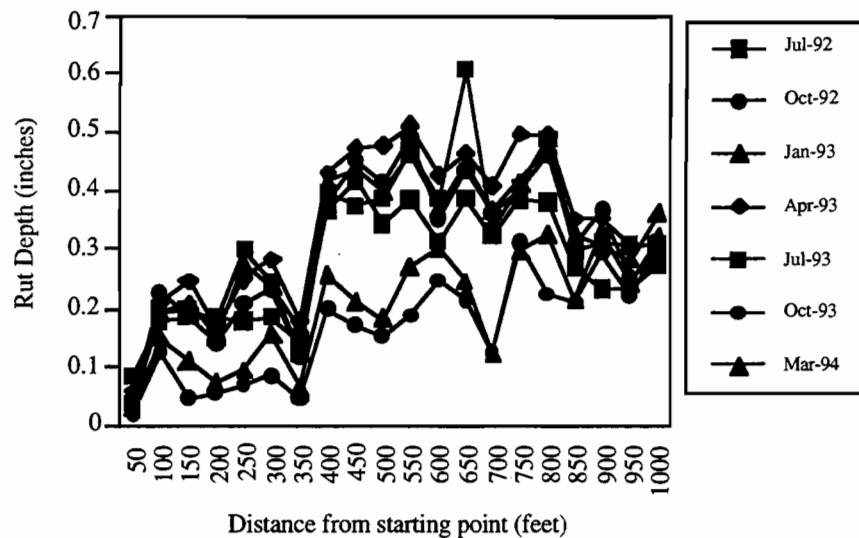
As discussed previously, the two sections that had flexible bases — R3 for the rigid sections and F5 for the flexible sections — also experienced severe rutting problems, though they performed adequately in protecting the overlay against reflective cracking. Along with severe rutting, these sections exhibited alligator cracking when the condition survey was performed in March 1994. Sections R2A and R2B also experienced significant rutting in the rigid sections. Thus, rigid test sections R2A, R2B, and R3 and flexible test section F5 were selected for further study in our effort to develop a rutting prediction model.

6.7.1. Rigid Sections

Figures 6.16 through 6.17 present the rut depth development for test section R3, from the beginning of the project to March 1994. As discussed previously, the outside wheel path of the right lane presented greater rut depths than the inside wheel path. The outside wheel path of the right lane for section R3 presented a maximum of 1.016 cm (0.4 in.) of rutting only 3 months after construction of the overlay, with the section ultimately developing a maximum of 1.524 cm (0.6 in.) in July 1993. The approximate increase rate for the maximum rut depth in section R3 was about 0.038 cm (0.015 in.) per month.

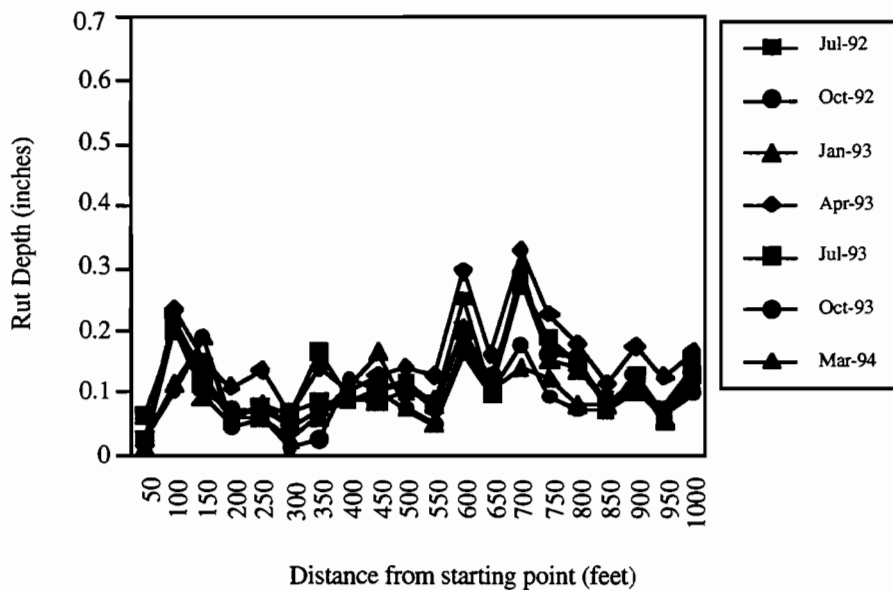
The rut depths increased continuously up until the July 1993 measurements. Surprisingly, the measured rut depths decreased significantly from July 1993 on, as shown in Figure 6.16. This could have been caused by lane marking change, rut depth measurement error, or by maintenance. No routine maintenance (e.g., patching) was applied to the test sections; and because no error on the rutting device was found, the decrease in rut depths may be attributed to the new striping applied to the rigid section. New lane markings, which had been moved 45.72 cm (18 in.) to the

right, were introduced to delay the formation of ruts and the correction of wrongly placed traffic markers.



1 inch=2.54 cm
1 foot=0.304 m

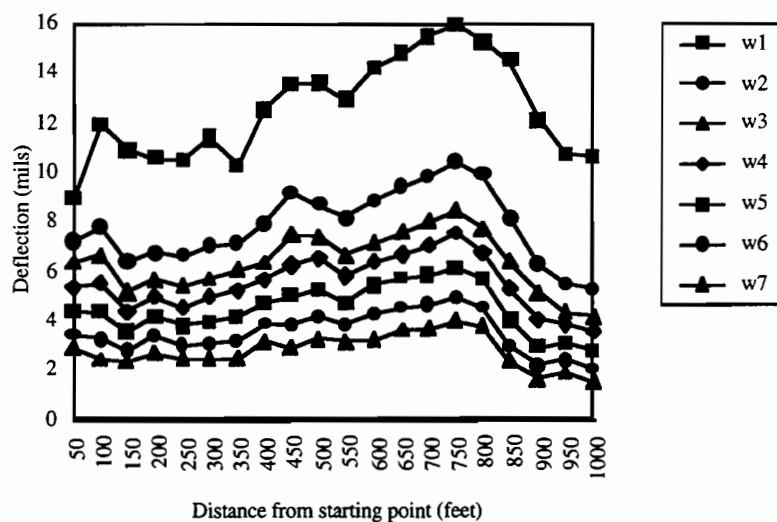
Figure 6.16 Rut depth variation along outside wheel path in right lane — R3



1 inch=2.54 cm
1 foot=0.304 m

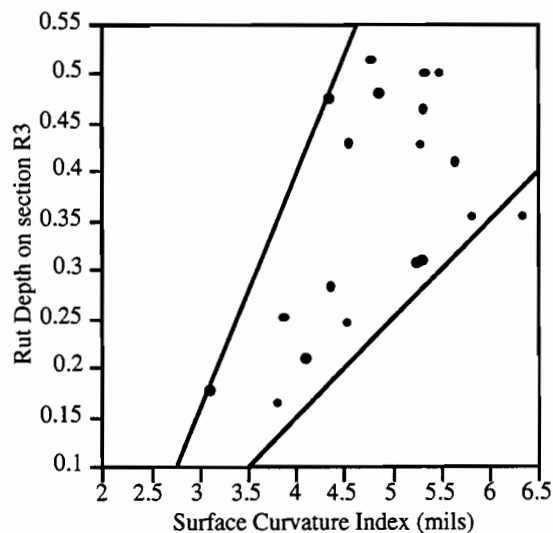
Figure 6.17 Rut depth variation along inside wheel path in right lane — R3

The first 106.68 m (350 feet) of section R3 exhibited smaller rut depths, while the rest of the section presented deeper rut depths. The plot of deflections along the section is presented in Figure 6.18. The deflection variation along R3 shows a similar trend, such that the latter part of the section had higher deflections. In addition, greater surface curvature index (SCI) values were observed at the same locations where the most severe rut development occurred. This finding suggests that SCI can be used in the development of a rutting prediction model for pavement sections similar to R3. Figure 6.20 shows the relationship between the rut depths and deflections measurements taken in March 1993; as shown, rutting increases as SCI increases.



1 mil=0.025 mm
1 foot=0.304 m

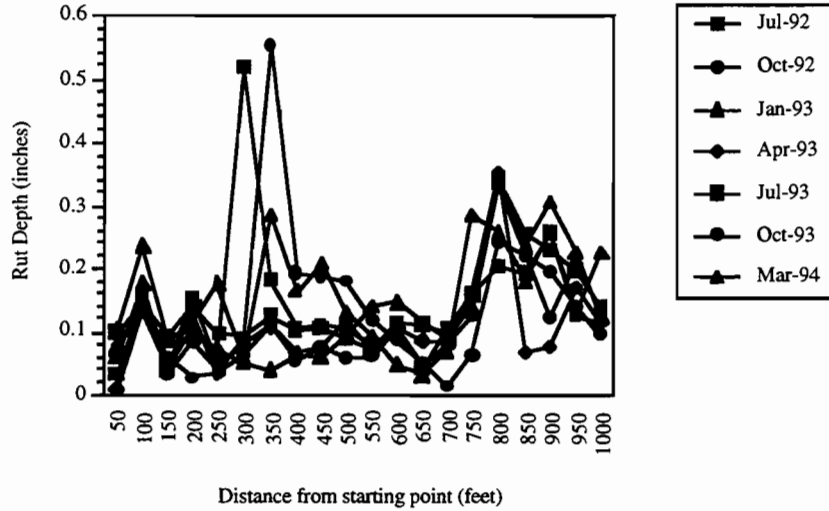
Figure 6.18 Deflection variation along the right lane of R3 in March 1993 — Second drop height



1 mil=0.025 mm

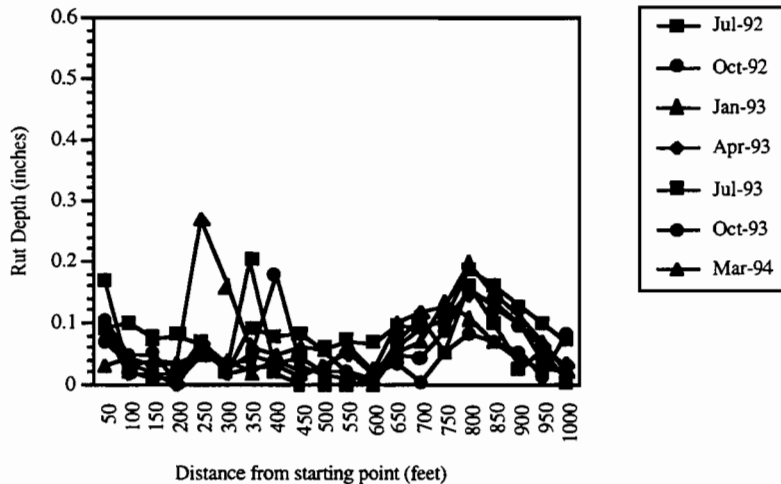
Figure 6.19 The relationship between the SCI and rut depth on the right lane in R3

Figures 6.20 and 6.21 summarize the rut depth development for section R2. It was difficult to find a unique rut depth growth pattern during the survey, as explained in the previous paragraph. Before the lane markings were changed, section R2B had relatively greater rut depths. However, the rut depth of R2A increased rapidly after the markings were changed. This section also showed that the outside wheel path developed greater rutting than the inside wheel path, indicating that there are different patterns of distress development between wheel paths as well as between traffic lanes.



1 inch=2.54 cm
1 foot=0.304 m

Figure 6.20 Rut depth variation along outside wheel path in right Lane — R2



1 inch=2.54 cm
1 foot=0.304 m

Figure 6.21 Rut depth variation along inside wheel path in right Lane — R2

In a procedure similar to that used for R3, the relationship between rut depths and SCI was plotted for section R3. The relationship between the rut depth and SCI does not present a good fit, as shown in Figure 6.23. The literature suggests that the surface curvature index is related to the condition of the material of the surface layer, while the seventh sensor reading is directly related to the subgrade layer stiffness (Ref 13). As may be observed in Figure 6.22, the deflections of the seventh sensor readings are generally over 0.075 mm (3 mil), which indicates a weakened subgrade. Thus, the rutting observed in test sections R2A and R2B is not strongly related to a surface material problem, but may be associated with the break and seat procedure applied prior to the overlay. In this case, a relationship between rut depths and the deflections of the seventh sensor of the FWD may be more appropriate for the development of a rutting model based on pavement deflection measurements. The relationship for rut depths versus the seventh sensor reading is presented in Figure 6.24.

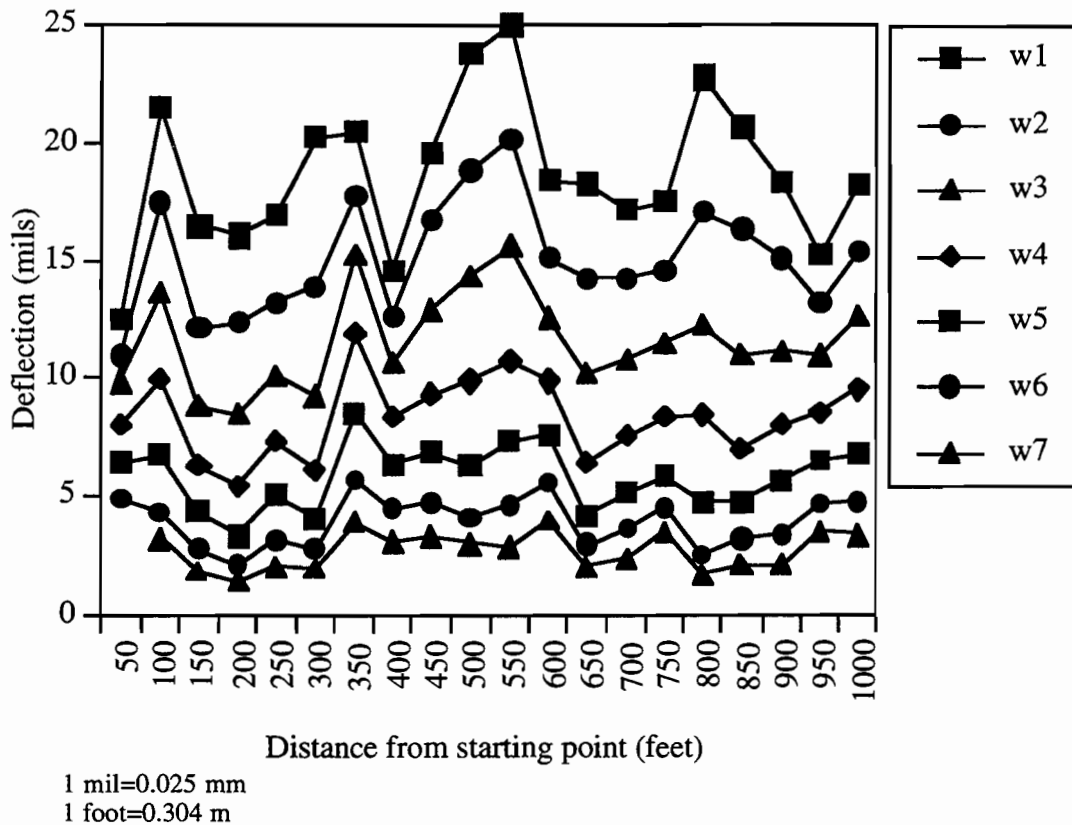
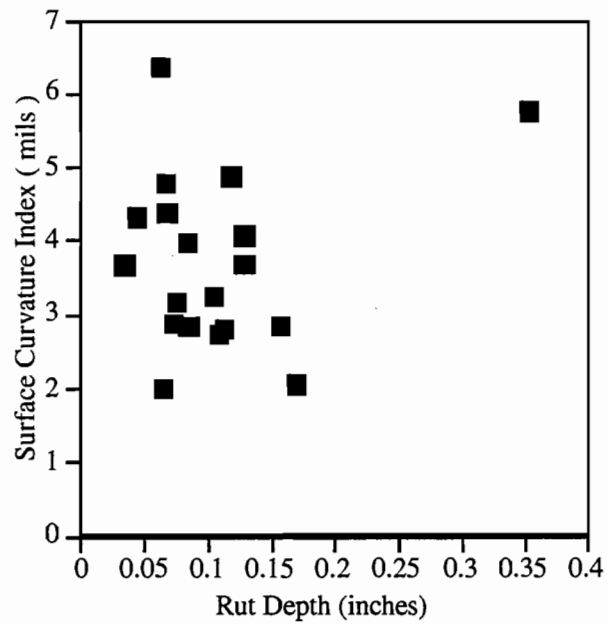
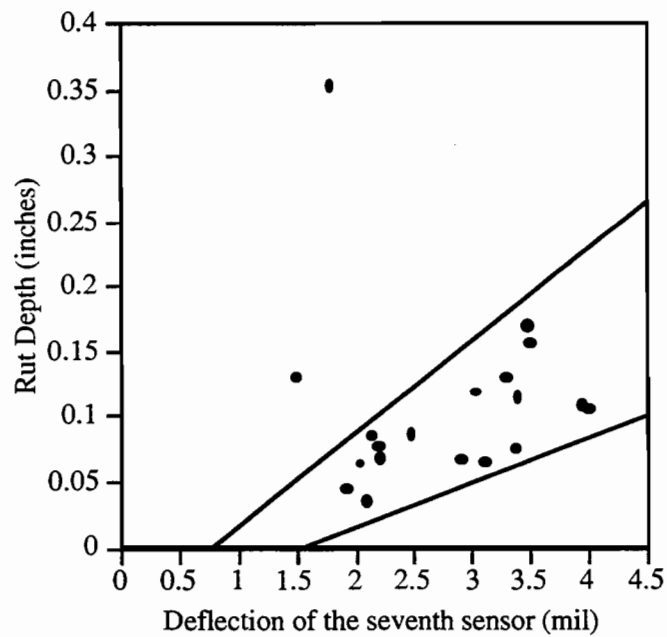


Figure 6.22 Deflection variation along the right lane of R3 in March 1993 — Second drop height



1 inch=2.54 cm
1 mil=0.025 mm

Figure 6.23 The relationship between the SCI and rut depth on the right lane in R2



1 inch=2.54 cm
1 mil=0.025 mm

Figure 6.24 The relationship between the W7 and rut depth on the right lane in R2

6.7.2. Flexible Section

Section F5, which had developed a severe rutting problem, was selected for studying the relationship of rut depths to pavement deflections. Figures 6.25 through 6.26 show the trends of rut depth development for each wheel path and lane on section F5. As seen in the charts, the left and right lanes have similar patterns of rut depth development; the differences in the magnitude of the rut depths may be explained by differences in the traffic volumes and loads between the two lanes. Unlike sections R2 and R5, the deflection-versus-rut-depth relationship was studied using the deflection data available for March 1994, since the deflection data available for March 1993 represented measurements taken every 30.48 m (100 feet). As shown in Figure 6.27, section F5 also presented a larger surface curvature index along the section, suggesting that the larger rut depths observed for section F5 may be caused by one of the upper layers, in this case probably the flexible base layer. The relationship between the SCI versus rut depth is shown in Figure 6.28; even though a strong relationship cannot be observed, it is still possible to observe a direct relationship between the SCI and rut depths. Based on the results summarized in this section, it is possible to associate the rutting observed in section F5 with the upper layers of the pavement, in this case particularly the flexible base.

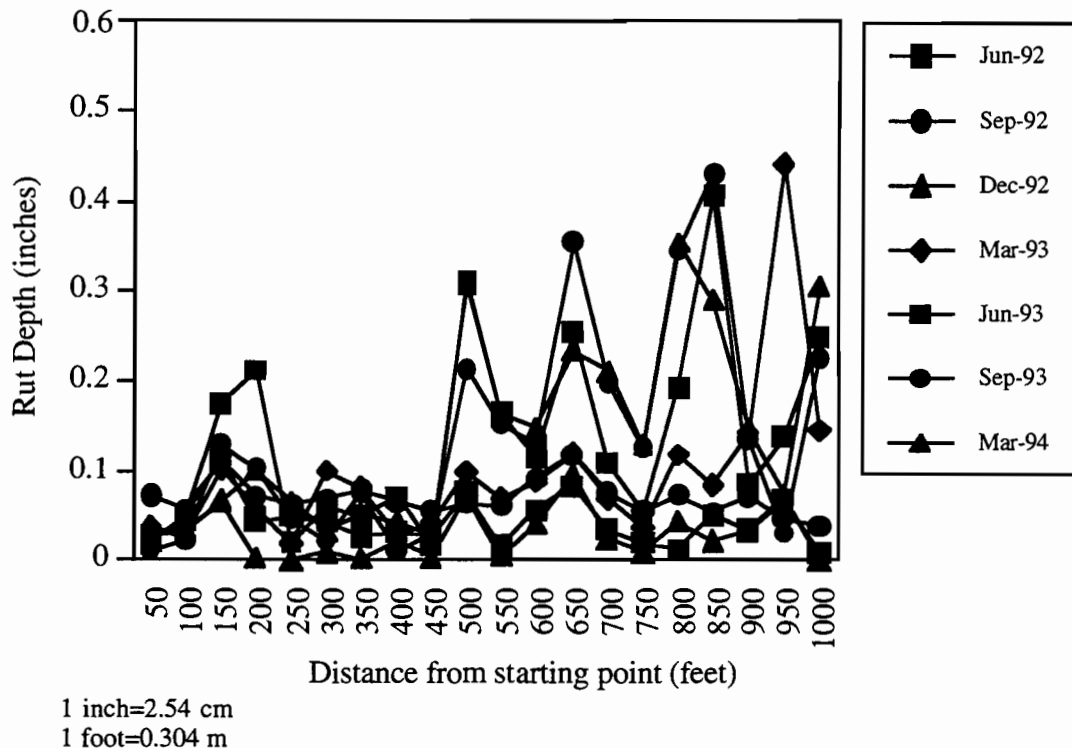
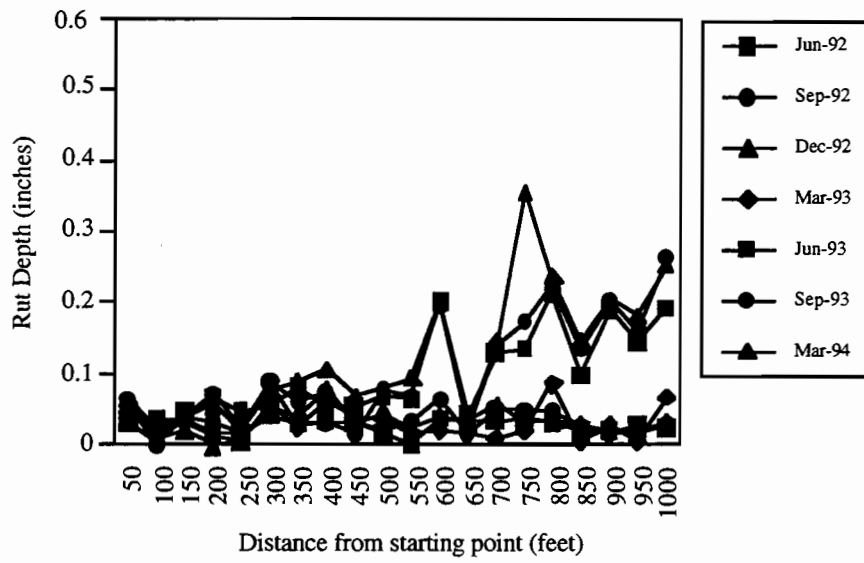
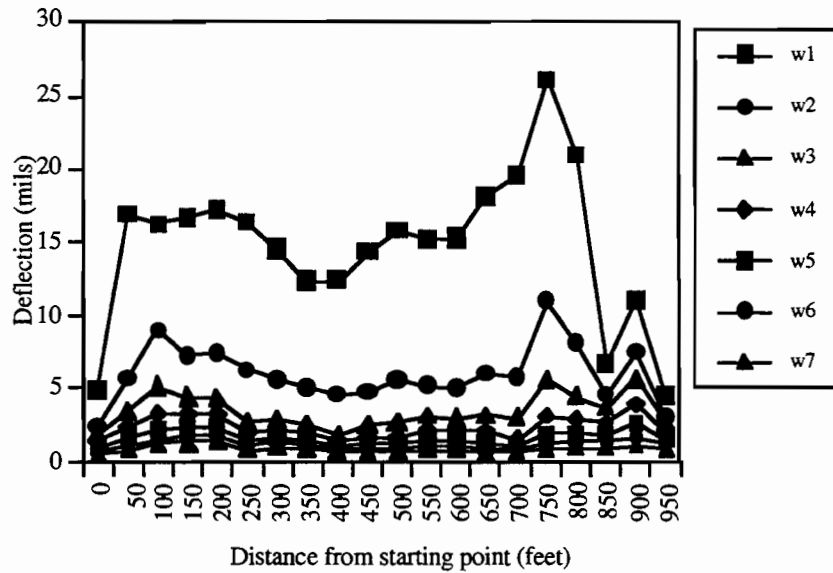


Figure 6.25 Rut depth variation along outside wheel path in right lane — F5



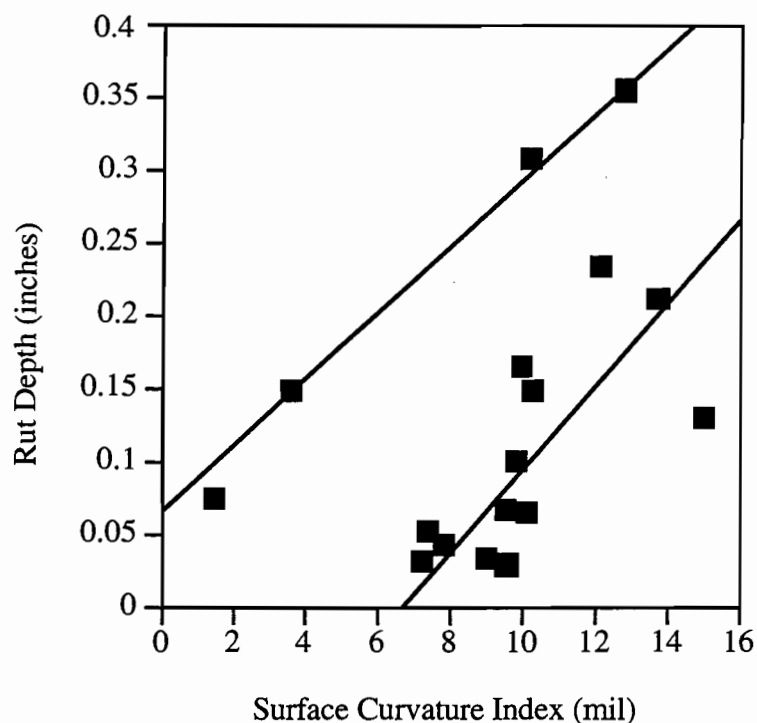
1 inch=2.54 cm
1 foot=0.304 m

Figure 6.26 Rut depth variation along outside wheel path in left lane — F5



1 foot=0.304 m
1 mil=0.025 mm

Figure 6.27 Deflection variation along the right lane of F5 in March 1994 — Second drop height



1 inch=2.54 cm
1 mil=0.025 mm

Figure 6.28 The relationship between the SCI and rut depth on the right lane in F5

6.7.3 Summary

Sections R2, R3, and F5 exhibited the most severe rutting problems. Sections R3 and F5 had structural problems in the upper layer, as suggested by their high SCI obtained from FWD deflection measurements. Section R2 exhibited a lower layer problem (broken concrete) that can be associated with the break and seat method applied during the construction of the overlay or with degradation of the subgrade support capacity due to pumping. This was supported by the FWD's seventh sensor deflections, which were above 0.075 mm (3 mil) for this test section. The seventh sensor readings are considered a good determination of subgrade condition.

Finally, the relationship between SCI versus rutting can be used in estimating the rut depths of the test section in the future for the test sections that experienced decreasing strengths at the upper layer (R3, F5), and for some of the other sections that had relatively large SCI (R4, R5, and R6).

CHAPTER 7. CONDITION SURVEY

7.1. INTRODUCTION

A walking condition survey was used to collect detailed distress information from the test sections. For the survey, two technicians walked along the test section, with one recording data while the other measured the length and area of the distresses. The data were collected in three stages — before milling, after milling, and after construction — so that performance comparisons could be made. After milling, information on only one section in the rigid set could be obtained, owing to the ongoing construction. The predominant distress observed in the rigid test sections was reflective cracking, while fatigue cracking caused by traffic loads was the main distress observed in the flexible test sections. This chapter describes these condition survey findings.

7.2. RIGID SECTIONS BEFORE CONSTRUCTION

7.2.1. Transversal Cracking

Prior to new overlay construction, the old asphalt overlay exhibited many reflective cracks. Almost all the transverse joints reflected through the old asphalt overlay, despite the overlay's total accumulated thickness of about 17.78 cm (7 in.). Figure 7.1 shows the total length of the transverse cracks in each test section. There was not a large variance between the two lanes: the crack lengths measured on the two lanes were almost identical. Even though all of the test sections had reflective transverse cracks on joints, sections R2 and R3 had the greatest incidence of transverse cracks among the test sections. Considering its length, test section R2B exhibited the worst condition among all test sections.

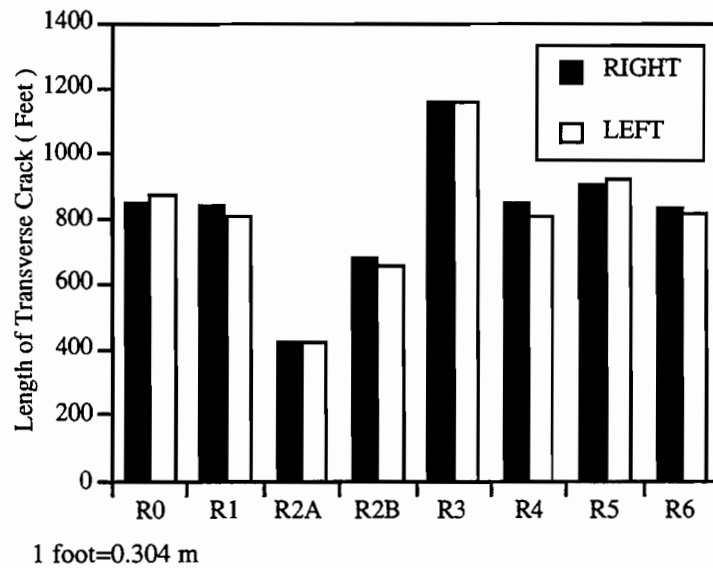


Figure 7.1 Transverse crack in the rigid sections — Before construction

Figure 7.2 summarizes the transverse crack spacing information. It can be observed that many of the test sections had an average crack spacing of about 4.57 m (15 feet). Two sections, R2B and R3, had half of the normal crack spacing, meaning these two sections had another transverse crack between two joint reflective cracks; why these cracks developed could not be determined from the condition survey, since these sections were exposed to the same traffic loading and temperature cycles as the other sections. However, based on the deflection data, some conclusions may be drawn. From the deflection data reported in Chapter 4, it may be observed that these two sections had a subgrade condition worse than the other sections.

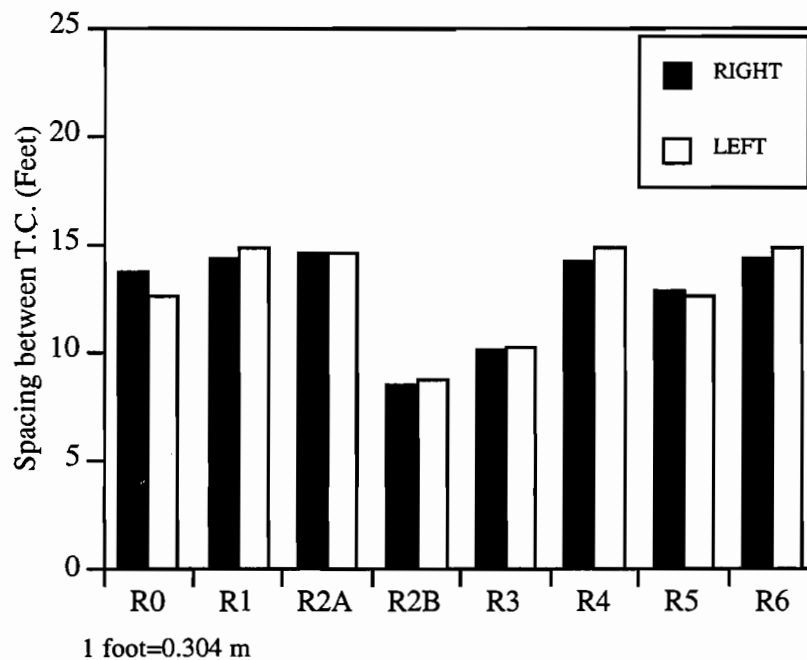


Figure 7.2 Transverse crack spacing in the rigid sections — Before construction

7.2.2. Longitudinal Cracking

Unlike the transversal cracking, longitudinal cracking was counted on a section basis only because longitudinal joint reflective cracking was dominant in the sections, where the difference between the two lanes could not easily be determined.

Figure 7.3 shows the total longitudinal crack length observed for each test section. Unlike the transversal cracks, the total longitudinal crack lengths among test sections did not present greater differences. The sections that had many transversal cracks did not show the same magnitude of longitudinal cracking. For example, R0, R3, R5, and R6 showed larger longitudinal cracking, while R2B and R3 had larger transversal cracking. If we assume that sections R2B and R3 had structural problems, and that longitudinal cracking is mainly associated with traffic-related problems, then these two sections should have exhibited larger amounts of longitudinal cracking

also. This discrepancy may indicate that longitudinal cracking is not as strongly related to traffic volumes as thought, at least for asphalt overlays on a rigid section.

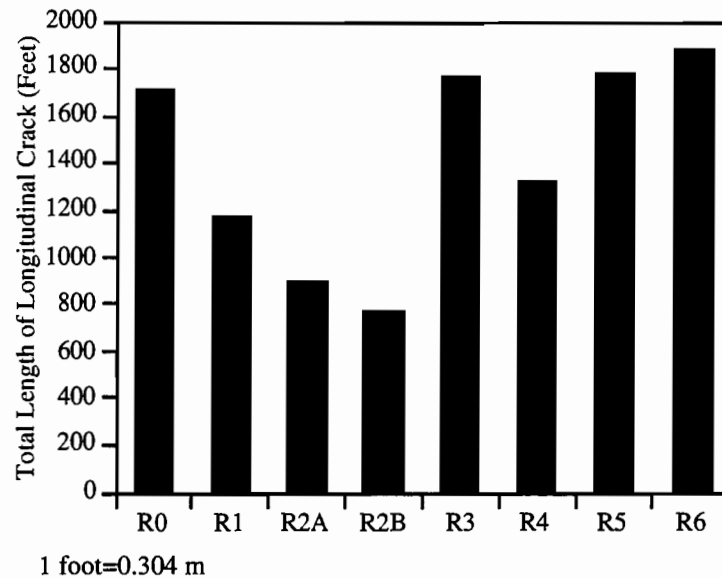


Figure 7.3 Total length of longitudinal crack in rigid section — Before construction

7.3. FLEXIBLE SECTIONS BEFORE CONSTRUCTION

The condition survey map used for the rigid sections was also adapted to record crack patterns for the flexible test sections. The flexible test sections showed dissimilar crack patterns and trends when compared with the rigid test sections.

7.3.1. Transversal Cracking

Figure 7.4 shows the total length of transversal cracking for both lanes. The results are significantly different for each lane, revealing that the right lane experienced more intense transverse cracking than the left lane, unlike what was observed for the rigid sections. It was also observed that some sections, including F1, F2, and F3, had relatively more transversal cracking than the other test sections. If the transversal cracking was caused mainly by thermal stresses, as was probably the case for the rigid sections, the amount of cracking would be rather uniform across the test sections. However, the difference in transversal cracking between sections F3 and F5 was about 152.4 m (500 feet) for the right lane; no large differences were observed for the left lane. This finding suggests that the mechanism for transverse crack development for the flexible sections may be traffic loadings.

The crack spacing data plot shown in Figure 6.5 shows that the transverse crack spacing for the right lane fluctuates from 3.96 to 7.62 m (13 to 25 feet). As discussed in the previous report for this project (Ref 5), the layer under the asphalt surface exhibited stripping problems that reduced the overall bearing capacity of the pavement. Considering the traffic volume differences between the two lanes (reported in Chapter 3) and the crack pattern reported in the condition survey

map, the observed cracks could be strongly related to traffic loadings, rather than to reflective cracking action.

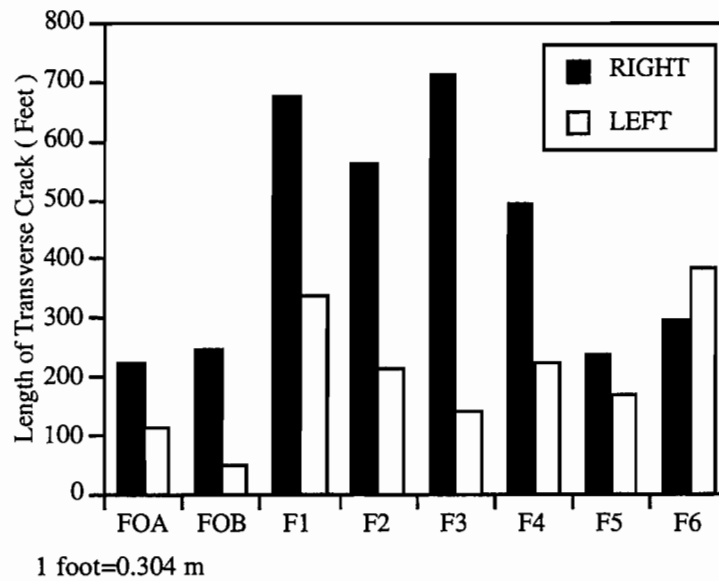


Figure 7.4 Transverse cracking in the flexible sections — Before construction

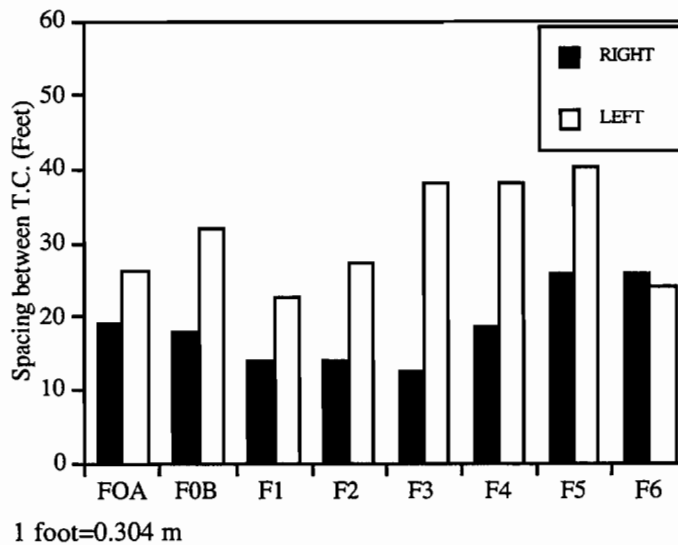


Figure 7.5 Transverse cracking spacing in the flexible sections — Before construction

7.3.2. Longitudinal Cracking

For the flexible sections, most of the longitudinal cracking occurred along the central line between the two lanes. This situation called for a different methodology for summarizing the longitudinal crack information — that is, one different from that used for the rigid sections, where

the longitudinal cracking was counted by section. The longitudinal cracking for the flexible sections is shown in Figure 7.6, where it is summarized in three different categories defined according to the position of the longitudinal cracks in the test section's transversal cross section — center, left, and right.

Figure 7.6 also shows that most of the cracking appeared on the right lane or in the center of the section, with little or no cracking exhibited on the left lane. Sections F1, F2, and F3 presented significant longitudinal cracking, while the other test sections presented less longitudinal cracking. These results indicate that the longitudinal cracking development on the flexible test sections was not related to reflective cracking, but, rather, to traffic loadings. The large differences between test sections can also be explained by other factors, such as subgrade strength, water level, and swelling clay occurrence.

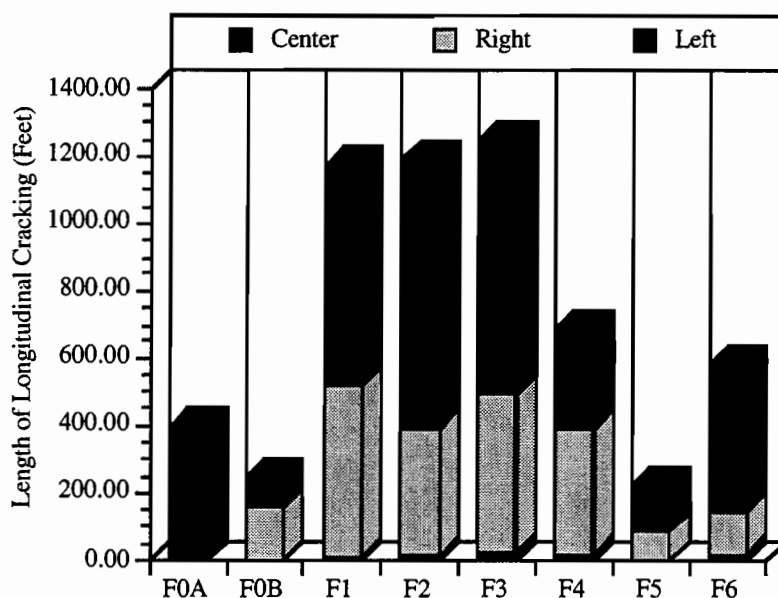


Figure 7.6 Longitudinal crack in the flexible sections — Before construction

In summary, the main cause of cracking in the rigid test sections before construction of the overlays was reflective cracking; cracking in the flexible sections was presumably the result of structural problems caused by moisture and traffic loading. Based on the results of the surveys, the sections that had the most severe cracking were R2 and R3 for the rigid sections, and F1, F2, and F3 for the flexible sections.

7.4. SURVEY AFTER MILLING OF THE EXISTING OVERLAY

The exposure of the original JCP of test section R1 (after milling) provided a good opportunity to compare the reflective cracking data available for the before-construction condition, where the existing overlay was still in place, with cracking observed on the exposed JCP section. Section R2 was excluded, since it had the crack and seat method applied after milling.

7.4.1. Transversal Cracking

Table 7.1 summarizes the length of transverse joints and transverse cracking (TJC) observed during the survey of the JCP milled section. Both lanes were almost identical in length; crack spacing was also uniform for both lanes. A comparison of these results with the results reported for the before-construction condition indicates that the transversal cracking on the existing asphalt overlay of R1 was caused by reflective cracking — a conclusion based on the fact that total crack lengths for the two situations were almost equal, about 243 m (800 feet) per lane.

Table 7.1 Summary table of test section R1 — After milling

	TJC (Right)	TJC Spacing	TJC (Left)	TJC Spacing
Total Length (FT)	840		836	
Average Length (FT)	11.51	13.75	11.94	14.35
Total Number	73		70	

1 foot=0.304 m

Another possible conclusion derived from the comparison of the results for the milled and non-milled situations is the qualitative effectiveness of an asphalt overlay in protecting the existing JCP from further damage. The existing JCP was in relatively good condition, even though it was built in 1943. Unfortunately, because condition survey data were not available for this pavement section before the first asphalt overlay was applied in 1953, it is not possible to determine precisely how much the previous overlay protected the existing JCP from further deterioration. However, the old overlay certainly prevented rapid deterioration of the concrete pavement, as evidenced by the lack of severe punch outs and spalling observed once the old overlay was removed; moreover, the average crack spacing for the left lane was almost the same as the joint spacing, 4.57 m (15 feet).

7.4.2. Longitudinal Cracking

Longitudinal cracking was observed on both lanes. The total length was approximately 146.3 m (480 feet) for the left lane, 106.68 m (350 feet) for the right lane, and about 91.44 m (300 feet) for the center. The fact that these results match the condition survey results for longitudinal cracking for the existing asphalt overlay reinforces the conclusion that initial cracking in the composite section was primarily caused by reflective cracking, not by traffic-related fatigue cracking.

7.5. RIGID SECTION AFTER-CONSTRUCTION CONDITION SURVEYS

After construction, five condition surveys were undertaken. Because the purpose of the condition surveys was to summarize the location and density of reflective cracks that are visible within the test section (no matter what orientation they had), we mapped these cracks on survey forms (Appendix B). After the field surveys, the data were stored in a personal computer for later

analysis. Recorded data included transverse and longitudinal cracks, patching, alligator cracks, and pot holes; segregation and water leaking problems were also reported.

7.5.1. Transversal Cracking

Monitoring reflective cracking development was one of the objectives of these condition surveys. While there are many methods for evaluating the development of reflective cracking on a composite pavement, one simple and popular method is to calculate the ratio between the length of reflective cracking observed and the length of previously existing joints and cracks for the non-overlaid pavement.

Unfortunately, no pre-overlay condition survey data were available for almost all the test sections. The exact condition of the existing rigid pavement was known only for test section R1, which, when milled, had a condition survey performed before the new overlay was placed. To allow for the study of the reflective cracking development for the remaining test sections, we assumed that the cracks on the old asphalt overlay consisted in their entirety of reflective cracks, and that they matched completely the cracking and joint spacing of the existing JCP. Based on these assumptions, the reflective crack ratio defined previously can be calculated.

The transverse crack development for each test section versus time is shown in Figures 7.8 and 7.9. If we assume that all transverse cracks are reflective cracks, then it may be concluded that efforts to prevent reflective cracking on sections R3, R4, and R5 will most likely be successful. Conversely, sections R2A, R0, and R1 exhibited more cracks than the other sections.

Figures 7.7 and 7.8 summarize other important information regarding transverse cracking development. A significant difference in reflective cracking development may be observed between the two lanes, with the right lane experiencing faster development of transverse cracking than the left lane, even though they experienced the same environmental conditions, same maintenance, and were provided the same overlay thickness and material. The only significant factor that differs for the two lanes is traffic loading, as discussed in Chapter 3. However, at the end, the amount of transverse cracking in the left lane will converge to a single value with the right lane (and will show a faster growth rate).

In addition, the slope of each curve in Figures 7.7 and 7.8 is different between measurements, though overall there is a steady increase. The trends for sections R1 and R0 in Figure 7.8 are a good example of this: These increase slowly until the second measurement, taken in May 1993; thereafter, they almost stop increasing until the third measurement, taken in October 1993. However, as may be observed during the winter season, cracking developed rapidly, as seen in the fourth and fifth measurements.

A similar trend is also observed for the other test sections shown in Figures 7.9 and 7.10, which summarize the total number and length of transverse cracks for all rigid sections by season. The increasing rate of crack development for the winter far exceeds the rate for the other seasons, regardless of lane. For example, for the left lane, during the first year (except for the winter season), transverse cracking increased only slightly. During the first winter, a nearly 50 percent increase in crack growth occurred for both lanes; during the second winter, a 100 percent increase in crack growth occurred for both lanes, suggesting that the crack growth rate for the winter season

is not linear but, rather, has an exponential trend. This may also indicate that thermal cracking is fatigue-oriented, since the second winter cycle experienced more accumulated thermal cycles than the first winter.

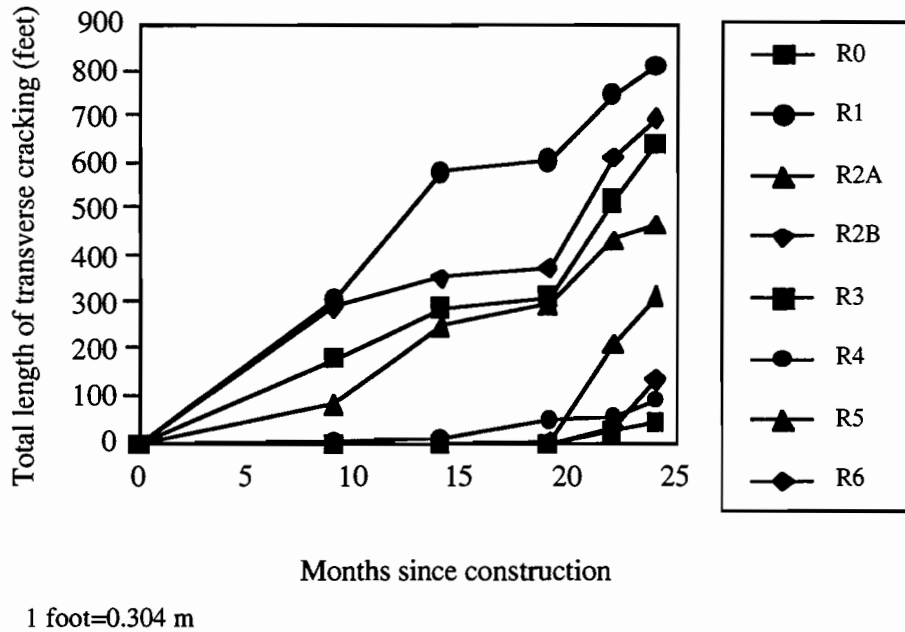


Figure 7.7 Total length of transverse cracking for the right lane for the rigid section

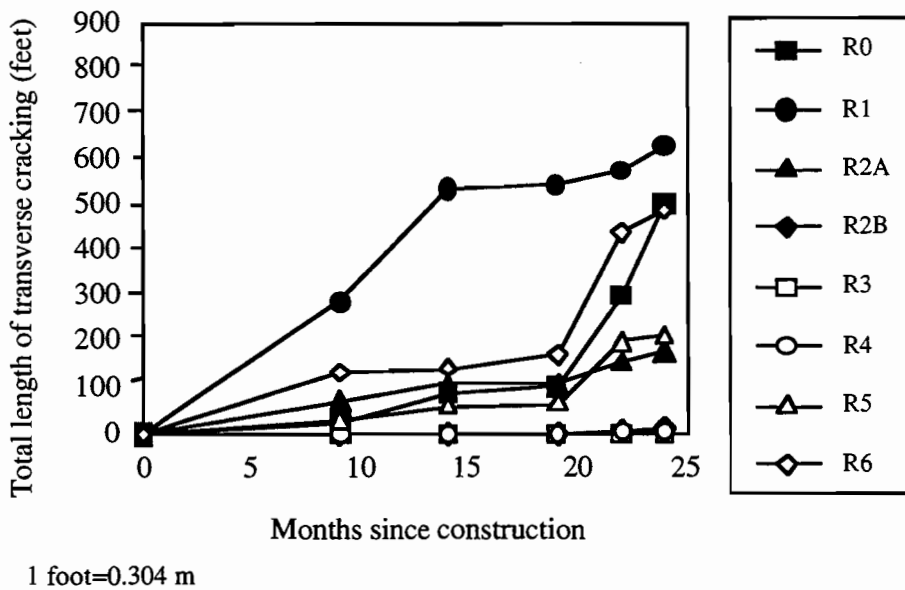


Figure 7.8 Total length of transverse cracking for the left lane for the rigid section

In summary, transverse cracking developed mainly during the winter and is primarily related to climatic loading (especially low-temperature fatigue cracking).

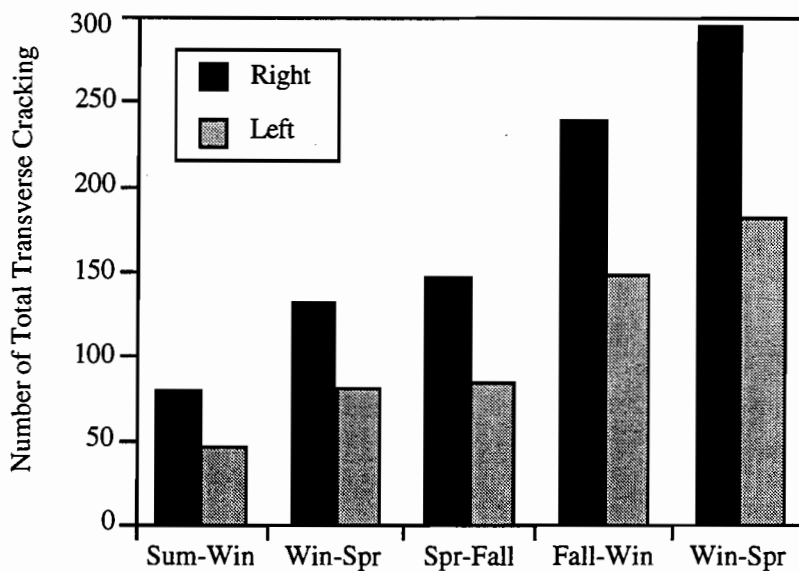


Figure 7.9 Total number of transverse cracks by season for the rigid test sections

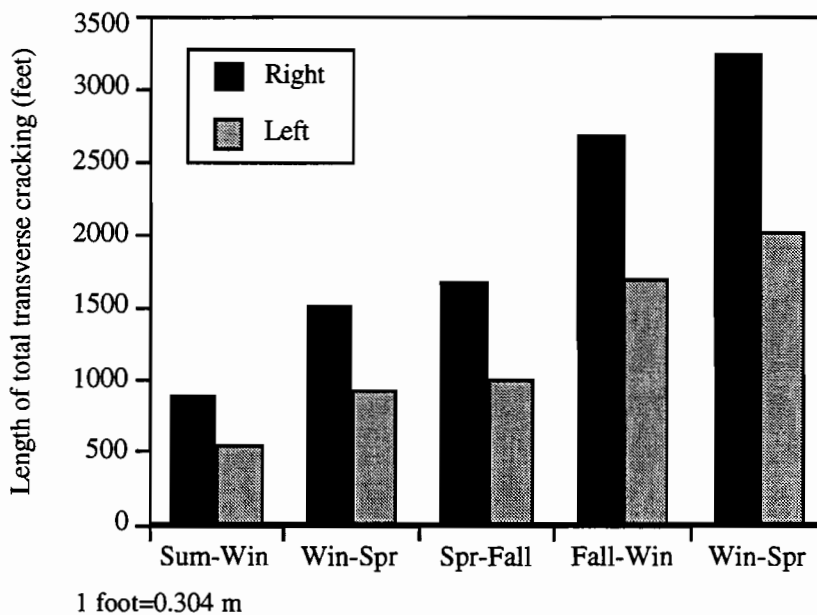


Figure 7.10 Total length of transverse cracks by season for the rigid test sections

Figures 7.11 and 7.12 summarize the average crack spacing for each section versus time. Crack spacing for both lanes, as expected, decreases as time goes on and converges to the original contraction joint spacing of 4.57 m (15 feet) of the existing JCP. According to the literature on the relationship of temperature loading and cracks (Ref 46), transversal crack development involves the following sequence: First, a crack develops at the center of the pavement (a result of temperature loading) when the tensile stresses caused by the thermal loading are greater than the tensile strength of the pavement. The subsequent cracks appear midway between the first crack and the edge, or between two adjacent cracks. The cracks then propagate, following the previously described cycle until equilibrium is attained.

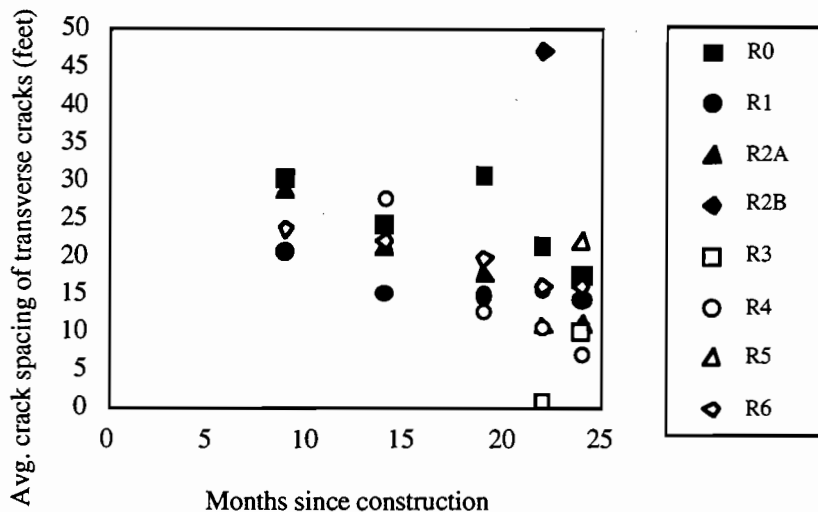
For test sections R1 and R6, once the crack spacing converges to 4.57 m (15 feet), the original joint spacing for the existing JCP, the transversal crack development rate decreases significantly. It is reasonable to assume that reflective cracking will not progress once the reflective transverse crack spacing reaches 4.57 m (15 feet). Of course, there are exceptions, such as test sections R3, R4, and R2A. The few transverse cracks observed on test sections R3 and R4 do not appear to be reflective cracking (i.e., they develop irregularly and do not run the length of the section).

Test section R2A merits special discussion regarding its transversal crack development. Like the other test sections, R2A presented reflective cracking from the beginning. However, unlike the other test sections, the spacing decreased continuously without converging to the 4.57 m (15 feet) joint spacing. At the last condition survey, crack spacing was down to 3.05 m (10 feet) for the right lane of section R2A. As shown in Figures 7.7 and 7.8, crack lengths continuously increased through the addition of fatigue cracks caused by traffic loadings. This trend may be attributed to the structural weakening caused by the crack and seat method used in this section. This is, in fact, corroborated by comparing the results of the right lane with those of the left lane, which experienced less traffic loading applications, as discussed in Chapter 3. The results obtained for the left lane show that the crack spacing for R2A was still above 4.57 m (15 feet) at the last survey. Based on these observations, it can be stated that the transverse cracking for test section R2A occurred mainly by reflective action in the first stages, which was accelerated by traffic-related fatigue in the later stages. As extensively discussed in the literature, the main driving factor for reflective transverse crack development is assumed to be temperature differentials, with traffic loadings acting as a minor factor (Ref 47). The condition survey results reported previously show good agreement with these assumptions.

7.5.2. Longitudinal Cracking

Figure 7.13 summarizes the development of longitudinal cracks in the rigid sections. The longitudinal cracking, which developed randomly on the test sections, could not be assigned to any particular lane. However, a specific pattern in the longitudinal crack development was observed. The longitudinal crack increases after a certain period of dormancy, even though the cracks increase step by step. This behavior is particularly evident in sections R1 and R2, where section R1 experienced an increase in longitudinal crack development immediately after 20 months of

service, while section R0 presented the same pattern after 22 months. The points at which longitudinal cracks developed were in the winter and after the transverse cracks had already propagated through the asphalt overlay from the existing crack.



1 foot=0.304 m

Figure 7.11 Average spacing of transverse cracking in right lane



1 foot=0.304 m

Figure 7.12 Average spacing of transverse cracking in left lane

The detailed condition survey map also shows that the cracks usually connected two transversal cracks. A possible explanation for this type of crack development is that the transverse crack spacing becomes shorter than the longitudinal slab length, a development that changes the main axis of thermal movement to the longitudinal direction, leading to a composite loading situation when traffic loading is combined. Traffic loading will induce a bending force that,

combined with the thermal loading, will lead to a tensile stress that is above the overlay strength, causing a longitudinal crack to appear between two transverse cracks. This cycle will be repeated continuously, leading to a block-crack pattern and then, finally, to alligator cracking and failure.

Figure 7.14, a summary of the seasonal effects on longitudinal cracking, presents the total length of longitudinal cracking in the test section per season. The chart shows that reflective cracking is strongly related to low temperature loading, since little or no increase of longitudinal cracking occurs during the summer. This again supports the failure mechanism discussed previously, where a longitudinal crack may develop between two transverse cracks as a result of low temperature, and only after a certain amount of transverse cracking has developed on the pavement section.

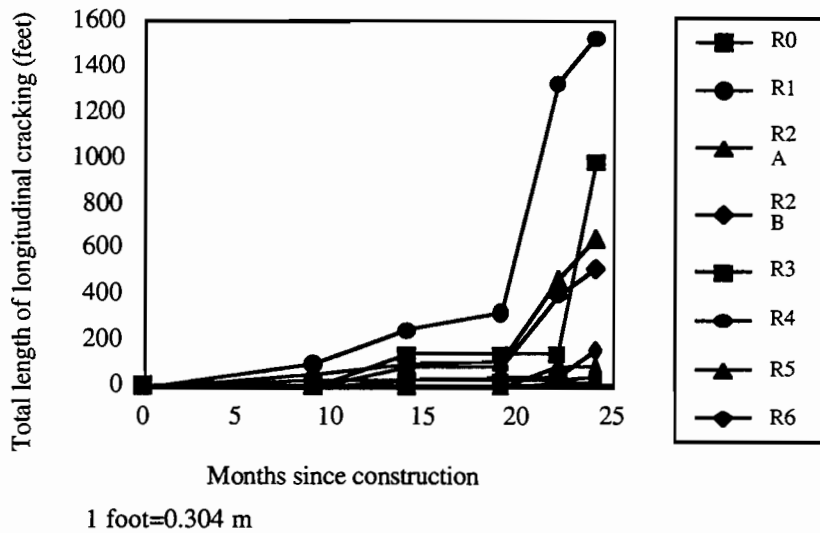


Figure 7.13 Total length of longitudinal cracking for the rigid sections

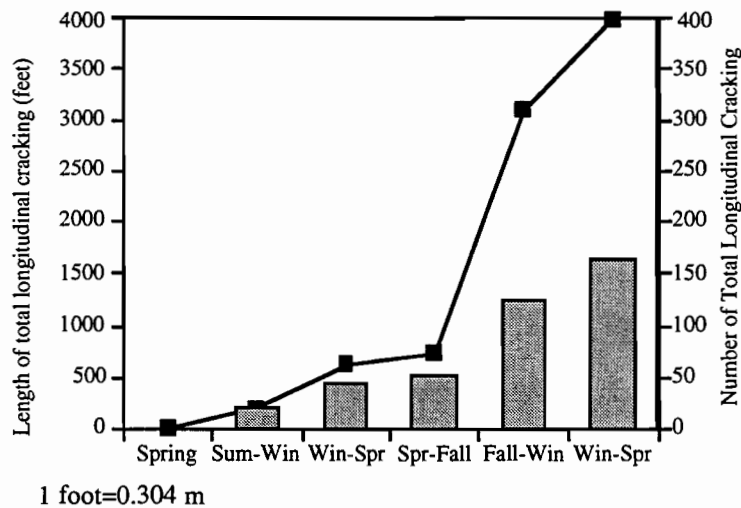


Figure 7.14 The trend of total length of longitudinal cracking in rigid section

7.5.3. Other Distresses

Besides longitudinal cracking and transverse cracking, other distresses, including patching, alligator cracking, segregation, and water leaking through the reflective cracks, were recorded during the condition surveys. Patching and alligator cracking were counted since they are strongly related to pavement performance (these were not, however, summarized by lane because almost all of these distresses appeared on the right lane). The total area of patching is summarized in Figure 7.15. Even though patching area is not a distress in itself, it is an indicator of serious pavement failure. Small amounts of patched area were observed in all the test sections, except for sections R1 and R2A. Section R2A showed the most rapid increase of patched area among the test sections, while test section R2B presented the smallest area. Even considering any mechanistic verifications, the difference of only 3.81 cm (1.5 in.) in thickness significantly differentiates the performance of the two test sections.

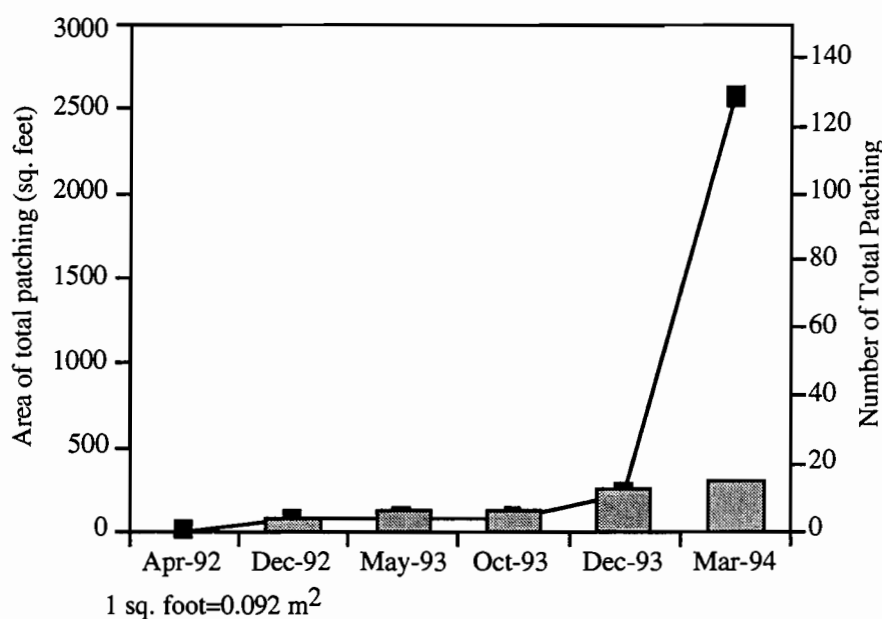


Figure 7.15 Total area of patching versus time in the rigid

Figure 7.15 summarizes the sections' alligator cracking, a distress that increases over time and traffic loadings. Among the test sections, R3, which has a flexible base and little reflective cracking, showed a dramatic increase in alligator cracking on the last survey, even though the level of severity was low. However, the amount and severity of the alligator cracking will inevitably expand, ultimately leading to failure of the test section. We attributed the apparent reduction in alligator cracking area for test section R2A in Figure 7.16 to patching.

If we divide the test sections into two groups — non-milled and milled or partial milled — the amount of alligator cracking development on the milled sections is much more significant than

that of the non-milled sections. The milled sections, R2A, R2B, and R3, are sections that ranked higher in terms of alligator cracking development, as compared with the non-milled sections, such as R0, R6 and R5, as may be observed in Figure 7.16. Section R1, an exception, was repaired after milling and, thus, does not show too much structural-related cracking. The trend of patching development also shows that the milled sections had a larger amount of patching area than the non-milled sections, as shown in Figure 7.15. This finding shows that the crack and seat and flexible base methods, which were used to prevent reflective cracks, may cause other severe problems (e.g., alligator cracking).

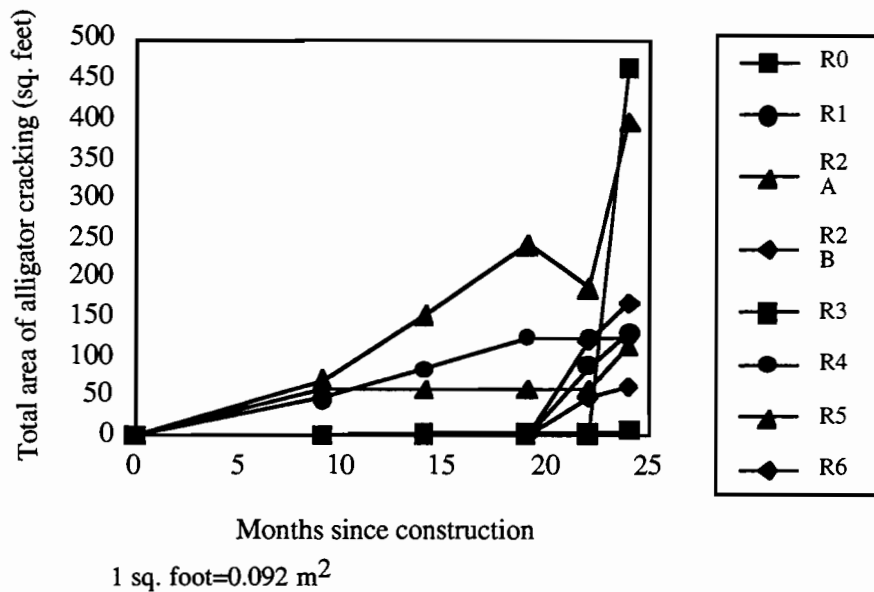


Figure 7.16 Total area of alligator cracking

Figure 7.17 shows the total length of alligator cracking development for all the rigid sections. Unlike the transverse cracking or longitudinal cracking seen in Figures 7.10 and 7.14, alligator cracking increases continuously, with little seasonal effect. The alligator cracking growth rate observed during the last 3 months (Dec. 1993–Mar. 1994) was higher than that for any other period. Section R3 was the main contributor to alligator cracking development in the last 3 months, a point at which it almost ended its structural life. This finding reinforces the view that alligator cracking, rather than being strongly related to thermal loadings, is a function of traffic load applications.

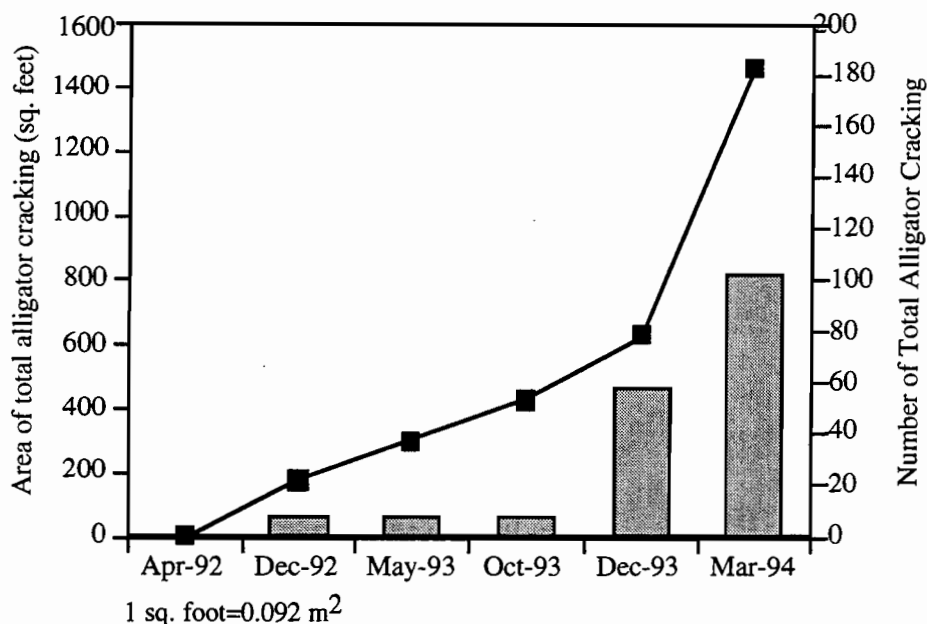


Figure 7.17 The trend of alligator cracking in test section

7.6. SUMMARY OF CONDITION SURVEY RESULTS FOR THE RIGID SECTIONS

From the condition survey results obtained from the rigid sections, the following conclusions can be drawn for each test section. Section R1, which had a 10.16 cm (4 in.) asphalt overlay and saw cuts every 4.57 m (15 feet), developed a relatively large reflective cracking problem, even though the existing JCP had its cracks repaired by various methods, including substituting severely cracked slabs with prestressed slabs, polymer concrete, and other methods. The subsection in which sawcuts were applied performed relatively well when the sawcut line met precisely with the existing transverse joints. If the sawcut joint did not agree with the existing transverse joint, premature failure at the sawcut usually developed. However, even when there was exact agreement between the sawcuts and the existing joints, failure at the sawcut could not be avoided under heavy traffic loadings. For example, in the last condition survey (March 1994), almost all the sawcuts on the right lane experienced joint deterioration, while few of the left lane sawcuts experienced joint problems. Since the joint cracking problem is mainly related to traffic loadings, a conclusion may be drawn that, while sawcuts may prevent reflective cracking, they may cause other problems, such as joint failure under heavy traffic volumes.

The fact that R2A and R2B are 152.4 m (500 feet) in length led to some interesting findings. First, the crack length between the two sections differs significantly, as shown in Figures 7.7 and 7.8. Section R2A has almost 243.84 m (800 feet) of transverse crack length in the right lane, and over 182.88 m (600 feet) in the left lane; section R2B shows less than half of the length of the right lane — the left lane of R2B presented less than 45.72 m (150 feet) of transverse cracking length. Considering that the only difference between these two sections is the thickness of the asphalt overlay — section R2A has a 10.16-cm (4-in.) thick overlay, while section R2B has

a 13.97-cm (5.5-in.) thick overlay — the thickness of the overlay proves to be a very significant factor in transverse cracking development. Second, the transverse cracks consist of both reflective cracks and fatigue cracks that are related mainly to traffic loadings. This can be explained by the fact that the average crack spacing on the right lane of section R2A goes below 4.57 m (15 feet), which was the original contraction joint spacing for the existing JCP. In addition, section R2A had many other failures that are related to structural deficiency of pavements (e.g., patching).

Section R3 experienced few reflective cracking problems up to this point. However, as observed in Figure 7.16, alligator cracking developed throughout the section; though not severe now, the problem will certainly grow over time.

Sections R4 and R5 are in relatively better condition than the other test sections. The Arkansas mix appears to be performing better than any other method used for protecting the overlay from reflective cracking. For either the right or left lanes, little reflective cracking developed on the pavement up to this point. Some transverse cracking developed within the 76.2 to 106.68 m (250 to 350 feet) line in the right lane. This distress may be more related to alligator cracking or to traffic load cracking than to reflective cracking. Sections R4 and R5 also experienced bleeding near these cracked areas along the wheel path (a problem that may be related to mix design, e.g., AC content or low void in mineral aggregates). Except for this 30.48 m (100 feet) length, the remainder of the test sections were in nearly perfect condition, especially if we compare their performance to the other test sections.

Section R5, which includes a stress relief layer between the existing pavement and the new overlay, also developed reflective cracking during the second winter after construction of the overlay. Even though the percentage of reflective cracking was relatively low compared with the other sections, the section may yet approach a condition similar to that of the other sections.

The overlay using 7.62 cm (3 in.) type C asphalt does not appear to be effective. In section R6, hair transverse cracking developed after the second winter. The section also developed a depressed area with alligator cracking at 243.84 m (800 feet) in the right lane after a few months. The Type C asphalt used in the overlay may postpone the development of reflective cracking, but its effectiveness is questionable, considering its thickness.

The type D overlay in the control section developed almost 100 percent of the reflective cracks on the surface over 2 years. It also developed hair cracks longitudinally throughout the shoulder. Even though no severe failures were observed in this test section, the severity of the next stage of distresses will be greater than that for any other test section, since reflective cracks act as an accelerator in decreasing the serviceability of the pavement.

In summary, for all the test sections, transverse cracks occurred mainly by reflective action, while traffic loadings had a minor effect. These transverse cracks developed mostly during the winter, with traffic loading affecting the rate of development of transverse cracking. The longitudinal cracks developed randomly (and not for a particular lane) and connected with transverse cracks. Alligator cracking increased continuously for the sections; by contrast, transverse cracks and longitudinal cracks had alternating periods of fast and slow development, reinforcing the conclusion that alligator cracking is mainly a function of traffic loadings.

7.7. CONDITION SURVEYS AFTER CONSTRUCTION FOR THE FLEXIBLE SECTIONS

Unlike the rigid sections, the flexible sections did not develop significant reflective cracking up to the last condition survey, though traffic-related cracking (alligator cracking or patching) was prevalent. Also affecting performance of the flexible test section was the wood debris falling from logging trucks. These particles created small, expanding holes in the pavement that led to raveling.

Figures 7.18 and 7.19 show the transverse-crack-versus-time relationship. Such cracking, not observed until the second winter, was not significant when compared with the cracking on the rigid sections. Sections F1 and F0B developed relatively large transverse cracking, though these were not the sections that had larger transverse cracking before the new overlay was placed (i.e., F1, F2, and F3). This finding supports the hypothesis that the cracking on the flexible sections did not develop from reflective action. Crack spacing was sometimes impossible to count because it usually appeared randomly, which again supports the hypothesis discussed above.

Other interesting results are related to lane differences. No notable differences could be found based on the charts included in Figures 7.18 and 7.19. As discussed in the condition survey of the old asphalt overlay before the new construction, the amount of transverse cracking between two lanes differed significantly. However, up to the last survey results, the total cracking between two lanes did not present any differences. This may indicate that the test sections are far from the end of their design lives.

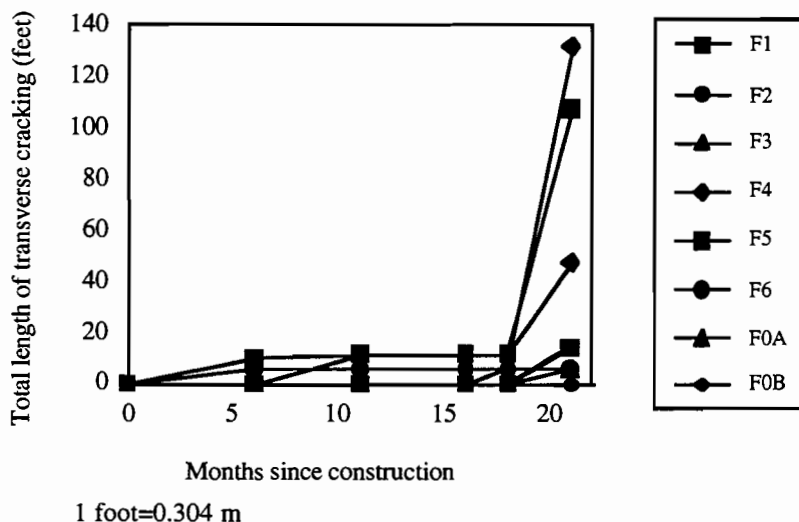


Figure 7.18 Total length of transverse cracking in right lane



Figure 7.19 Total length of transverse cracking in left lane

Longitudinal cracking was not common in the flexible sections, as shown Figure 7.20. A longitudinal crack of 5.18 m (17 feet) detected in test section F0B was studied by coring. According to the information obtained from the cores, the 5.18-m (17-foot) crack developed from an existing pavement surface crack, which should have been repaired during construction. This crack, which was entirely on the surface of the asphalt (i.e., not related to a structural problem), demonstrates how important it is to prepare and repair the existing pavement surface before a new overlay is applied. After the second year, longitudinal cracking developed at a faster rate on sections F0B and F4 (almost entirely on the right lane), while the other sections did not develop any longitudinal cracks.

Before the new overlay was placed, the worst sections, based on longitudinal cracking, were F1, F2, and F3, while after the overlay was placed, the poorest performing sections, again in terms of longitudinal cracking, were F0B and F4. This longitudinal cracking development was probably mostly due to traffic loadings and to interaction with transverse cracking. This follows the standard pattern leading to failure, where if sufficiently extensive transverse cracking develops, then the transverse direction will exceed the longitudinal direction, which will lead to another longitudinal crack caused by the bending action from traffic loadings combined with axial forces induced by thermal loading.

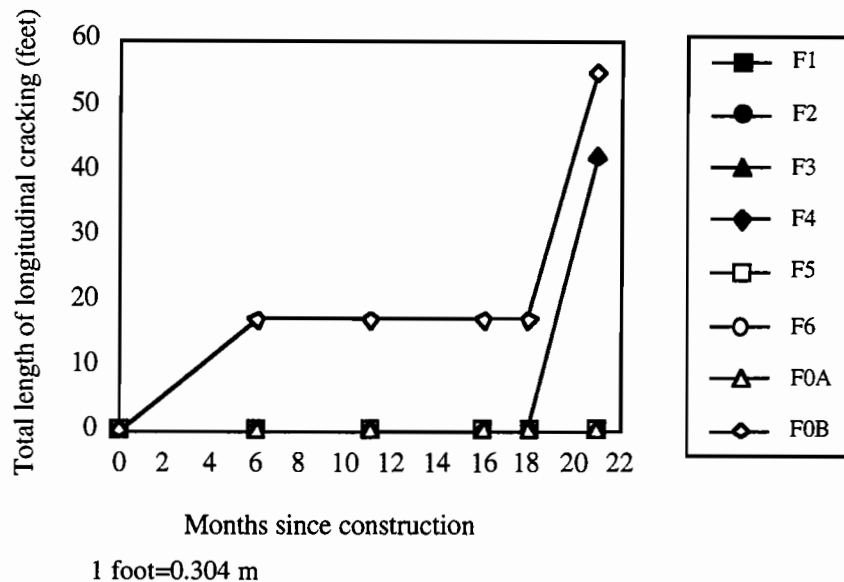
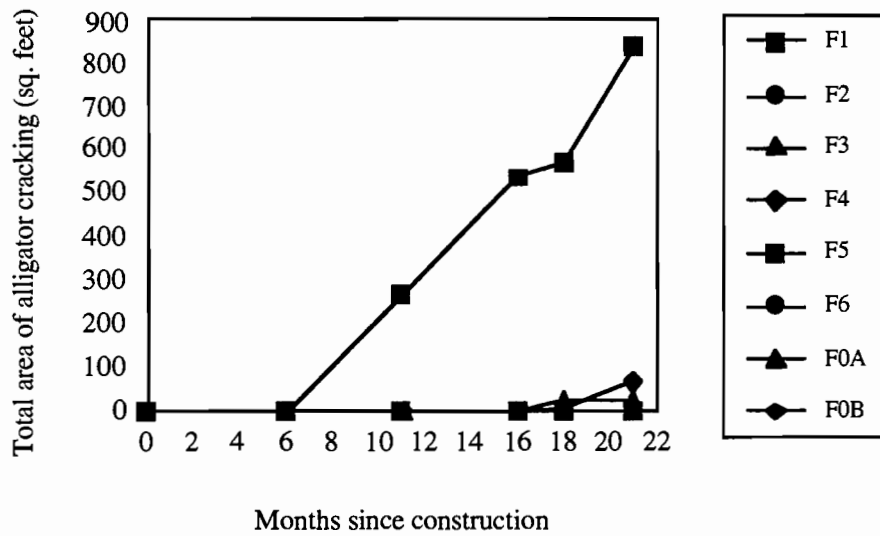


Figure 7.20 Total length of longitudinal length

Alligator cracking was the result mostly of structural failure under traffic loadings. As the material is repeatedly subjected to an accumulation of stress applications, some parts of the pavement subjected to stresses in excess of the tensile strength fail in the form of block cracks through fatigue. Alligator cracking generally progresses through the development of hairline longitudinal cracks that are subsequently connected with transverse hairline cracks. Through the traffic load repetitions, this process progresses until failure. This type of cracking development is strongly related to traffic loadings and to the structural bearing capacity of the subgrade layers.

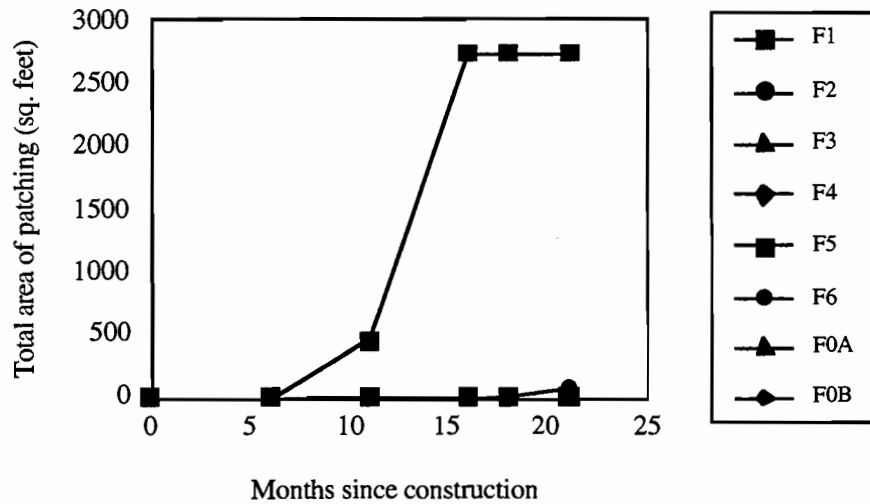
As shown in Figure 7.21, test section F5 developed extensive alligator cracking on a rather continuous basis. These results are similar to those observed for the rigid test sections that also have a flexible base. The flexible base prevents the development of reflective cracks, though at the same time it can also cause problems because of its structural weakness, as indicated by the significant development of alligator cracking for the rigid section R3 that included a flexible base.

Figure 7.22 shows patching versus time; as expected, the pattern was identical to the pattern for alligator cracking development. All the patching areas are located in the right lane only, again supporting the hypothesis that traffic loadings cause alligator cracking and consequent patching. As was the case for alligator cracking development, the data for patching for test section F5 show that it failed after only 2 years of traffic loading applications.



1 sq. foot=0.092 m²

Figure 7.21 Alligator cracking in the test section



1 sq. foot=0.092 m²

Figure 7.22 Total patching accumulation in the test section

In summary, the prevalent mode of failure for the flexible test sections was traffic-related fatigue cracking (e.g., alligator cracking). Reduced transverse and longitudinal cracking developed on all the test sections. Comparing the results for the cracking surveys before and after the overlay for the test sections, we determined that these cracks did not develop from reflective action, but, rather, from traffic-induced fatigue. Debris falling from the logging trucks also caused raveling and other problems on the flexible test sections.

CHAPTER 8. ROUGHNESS

8.1. BACKGROUND

A highway designer expects a pavement to provide a smooth ride and long service. A user's perception of pavement condition, termed the "serviceability of a pavement," has been recognized as one of the criterion in successful pavement design. The AASHO Road Test showed that the serviceability of a pavement was largely a function of its roughness (Ref 48), with about 95 percent of serviceability being influenced by the roughness of the pavement surface profile. Roughness can be defined as a distortion of the pavement surface, which is a function of the vehicle and pavement interaction; roughness is also a determining part of the riding quality of pavements. Pavement roughness can cause many problems to both the user and vehicle, including poor riding quality, safety hazards, discomfort, possible cargo and vehicle damage, and rapid deterioration of the pavement by dynamic loading impacts. However, because most travelers drive within a uniform range of speed on a highway, and because the riding quality of most passenger cars is similar, the riding comfort of a user is mainly a function of pavement roughness. Components of pavement profile can be classified into three parts: longitudinal, transverse, and horizontal variation (Ref 11). Among these, longitudinal variation of profile is considered the dominant factor contributing to pavement roughness.

8.1.1. Equipment for Measuring Roughness

Research efforts to objectively measure the effects of roughness on a highway user (Ref 49) have led to such devices as the roughometer (called BPR), Ontario's RRL type profilometer, and the Surface Dynamics Profilometer (SDP), which was used in this project. These types of devices estimate ride quality by objectively measuring the dynamic response of a passenger car to pavement roughness. The SDP, shown in Figure 8.1, consists of two wheels mounted on trailing arms beneath the measuring vehicle, one in each wheel path. A potentiometer measures relative motion between the wheel and the vehicle to obtain the surface profile (Ref 11). It has several advantages over other devices, including (1) capability of handling large amounts of data, (2) operating speed sufficient to cover a reasonable amount of pavement in a reasonable amount of time, and (3) excellent repeatability

The AASHO Road Test used the PSI concept for scaling roughness, while an important World Bank study used the Quarter-car Index (QI). In addition, the Bump Integrator trailer (BI) developed at the Transportation Road Research Laboratory (TRRL) defines roughness of a pavement in a different way (Ref 50). To provide a common scale to represent pavement roughness, the World Bank developed a standardized objective method for measuring pavement roughness, termed the International Roughness Index (IRI) (Ref 51). Guidelines for correlation with other indexes were also developed and summarized in this study (Ref 52). The IRI concept was applied during this research project to summarize roughness development in the pavement test sections. The standardized IRI is derived from a computer simulation using a set of standard

suspension parameters and a recorded profile. It mathematically accumulates the longitudinal surface profile effects of pavements in a passenger car, which can then be defined by the reference average rectified slope (RARS 80, the ratio of accumulated suspension motion to the distance a standard car simulation travels at a speed of 80 km/h [49.7 mph]). Thus, the higher the IRI, the rougher the pavement.



Figure 8.1 The Surface Dynamics Profilometer (SDP)

Guidelines for classifying pavement condition based on IRI have been developed in recent bonded concrete overlay research (Ref 53). According to these guidelines, if a pavement exhibited an IRI below 90, then it was considered in relatively good condition; if the pavement exhibited an IRI over 270, it needed rehabilitation.

Because roughness was one of the components of the serviceability index function derived from the AASHO Road Test, there may be a misconception that only the roughness measured represents pavement serviceability. Of course, both can be correlated with each other, as shown in Figure 8.2; but there are considerable variations in the relationship between roughness and serviceability index derived from different sources. The Texas relationships, for example, could represent a road user who has a relatively high expectation about pavement serviceability; the same roughness profile could correlate differently with the serviceability index, depending on the agency performing the measurements. From their research on the relationship between roughness and serviceability index, Paterson (Ref 54) and Janoff (Ref 55) suggest using linear functions between roughness and SI over normal ranges of paved highway.

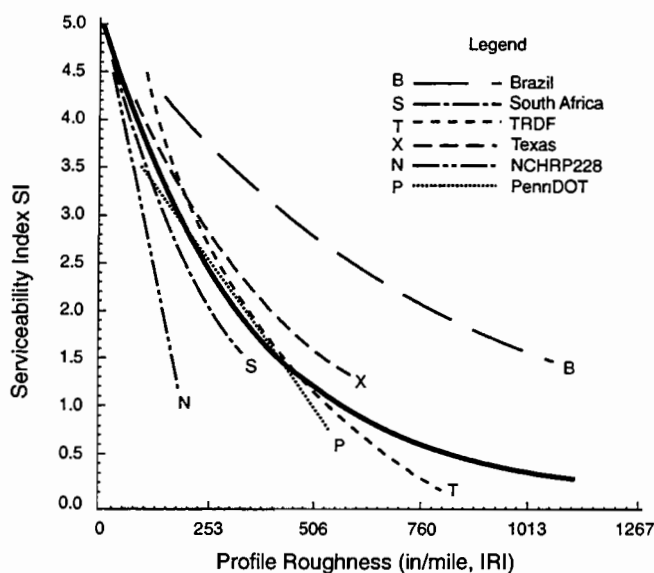


Figure 8.2 Approximate relationship between AASHO serviceability index and IRI

8.1.2. Data Collection Procedure

To collect roughness data, we drove the Surface Dynamics Profilometer four times over the test sections at 72.4 km/h (45 mph). All data were stored in a computer and transferred to CTR in floppy diskettes. The analysis program IRIE was run to calculate the IRI and the serviceability index. This program summarizes the fluctuation of profile along the road section and calculates the IRI of the left and right wheel paths. In order to exclude the transition effect between two test sections, 30.48 m (100 feet) at the beginning and end of each test section were bypassed when calculating the IRI. For R2A and R2B in the rigid sections, and for F0A and F0B in flexible sections, 15.24 m (50 feet) were excluded from both ends of their 152.4 m (500 feet) length. To test repeatability, we took three measurements on the same test section in March 1992, with these measurements indicating good repeatability. Further measurements were, therefore, taken only once.

8.2. PROFILE DATA COLLECTION BEFORE CONSTRUCTION

8.2.1. Rigid Sections

Before construction, roughness was measured to verify how efficiently the new overlay improves serviceability, and how existing conditions of the pavement affect the performance of the overlaid pavement structure. Overlays have been recognized as an efficient pavement rehabilitation method *if* the pavement is not severely damaged. It is commonly known that an overlaid pavement will fail earlier if the original pavement is in poor condition. Conversely, the overlaid

pavement performance will be improved if the original pavement presented relatively high riding quality before being overlaid.

Some of the rigid sections were already at the end of their performance period before the overlay was applied, as shown in Table 8.1. These test sections can be classified into three groups, based on the IRI. The rougher sections were R1, R2, and R6, especially the outside wheel path of R2. Relatively smooth sections included test sections R4 and R5. The test sections that exhibited larger IRIs show a significant difference between the inside and outside wheel paths, while the remaining sections that exhibited smaller IRI values did not show much difference between the wheel paths. The overall condition of the right lane was worse than that of the left lane. Figures 8.3 and 8.4 also indicate that the outside wheel path exhibited larger IRI values. This fact may be explained by geometric effects (i.e., the outside wheel path area is more susceptible to moisture damage and may have lost support by an improperly designed shoulder). The maximum observed IRI was 250 for R2, while the minimum was 70 for test section R4; the overall condition of the rigid test sections was relatively good (except for test section R2).

Table 8.1 International Roughness Index before construction — Rigid sections

Section Wheel Path	Right Lane		Left Lane	
	Inside	Outside	Inside	Outside
R1	149.62	138.88	114.55	116.99
R2	187.39	250.14	82.91	86.67
R3	166.92	94.08	78.66	92.39
R4	93.64	108.78	74.09	70.71
R5	103.45	133.77	81.19	89.13
R6	133.95	144.01	86.82	90.01
R0	78.41	99.29	74.93	96.01

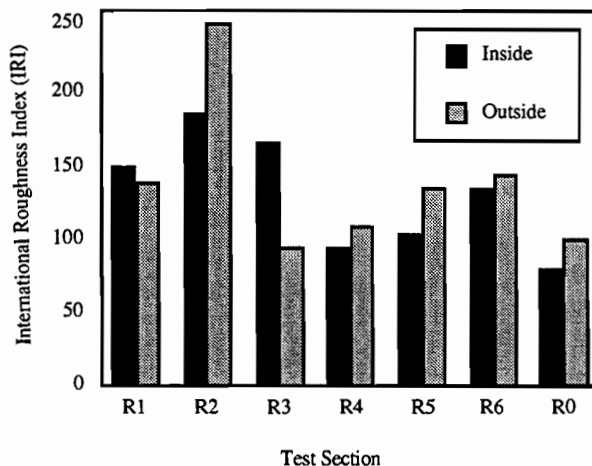


Figure 8.3 IRI of Right lane before construction — Rigid section

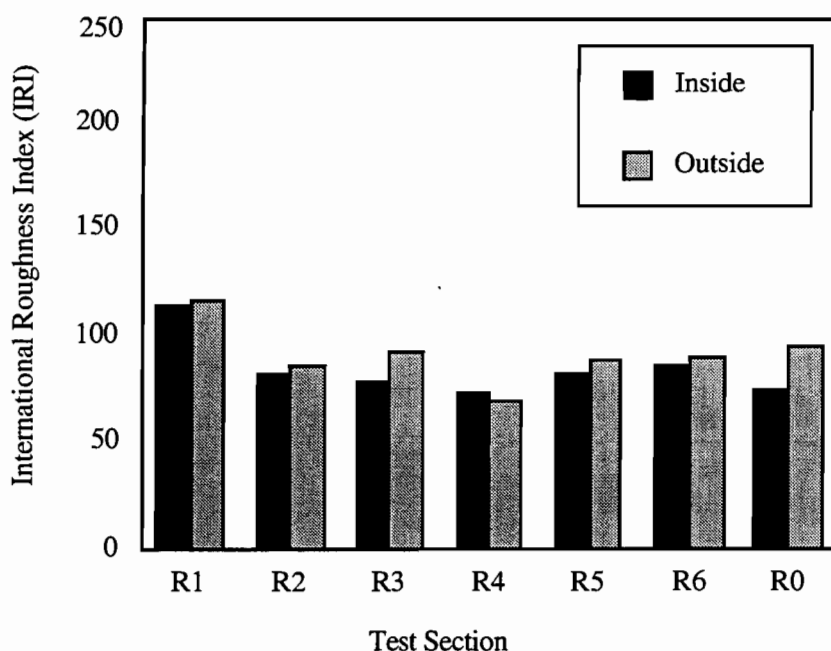


Figure 8.4 IRI of Left lane before construction — Rigid sections

8.2.2. Flexible Sections

Before construction, the flexible sections were in excellent condition, based on the IRI (Table 8.2); for either the right or left lanes, overall IRI was below 80. Test sections F3, F4, and F5 presented a slightly higher IRI than the other test sections, though with no large differences. Unlike what was observed for the rigid sections, no big difference existed between wheel paths, as shown in Figures 8.5 and 8.6.

Table 8.2 International Roughness Index before construction — Flexible sections

Section	Right Lane		Left Lane		
	Wheel Path	Inside	Outside	Inside	Outside
F1		66.22	65.19	53.87	55.12
F2		64.76	62.22	53.86	54.12
F3		73.75	67.75	54.53	68.26
F4		78.43	78.89	50.35	55.10
F5		78.03	77.12	48.88	56.81
F6		67.47	62.48	53.96	56.39
F0		62.70	58.14	62.15	65.50

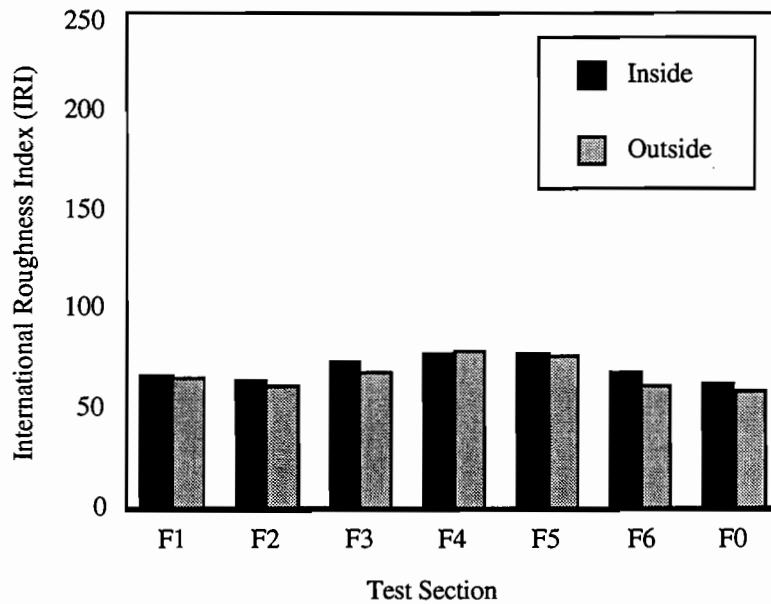


Figure 8.5 IRI of right lane before construction — Flexible sections

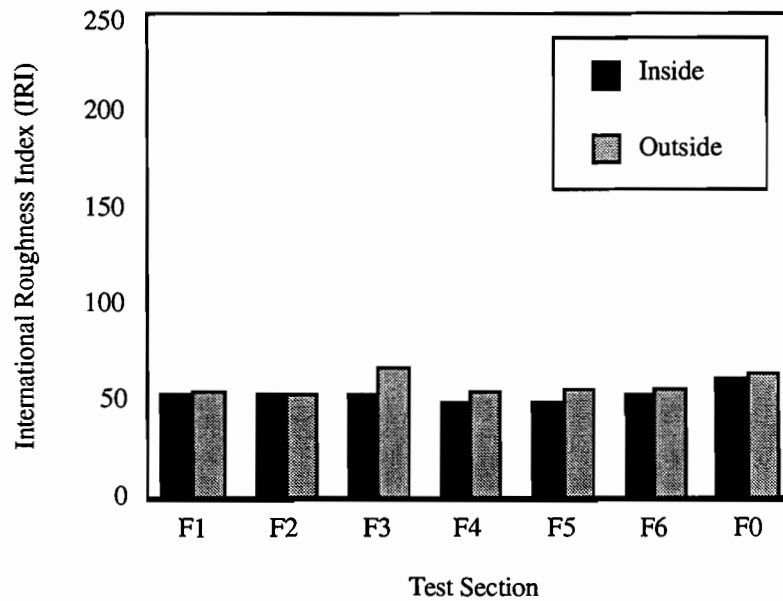


Figure 8.6 IRI of left lane before construction — Flexible sections

8.2.3. PSI for the Rigid and Flexible Sections

As expected from the previously reported IRI results, PSI for the rigid sections was relatively low, such that these sections required suitable maintenance; again, the right lane exhibited

a much lower PSI than the left lane. The right lane of test section R2 was at the end of its performance period, with a PSI of 2.25. However, the left lane showed a good surface condition, a finding that may be explained by differences in traffic between lanes. The flexible sections also exhibited the same trend as the rigid section, though the condition was as good as new pavement.

Table 8.3 PSI for the rigid and flexible test sections before construction

Section	Rigid		Section	Flexible	
	Right	Left		Right	Left
R1	2.78	3.49	F1	4.62	4.74
R2	2.25	4.19	F2	4.63	4.72
R3	3.41	4.26	F3	4.49	4.55
R4	3.79	4.33	F4	4.32	5.03
R5	3.54	4.18	F5	4.31	4.78
R6	2.97	4.19	F6	4.59	4.77
R0	3.92	4.10	F0	4.63	4.52

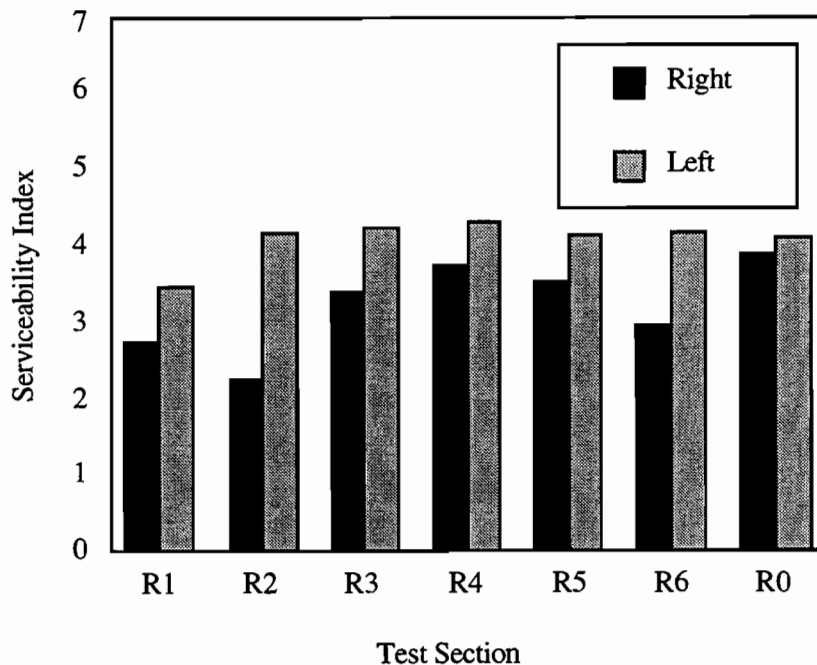


Figure 8.7 Serviceability Index before construction — Rigid sections

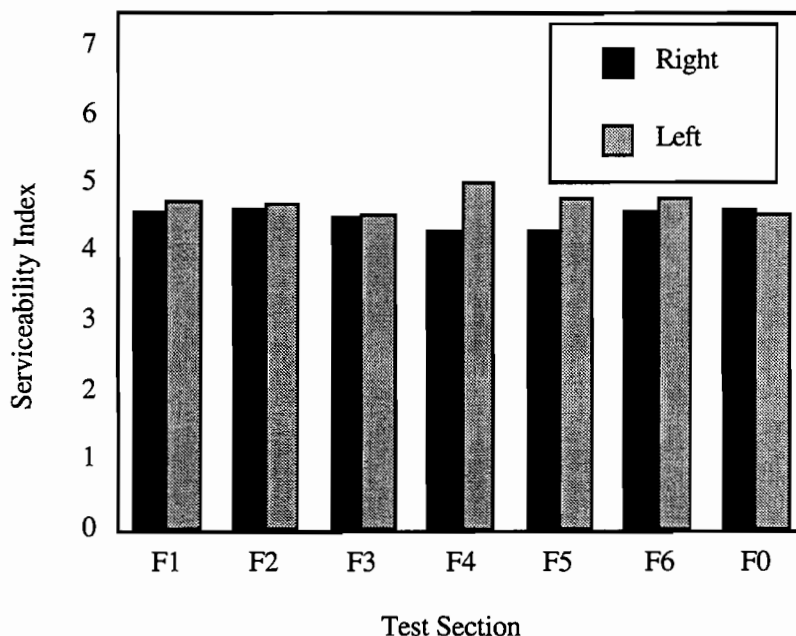


Figure 8.8 Serviceability Index before construction — Flexible sections

8.3. RIGID TEST SECTION ROUGHNESS PERFORMANCE AFTER OVERLAY

Test section roughness was measured using the Surface Dynamics Profilometer. IRI and PSI were calculated using the same methodology described for the measurements before construction of the different overlay options (detailed results are included in Appendix A).

Comparison of the results between lanes and wheel paths shows again that the right lane of the test sections generally developed larger IRIs than those observed for the left lane. This was expected, considering that the ESALs for the right lane were 10 times larger than those observed for the left lane (see Chapter 3), indicating that traffic loadings directly affect the smoothness profile of the pavement. However, there does not seem to be a major variance between the profile of the two wheel paths, because the outside wheel path on the right lane exhibited a slightly higher IRI.

To compare the effects of the new overlay, we classified test sections into three groups: milled, non-milled, and partially milled sections. Test sections R1, R2A, and R2B, which had the existing asphalt overlay milled off, show relatively larger values for the IRI; among the rigid sections, R2A and R2B have been exhibiting rapid deterioration, as shown in Figures 8.9 through 8.12. These two sections showed almost the same magnitude of IRI for the right lane, while R2A exhibited a larger IRI for the left lane. As discussed in Chapter 7, cracking in test section R2B was minor compared with the cracking observed in test section R2A. Section R2B did, however, develop relatively deep ruts (like R2A), indicating that roughness follows the rut depth development pattern rather than the crack development pattern. The rapid deterioration of the crack and seat pavement sections R2A and R2B could have been the result of the movement of cracked pieces under heavy loadings — movement that can ultimately lead to a loss of structural integrity.

However, for the low level of ESALs observed for the left lane, the crack and seat method may provide reasonable structural support. As heavy traffic loads are applied to the pavement, hairline fatigue cracking will develop; this will then be combined with the movement of the underlying JCP, a process that will certainly accelerate roughness.

Section R1, which was considered one of the rougher sections before construction, exhibited a smooth profile up to this point. Even though reflective cracking was observed, as discussed in Chapter 7, the underlying JCP, which was repaired by various maintenance methods before the overlay, provided good structural support for the asphalt overlay, such that the section showed a good profile. This finding underscores the importance of repairing the existing pavement before overlay operations.

Partially milled sections included test section R3. Even though section R3 developed a severe rutting problem, as discussed in Chapter 6, its current IRI was still acceptable. The IRI for test section R3 increased continuously up to the point when the traffic lane layout was changed. After the lane layout changes, the roughness even decreased slightly, as already discussed in Chapter 6.

Non-milled sections included R4 (Arkansas mix), R5 (with a stress relief layer between the new and old overlays), R6 (with a type C asphalt overlay), and the control section R0. This group exhibited the best performance among the three groups. Section R5 was in the best condition among the rigid sections. R4 and R0 became slightly rougher before changing the traffic lane markings; there was no consequent rise in IRI for section R5. Based solely on roughness, sections R4 and R5 can be considered the best performing rigid sections of the group.

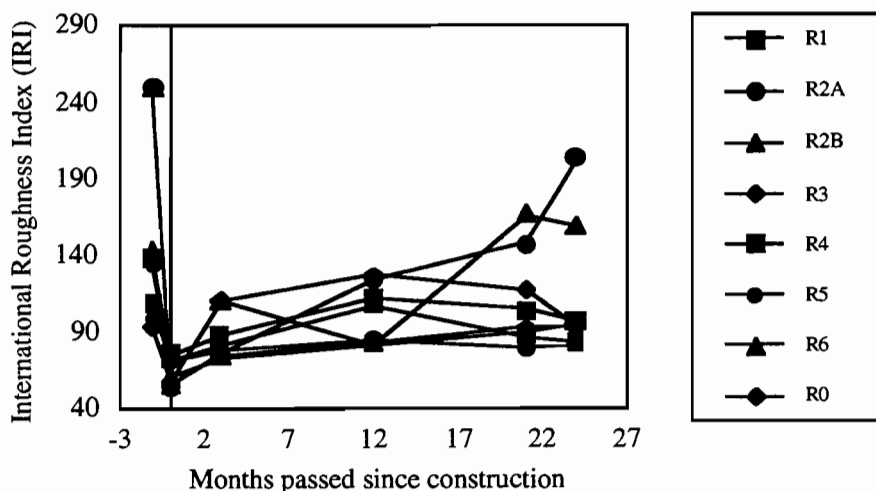


Figure 8.9 IRI versus time at outside wheel path of right lane — Rigid section

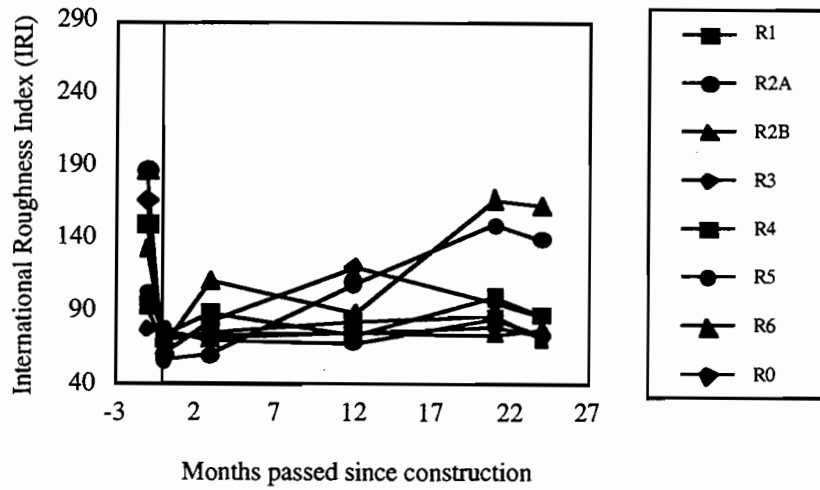


Figure 8.10 IRI versus time at inside wheel path of right lane — Rigid section

The effects of the before-construction condition on the new overlay can be observed in Figures 8.9 and 8.10. The pavement surfaces in sections R1, R2A, R2B, and R3 were rougher before the overlay than the pavement surface for the other sections. After the overlay, the profiles of R2A and R2B returned to their original status after 2 years. However, sections R1 and R3 showed relatively good profiles up to the last roughness measurements. The decrease in IRI in section R3 was strongly related to the change in lane markings on the rigid sections. The test section with the largest IRI, R1, stabilized after new overlay construction, apparently because cracks and joints were repaired before construction of the new overlay. From these observations, we may conclude that while the previous profile condition affects the performance of a new overlay, the performance also depends strongly on the overlay method.

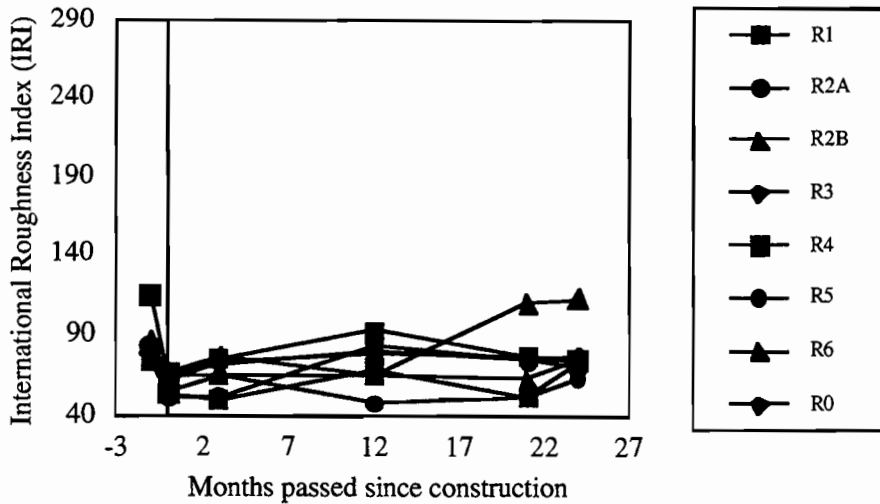


Figure 8.11 IRI versus time at inside wheel path of left lane — Rigid section



Figure 8.12 IRI versus time at outside wheel path of left lane — Rigid section

8.4. PERFORMANCE OF THE RIGID TEST SECTIONS AFTER OVERLAY

As expected, PSI performance for the rigid sections showed the same trend as the IRI. After construction, before being subjected to traffic, the rigid sections showed an initial PSI that ranged from 4.3 and 4.7. As traffic loadings accumulated, the initial PSI decreased consistently, except for a few test sections (which presented unexpected results, including increasing PSI, as may be observed for test section R3). Unlike the results obtained for the IRI, the differences between the two lanes are significant. The right lane of section R2A almost came to the end of its service life after about 900,000 ESALs, while the left lane, subjected to fewer ESALs, presented acceptable results for the PSI (PSI = 3.6). Before the new overlay, two sections (R1 and R2) could be regarded as failed sections (because of low PSI). However, R1 still presented a good degree of serviceability up until the last measurements. This again underscores the importance of repairing cracked concrete before overlays. The other non-milled or partially milled sections still presented a good level of rideability.

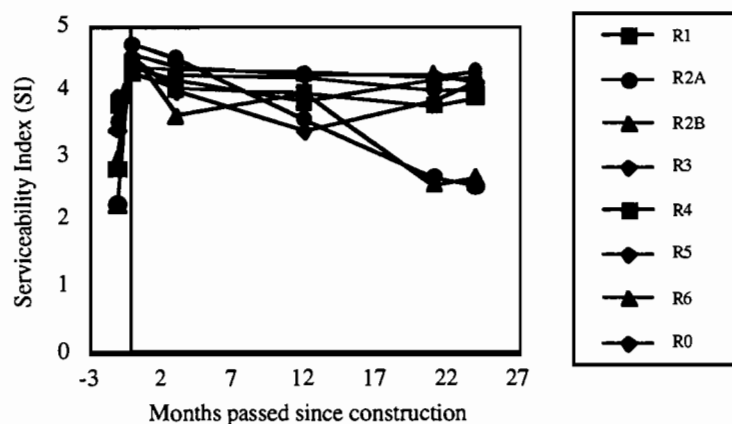


Figure 8.13 PSI variation of the right lane — Rigid section

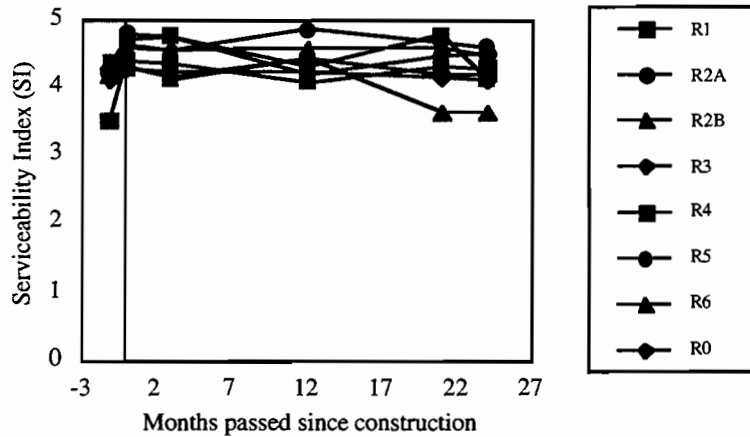


Figure 8.14 PSI variation of the left lane — Rigid section

8.5. FLEXIBLE SECTION ROUGHNESS PERFORMANCE AFTER OVERLAY

Figures 8.15 to 8.18 show the roughness development for the flexible test sections, as summarized by the IRI. Like the rigid sections, the right lanes presented rougher surface conditions than the left lanes. This can be particularly noticed in test section F5. However, no significant differences can be observed for the different wheel paths. Two sections, F5 and F0, developed relatively high roughness; except for these two sections, there was no evident sensitivity to the traffic or time up to the last measurements.

The right lane of test section F5 experienced severe rutting problems and slightly severe alligator cracking. Section F5 consists of a flexible base and type C asphalt overlay similar to that incorporated in rigid test section R3, which demonstrated the worst level of serviceability. Like R3, F5 is highly sensitive to traffic volumes: The right lane showed significantly higher IRI values, while the left lane retained an IRI below 90 (i.e., a good pavement condition). This finding shows that the flexible base sections are highly sensitive to traffic volumes, indicating that this may be an acceptable way to protect low volume roads from reflective cracking (though unacceptable for high-volume roads).

The control section F0, which presented relatively good serviceability before the new overlay, developed a slightly rough surface condition for the left lane, in contrast to the general trend in which the right lane deteriorated faster than the left lane as a result of higher traffic loads. Accordingly, it may be that the roughness was caused by factors other than heavy traffic. No rutting and no deflection problems were observed on the left lane of test section F0; the transverse cracks on the left lane were relatively larger than those for the other sections, but, again, the right lane also presented the same level of transverse cracks (as discussed in Chapter 7). The roughness may be attributed to construction, since the initial roughness was relatively high and since the rougher conditions persisted during the monitoring period, as shown in Figure 8.17.

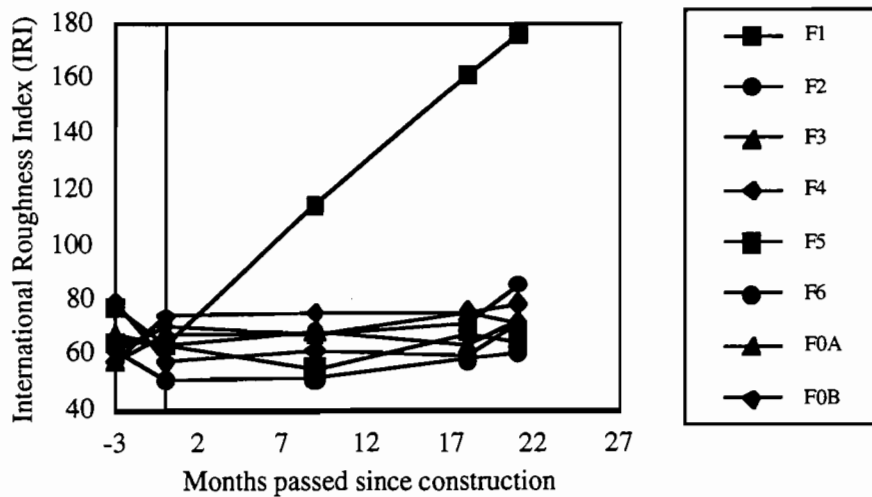


Figure 8.15 IRI versus time at outside wheel path of right lane — Flexible section

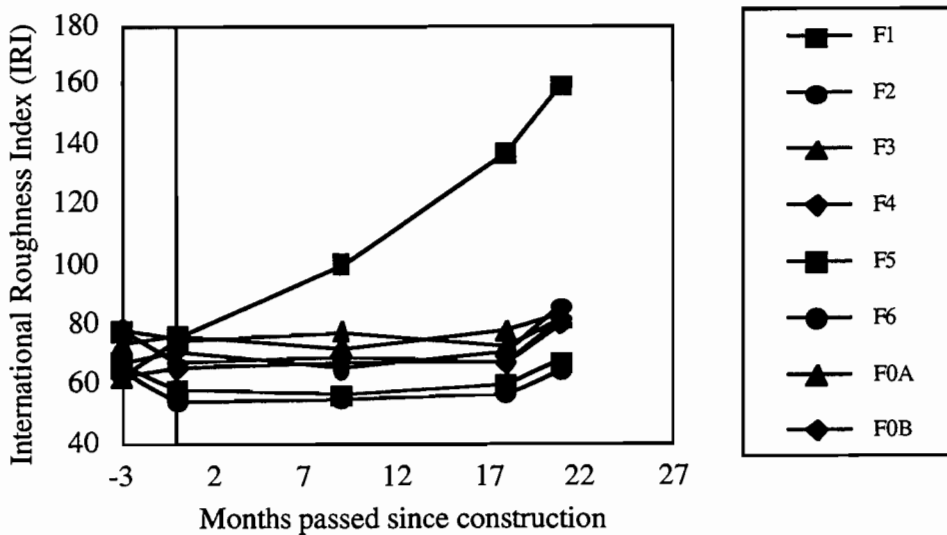


Figure 8.16 IRI versus time at inside wheel path of right lane — Flexible section

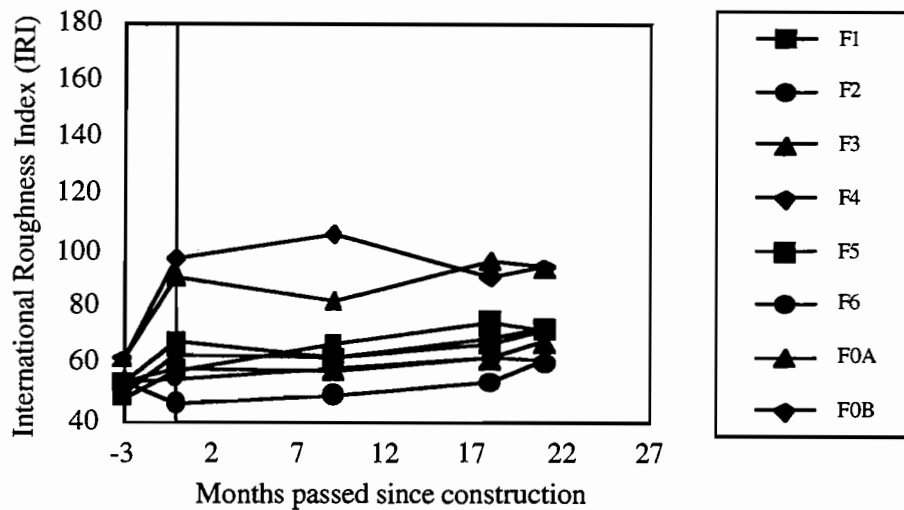


Figure 8.17 IRI versus time at inside wheel path of left lane — Flexible section

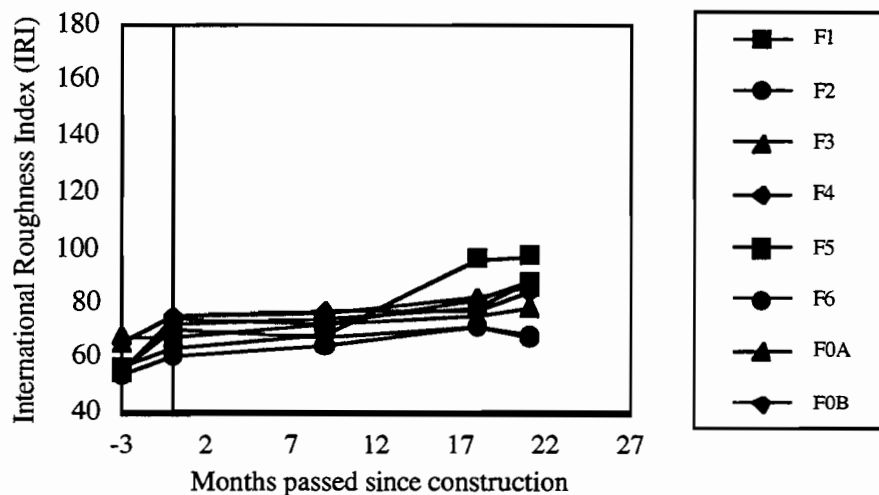


Figure 8.18 IRI versus time at outside wheel path of left lane — Flexible section

8.6. PERFORMANCE OF THE FLEXIBLE TEST SECTIONS AFTER OVERLAY

Figures 8.19 and 8.20 summarize the PSI performance of the flexible test sections. Section F5 shows sensitivity of the PSI to traffic: The right lane almost came to the end of its serviceability, while the left lane was still in good condition, with the serviceability index at the last survey estimated at 4.15. The control section F0 shows slightly decreasing serviceability in the left lane, with the same trend as shown for the IRI results. With a PSI above 4, the remaining test sections were in good condition, with most test sections still presenting good riding conditions (the exception was test section F5). Considering the overall performance of the flexible test sections,

where almost all the test sections remained at their initial stages of PSI, there is a need to collect serviceability data continuously throughout the sections to establish the long-term asphalt overlay performance information.

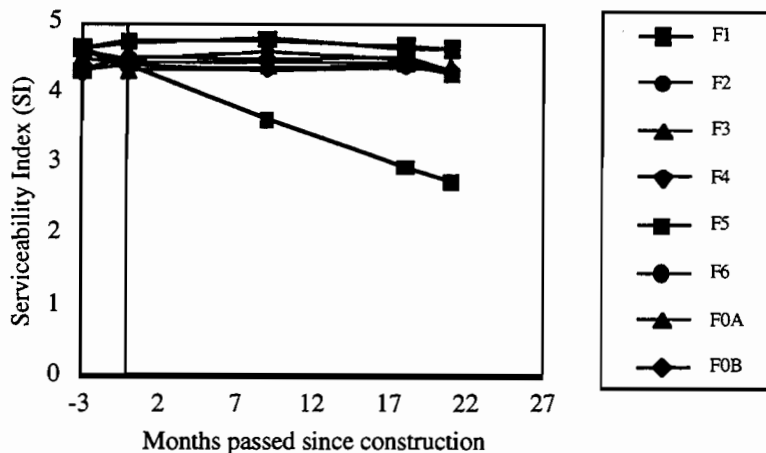


Figure 8.19 PSI variation of right lane — Flexible

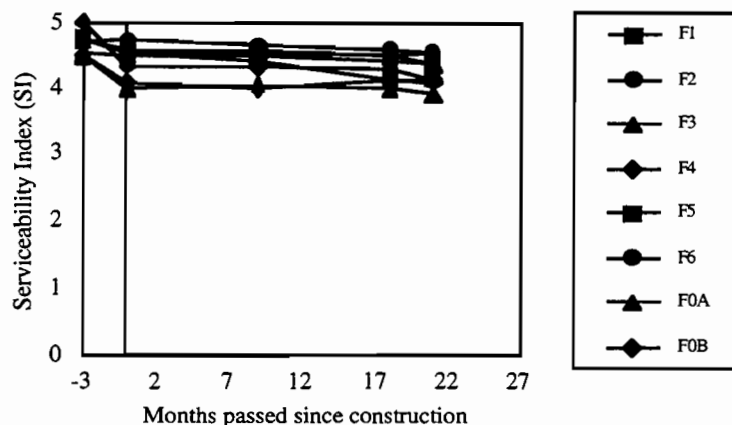


Figure 8.20 PSI variation of left lane — Flexible

8.7. SUMMARY

The overall performance of most of the test sections was good, the exceptions being test sections R2A and R2B, which used the break and seat method. The IRI between the left and right lanes shows a large difference, especially in sections R3 and F5, which have a flexible base layer. However, the IRIs obtained from between the wheel paths in the rigid and flexible sections did not show large differences. Our findings indicate that rutting is correlated with serviceability or longitudinal roughness. However, cracking did not seem to be strongly related to pavement serviceability. While section R3 developed significant cracking, as reported by the most recent survey, its serviceability index was still reasonable.

CHAPTER 9. CONCLUSIONS AND RECOMMENDATIONS

9.1. CONSTRUCTION AND MAINTENANCE OF THE TEST SECTIONS

Fourteen test sections (six alternative and one control section of both flexible and rigid pavement) were constructed on US 59 in an experiment designed to observe pavement performance under mixed traffic and environmental conditions. As part of our effort to identify optimal overlay designs, we monitored the construction and maintenance of these test sections. The following pavement-related data were collected:

1. The longer-than-expected construction time required for the rigid sections was partially a result of excessive rainfall occurring during the construction period. This delay increased indirect costs (e.g., user costs and vehicle operating costs) during rehabilitation.
2. Failed sections F5 and R2A were repaired by routine maintenance (e.g., patching and replacing subbase material). The time and costs associated with these maintenance procedures must be added to the total construction costs.

9.2. INFORMATION RECORDED BY THE WIM STATION

1. A weigh-in-motion (WIM) station was installed to collect such traffic information as axle type, weight, speed, and lateral distribution; these data were then related to pavement damage.
2. The lane distribution based on traffic volume was 75:25; based on ESALs, the distribution was 89:11. For design purposes, we recommend the larger number be used.
3. The lateral position of a truck — .91 m (3 feet) from the shoulder — provides basic input data useful in predicting pavement behavior under traffic loadings.
4. The daily temperature distribution followed a sine curve, with the maximum pavement temperature for the flexible sections almost 60° C (140° F) during the summer. Such temperatures may accelerate rutting in these test sections.

9.3. PERFORMANCE OF THE ASPHALT OVERLAYS ON THE TEST SECTIONS

We also analyzed pavement deflections and corresponding backcalculated stiffness. The distresses (rutting, profile, and cracks) were surveyed and measured within certain time intervals. From the deflection monitoring, we found the following:

1. Three stages of construction — before milling of the existing overlay, after milling, and after construction of the new overlay — summarize the structural response of the different pavement systems. The structural integrity of section R1 increased after

cracks and joints were repaired. The stiffness of the other sections (R2A and R2B) decreased after crack and seat. The other rigid sections did not show large before-and-after-construction differences.

2. The load transfer of the composite pavements shows higher load transfer efficiency. This finding suggests that the main cause of reflective cracking is not unequal displacement under traffic loadings, but, rather, other factors (such as slab movement caused by temperature cycles).
3. The deflection variations observed during the monitoring period for the rigid sections did not agree well with the conventional wisdom that suggests deflections should increase with the accumulation of traffic applications; the deflection results agree well for the flexible test sections. Identifying the temperature effects on the deflections of composite pavements will require further research.
4. The deflection between wheel path and on wheel path is not generally different, except for the sections that had higher rutting problems on the wheel path, including sections R3 and F5. The deflections taken on the wheel path were larger than those obtained between the wheel paths on these sections.

Backcalculation of stiffness for the different layers of the pavement for each test section were performed using two computer programs available for composite pavement and flexible pavements. The variation of effective stiffness is so high that the reliability of the process is questionable. However, general trends can be drawn from this backcalculation procedure:

1. The backcalculated stiffness using the two programs resulted in similar trends, supporting the view that the backcalculated stiffnesses can at least be used to estimate the trends of stiffness under traffic-load applications.
2. Stiffness recovery for repaired concrete pavements was demonstrated by the backcalculation results for test section R1 after milling and repair; stiffness decrease caused by the crack and seat method was demonstrated by the backcalculation results obtained for the stiffness of section R2.
3. The pavement system stiffness backcalculation procedure for the flexible section was difficult owing to the limitations of the two programs. The concept of effective stiffness provided acceptable results in most cases (the exception was section F5).
4. The structural number (SN) was estimated from the backcalculated stiffnesses for both sections. The SN, which provided a basic input for calculating ESALs, will be used to develop overlay design models.

Rut depth development for the test sections was monitored every 3 months. The results verified that a pavement that had rutting problems in the original pavement experienced a continuous increase in rut depths. Some specific conclusions based on the monitoring of rut depth developments in the test sections are as follows:

1. The rut depth development in the composite pavement section has three stages. In the first stage, the rapid increasing of rut depths is caused by post-compacting of asphalt

material by heavy traffic loadings. After initial densification, the ruts decrease or disappear. This may be strongly related to the lateral distribution of traffic loadings on the pavement, such that the entire pavement is compacted from the traffic loadings, leveling the ruts. In the third stage, there is a rapid increase in rutting over a short period (this was not formerly observed on the test sections). Flexible base sections R3 and F5 represented exceptions to these three stages of rut development. These test sections, which have a structurally weaker interlayer to prevent reflective cracking, experienced a rapid increase in rutting in the early stages after construction (and lesser increases in later stages).

2. The rut depths between lanes have different patterns as a result of the larger traffic loadings on the right lane for both the rigid and flexible test sections, with the right lane experiencing deeper ruts than the left lane.
3. The wheel path effect is significant for the rigid sections; no significant differences were found for the flexible sections.
4. After June 1993, the rut depths decreased for all rigid sections. This was certainly caused by moving the lane markings 45.72 cm (18 in.) to the outside; this finding shows the influence of lateral traffic distribution on rutting development.
5. Rutting is strongly related to the surface curvature index (SCI), which is calculated based on the FWD deflections. Sections F5 and F6 have higher SCIs and more rutting problems. Sections R3 and F5 showed large SCIs and greater rutting development.

Condition surveys were performed to collect detailed distress information throughout the test sections. The following conclusions may be drawn from these condition surveys:

1. The transverse cracks in the rigid sections are considered to be reflective cracks because they developed every 4.57 m (15 feet), which corresponds to the spacing of the contraction joints of the existing JCP. The transverse cracking increased during the winter, suggesting that the main mechanism of reflective crack development is thermal movement of the existing JCP.
2. The transverse cracks in the flexible section are considered a combination of fatigue-related cracking and reflective cracking, since some cracks appeared earlier in the life of the pavement, and because many of the transverse cracks appearing in the right lane can be associated with alligator cracking, which is a typical form of fatigue cracking.
3. The longitudinal reflective cracks appeared after the second winter on the rigid sections and seem to connect two transverse reflective cracks.
4. The alligator cracking and patching increased significantly after the rutting problem developed in sections R3 and F5. This finding shows that fatigue cracks become visible after severe rutting.

Profile information was collected using the Surface Dynamic Profilometer (SDP). The pavement roughness was summarized using the International Roughness Index (IRI) and the Pavement Serviceability Index (PSI).

1. Overall serviceability for both sets of test sections is over 4.0, except for sections R2A and R2B, which were subjected to a break and seat method during construction.
2. The IRIs between lanes show a large difference, especially for sections R3 and F5, which have a flexible base layer.
3. IRIs between wheel paths for the rigid and flexible sections do not show large differences.
4. Rutting seems to be correlated with serviceability or longitudinal roughness. However, cracking is not strongly related to roughness. While section R3 has begun to show cracks, as determined from the most recent survey, its PSI is still acceptable.

9.4. PERFORMANCE EVALUATION OF EACH REHABILITATION ALTERNATIVE FOR THE RIGID SECTIONS

Six alternative and one control section for each set of test sections, flexible and rigid, show different performance under the same traffic loadings and environmental conditions. While reflective cracking, the main study objective for the rigid test sections, could not be eliminated, it was kept at acceptable levels by many of the rehabilitation alternatives studied. Table 9.1 presents an overall summary of the performance of the rigid test sections for the different pavement attributes monitored throughout this study.

Table 9.1 Performance summary for the rigid test sections

	R1	R2A	R2B	R3	R4	R5	R6	R0
Deflection	G	B	B	B	G	G	N	N
Rutting	G	B	N	B	G	G	G	N
Condition Survey	N	B	G	N	G	N	N	N
Profile	N	B	B	N	G	G	G	G
Comment	RC, but sawcuts may help prevent RC	RC with structural deficiency failure	RC without structural failure	No RC, but rutting and structural failure	Best service-ability section	Slight RC cost-effective section	Moderate RC	100% of RC Haircracks

*G=Good, N=Normal, B=Bad, RC=Reflective Cracking

We drew the following conclusions for the rigid sections:

1. Section R1, which did not have sawcuts, exhibited reflection of 100 percent of the cracks. The sawcut section also exhibited reflective cracking when the sawcut line did not match well with the existing joints. Even when the reflective cracks did not appear in the sawcut sections, joint failure occurred as traffic loadings accumulated, as shown in the right lane. The pre-overlay repair of the existing JCP resulted in a structurally

stronger base layer, which translated into good rutting performance. Because of the large amount of cracks and high severity of these cracks, a relatively large IRI was observed for this test section.

2. Section R2A exhibited both reflective cracks and fatigue cracks as a result of low structural strength caused by the crack and seat method. Along with the decrease in stiffness, relatively large ruts were observed for this test section. The section also experienced pumping problems. These kinds of structural deficiencies led to functional failure earlier than expected. Section R2B experienced far fewer problems than R2A, which was 10.16 cm (4 inches) thick; the fewer problems can perhaps be attributed to the 3.81 cm (1 and 1/2 inches) difference in overlay thickness. It shows that the minimum asphalt thickness of 10.16 cm (4 inches) on the break and seat method suggested by the AASHTO Guide is not sufficient to provide better serviceability.
3. While section R3 experienced almost no reflective cracking problems up to now, it did exhibit severe rutting followed by alligator cracking. The deflections indicate a large surface curvature index, which is associated with a shear mode of failure, such as rutting. This section, however, showed a trade off between reflective cracking and rutting. Considering the good performance in the left lane, we recommend that the highway that has relatively low traffic volume and high reflective cracking be used.
4. Section R4 may be the best rehabilitation solution, based on condition survey results, rut depth measurements, deflections, and profile. Besides slight reflective cracking, it has the smallest deflections among the test sections. It also did not develop any rutting problems. All these factors suggest that this section provides the best serviceability, as supported by the small IRI and the highest serviceability index among the test sections.
5. Reflective cracking developed after the second winter in test section R5. This section presented the best surface condition during the first year, though it later deteriorated because of hairline cracking caused by reflective action. Deflection was not significant, and no rutting problems were observed. In summary, while the stress relief layer effectively delays reflective cracking development, it does not guarantee complete protection against it.
6. Test section R6 (with type C mix) resisted reflective cracking; its effect is definitely better than the typical type D asphalt mix that was used in the control section R0. Hairline cracks reflected after 2 years in test section R6. This section also presented low deflections, as compared with the other test sections, and no rutting problems. During the last measurements, this section was still providing good serviceability.
7. Test section R0 developed 100 percent reflective cracks of 4.56 m (15 feet) crack spacing just after 2 years of temperature loading cycles. A rapid increase in deflection was observed; roughness also increased with traffic load accumulations. This test section presented fair serviceability, as measured by the IRI, and no rutting problems. On the basis of the reflective cracking development, the type D asphalt mix should be avoided in future asphalt overlays of rigid pavements.

9.5. PERFORMANCE EVALUATION OF EACH REHABILITATION ALTERNATIVE FOR THE FLEXIBLE SECTIONS

Although the flexible sections experienced insignificant reflective cracking, fatigue cracks (alligator cracks and hair longitudinal cracks) were common. The patching area also increased as time and traffic accumulated. The milled sections (e.g., F5 and F6) generally deteriorated at a faster rate than the non-milled sections. Non-milled sections showed relatively better serviceability. Table 9.2 presents an overall summary of the performance of the flexible test sections for the different pavement attributes monitored throughout this study.

Table 9.2 Performance summary for the flexible test sections

	F1	F2	F3	F4	F5	F6	FOA	FOB
Deflection	G	G	N	G	B	N	N	N
Rutting	G	N	G	G	B	N	B	B
Condition Survey	B	G	G	N	B	G	N	B
Profile	G	G	N	G	B	G	N	N
Comment	Many TCs	Best performance section	Second best performance	A few TCs	Worst condition structural failure	Slight rutting large SCI	Moderate rutting	Many TC moderate rutting

* G=Good, N=Normal, B=Bad, TC=Transversal Cracks, SCI=Surface Curvature Index

1. For section F1, a relatively large amount of transverse cracks appeared on the surface layer for both lanes. No rutting problems developed, and relatively small deflection was observed.
2. The best performer among the test sections was F2. It developed shorter transverse cracks and no rutting problems; it also exhibited smaller deflections. At last survey, the section still had a high serviceability index value (PSI = 4.3). The modified type C asphalt seems to do a good job in protecting against thermal cracks and rutting.
3. The type B asphalt binder with type C asphalt used in test section F3 also provided good serviceability to this flexible section. This section developed neither rutting problems nor high deflections.
4. Section F4 developed transverse cracks. This section developed neither rutting problems nor high deflections. As in the comparison between test sections R6 and R0, the type C mix used in test section F4 performed better than the type D asphalt mix used in control section F0, primarily because of the better rutting and transverse cracking performance observed for the F4 test section.
5. Section F5 is probably the worst performer among the rehabilitation alternatives studied on the flexible test sections. Serious structural problems, including alligator cracks, longitudinal and transverse cracks, and patching, developed in this section. While rutting also developed, its magnitude was relatively less than that observed for

the rigid sections. It also presented large deflections and a large surface curvature index. In summary, while the flexible base prevented reflective cracks, it did cause other traffic-related problems, including rutting (as we saw with rigid test section R3).

6. Despite section F6 showing decreasing pavement serviceability, it still maintained reasonably good performance. It developed a slight rutting problem and a relatively large SCI.
7. Control section F0 did not perform well. It developed large transverse cracks lengths (reflective cracks and fatigue cracks), slight alligator cracking, and moderate rutting.

REFERENCES

1. Highway Research Board, "AASHO Road Test Report 7 — Summary Report," Special Report 61G, Highway Research Board, 1962.
2. Hoskins, B. E., B. F. McCullough, and D. W. Fowler, "The Development of a Long-Range Rehabilitation Plan for US-59 in District 11 — Preliminary Report," Research Project 987-1, Center for Transportation Research, The University of Texas at Austin, 1991.
3. Lee, Clyde E., and Safry Kamal Ahmad, "Effect of Work Zone Detours on Rural Highway Traffic Operations," Research Project 987-2, Center for Transportation Research, The University of Texas at Austin, May 1993.
4. Elmore, William E., Thomas W. Kennedy, Mansour Solaimanian, and Pablo Bolzan, "Long-term Performance Evaluation of Polymer-Modified Asphalt Concrete Pavements," Research Project 1306-1F, Center for Transportation Research, The University of Texas at Austin, November 1993.
5. Allison, B., and B. F. McCullough, "Construction of Rehabilitation Test Sections on U.S. 59 in the Lufkin District," Research Report 987-3, Center for Transportation Research, The University of Texas at Austin, August 1994.
6. American Society for Testing and Materials, "Standard Specification of Highway Weigh-in-Motion (WIM) Systems with User Requirements and Test Method," ASTM Designation: E 1318-90.
7. AASHTO, "AASHTO Guide for Design of Pavement Structures 1986," AASHTO, 1986.
8. Richardson, Joseph M., and Jamshid M. Armaghani, "Stress Caused by Temperature Gradient in Portland Cement Concrete Pavements," TRR 1121.
9. Kwasi Badu-Tweneboah, Mang Tia, and Byron E. Ruth, "Procedures for Estimation of Asphalt Concrete Pavement Moduli at In-Situ Temperatures," TRR 1121.
10. Kennedy, Thomas W., "Tensile Characterization of Highway Pavement Materials," Research Report 183-15F, Center for Transportation Research, The University of Texas at Austin, July 1983.
11. Haas, Ralph, and W. Ronald Hudson, *Pavement Management Systems*, McGraw Hill, 1986.
12. Washington State Department of Transportation, "State-of-the Art on Pavement Overlay Procedures, Vol I, State-of-the-Art Review and Research Plan," Washington State Department of Transportation, pp 29-59, 1983.
13. Anderson, D. T., and C. K. Koskey, "Advances in Asphalt Overlay Design Procedures," Sixth International Conference, Structural Design of Asphalt Pavements, Volume I, Proceedings, University of Michigan, pp 748-761, Ann Arbor, Michigan, July 1987.
14. "Asphalt Overlays for Highway and Street Rehabilitation," Asphalt Institute, Manual Series No. 17, June 1983.

15. McDaniel, Mark, "Accelerated Trafficing with the Model MLS," paper submitted to the First Annual CTR and TTI Student Seminar, April 1993.
16. McCullough, B. F., and James R. Lundy, "The Performance of Bonded Concrete Overlay in Texas," Annual Transportation Convention, The Republic of South of Africa, 1988.
17. "Manual for FWD Testing in the Long-Term Pavement Performance Program," SHRP-P-661, 1993.
18. Austin Research Engineers Inc., "Overlay Design and Reflective Cracking Analysis for Rigid Pavements, Volume I - Development of New Design Criteria," FHWA Report No. FHWA-RD-77-66, August 1977.
19. Wei, Chao, and B. F. McCullough, "Development of Load Transfer Coefficients for Use with the AASHTO Guide for Design of Rigid Pavements Based on Field Measurements," Research Report 1169-3, Center for Transportation Research, The University of Texas at Austin, February 1992.
20. Ricci, Eduardo A., and A. H. Meyer, "Falling Weight Deflectometer for Nondestructive Evaluation of Rigid Pavements," Research Report 387-3F, Center for Transportation Research, The University of Texas at Austin, November 1985.
21. McCullough, B. F., Jose Weissmann, Terry Dossey, and Yoon-Ho Cho, "A Case Study of Overlay Performance of Continuously Reinforced Concrete Pavement (CRCP) Located on IH-35, Bowie County, Texas," Research Report 1342-1, Center for Transportation Research, The University of Texas at Austin, February 1994.
22. Hall, Kathleen T., and Alaeddin Mohseni, "Backcalculation of Asphalt Concrete-Overlaid Portland Cement Concrete Pavement Layer Moduli," Transportation Research Board 1293, 1991.
23. Anderson, M., "A Data Base Method for Backcalculation of Composite Pavement Layer Moduli," ASTP 1026, 1989.
24. Vzan, J., T. Scullion, C. H. Michalok, M. Paredes, and R. L. Lytton, "A Microcomputer-Based Procedure for Backcalculation Layer Moduli From FWD Data," Research Report 1123-1, Texas Transportation Institute, Texas A&M University, July 1988.
25. Rhode, G. T., and T. Scullion, "Modulus 4.0: Expansion and Validation of the Modulus Backcalculation System," Research Report 1123-3, Texas Transportation Institute, Texas A&M University, November, 1990.
26. Koseno, Koestomo, and B. F. McCullough, "Evaluation of the Performance of the Bonded Concrete Overlay on Interstate Highway 610 North, Houston, Texas," Research Report 920-2, Center for Transportation Research, The University of Texas at Austin, December 1987.
27. Strategic Highway Research Program, "Layer Moduli Backcalculation Procedure: Software Selection," Strategic Highway Research Program, January 1993.
28. Scullion, Tom, and Chester Michalok, "Modulus 4.0 User's Manual," Research Report 1123-4, Texas Transportation Institute, Texas A&M University, January 1991.

29. Zhou, Haiping, Jim Huddleston, and James Lundy, "Implementation of Backcalculation in Pavement Evaluation and Overlay Design in Oregon," Transportation Research Record No. 1377, 1992.
30. Hossain, Mustaque, and Larry A. Schofield, "Interpretation of Backcalculated Layer Moduli Crack-and-Seat Pavement from Falling Weight Deflectometer Data," Transportation Research Record No. 1377, 1992.
31. Viljeon, Adrianus W., and B. F. McCullough, "Implementation of a Comprehensive Rigid Pavement Overlay Design System into a Condensed Overlay Design Manual," Research Report 388-4, Center for Transportation Research, The University of Texas at Austin, May 1985.
32. Sharma, Ashwani K., and Lynn L. Larson, "Rut Resistant Asphalt Concrete Overlays in Wisconsin," Transportation Research Record 1259, pp 163-168.
33. Eisemann, J., and A. Hilmar, "Influence of Wheel Load and Inflation Pressure on the Rutting Effect at Asphalt Pavement — Experiments and Theoretical Investigations," 6th International Conference, Structural Design of Asphalt Pavements, Volume I, Proceedings, pp 392-403, University of Michigan, Ann Arbor, Michigan, July 1987.
34. Claessen, A. I. M., and R. Ditmarsch, "Pavement Evaluation and Overlay Design: The Shell Method," 4th International Conference, pp 649-662, Ann Arbor, Michigan, 1977.
35. Cross, S. A., and E. R. Brown, "A National Study of Rutting in Hot Mix Asphalt (HMA) Pavements" National Center for Asphalt Technology, January 1992.
36. Moore, Raymond K., "Wide-Base Truck Tire Effects on Pavement Performance and Vehicle Regulatory Legislation," Kansas Department of Transportation, June 1992.
37. Sebaaly, P., and Nader Tabatabaee, "Effect of Tire Pressure and Type on Response of Flexible Pavement," Transportation Research Record 1227, pp 115-127.
38. Huhtala, Matti, Jari Pihlajamaki, and Markku Pienimaki, "Effect of Tires and Tire Pressures on Road Pavements," Transportation Research Record 1227, pp 107-114.
39. Bonaquist, Ramon, Roger Surdahl, and Walla Mogawer, "Effect of Tires Pressure on Flexible Pavement Response and Performance," Transportation Research Record 1227, pp 97-106.
40. Roberts, Freddy L., Prithvi S. Kandhal, E. Ray Brown, Dah-Yinn Lee, and Thomas W. Kennedy, "Hot Mix Asphalt Materials, Mixture Design, and Construction," NAPA Education Foundation, 1991.
41. Button, Joe W., Dario Perdomo, and Robert L. Lytton, "Influence of Aggregate on Rutting in Asphalt Concrete Pavements," Transportation Research Record 1259, pp 141-152.
42. Mahboub, Kamyar, and Dallas N. Little, "Improved Asphalt Concrete Mixture Design Procedure," Report 474-1F, Texas Transportation Institute, Texas A&M University, College Station, Texas.

43. Asphalt Institute, "The Asphalt Handbook," Asphalt Institute, 1989.
44. Saraf, C. L., B. F. McCullough, and M. F. Aslam, "Rutting of ACP Overlays on CRCP in the State of Texas," TRR 1109, January 1987.
45. Ford, Jr., Miller C., "Development of a Rational Mix Design Method for Asphalt Bases and Characteristics of ARKANSAS Asphalt Mixtures," Arkansas State Highway and Transportation Department, July 1985.
46. Won., M., K. Hankins, and B. F. McCullough, "Mechanistic Analysis of Continuously Reinforced Concrete Pavements Considering Material Characteristics, Variability, and Fatigue," Research Report 1169-2, Center for Transportation Research, The University of Texas at Austin, April 1990.
47. Cho, Yoon-Ho, and B. F. McCullough, "Development of Reflection Cracking on US 59 in Lufkin, Texas," 3rd International Workshop on the Design and the Evaluation of Concrete Pavements, October 1994.
48. Carey, W. N., and P. E. Irick, "The pavement serviceability - performance concept," HRB Bulletin 250, 1960.
49. Hegmon, Rudolph R., "A Close Look at Road Surface," *Public Roads*, summer 1993.
50. Paterson, W.D.O., "Prediction of Road Deterioration and Maintenance Effects: Theory and Quantification," Highway Design and Maintenance Standard Study, Vol III. Transportation Department, World Bank, 1987.
51. Sayers, Michael W., Thomas D. Gillespie, and Caesar A. V. Queiroz, "The International Road Roughness Experiment: Establishing Correlation and a Calibration Standard for Measurement," World Bank, 1986.
52. Sayers, Michael W., Thomas D. Gillespie, and Caesar A. V. Queiroz, "Guidelines for Conducting and Calibrating Road Roughness Measurements," World Bank, 1986.
53. Koesmo, Loestomo, and B. F. McCullough, "Evaluations of the Performance of teh Bonded Concrete Overlay on Interstate Highway 610 Northm, Houston, Texas," Report 920-2, Center for Transportation Research, The University of Texas at Austin, 1989.
54. Paterson, W.D.O., "International Roughness Index: Relationship to Other Measures of Roughness and Riding Quality," Transportation Research Record, 1084.
55. Janoff, M. S., J. B. Nick, P. S. Davit, and G. F. Hayhoe, "Pavement Roughness and Rideability," NCHRP Report 275, TRB, 1985.

APPENDIX A:

IRI AND PSI VARIATION DURING FIRST STAGE

• Rigid Section

Table A.1 IRI in the outside on Right Lane - rigid Section

	Pre-const.	Mar-92	Jul-92	Mar-93	Dec-93	Mar-94
R1	138.88	75.37	88.32	112.44	104.63	97.10
R21	250.14	54.77	75.49	125.48	148.86	204.25
R22	250.14	56.31	110.58	82.83	167.70	160.31
R3	94.08	56.53	110.69	127.57	117.54	92.51
R4	108.78	72.14	82.43	108.83	87.29	83.48
R5	133.77	69.98	78.40	85.02	79.88	82.00
R6	144.01	60.35	73.68	82.35	90.59	96.52
R0	99.29	*	75.40	83.58	92.81	95.08

*) Missing due to WIM installation

Table A.2 IRI in the inside on Right Lane - rigid Section

	Pre-const.	Mar-92	Jul-92	Mar-93	Dec-93	Mar-94
R1	149.62	72.90	89.08	73.71	99.68	87.69
R21	187.39	58.24	60.90	109.87	148.86	139.37
R22	187.39	66.47	110.91	88.79	167.70	163.14
R3	166.92	60.91	82.72	121.17	95.98	86.67
R4	93.64	70.79	76.26	82.89	86.66	72.58
R5	103.45	77.92	70.30	69.24	84.98	72.84
R6	133.95	73.28	72.73	76.45	75.22	78.37
R0	78.41	*	71.41	76.08	78.97	73.19

*) Missing due to WIM installation

Table A.3 PSI on the Right Lane - rigid Section

	Pre-const.	Mar-92	Jul-92	Mar-93	Dec-93	Mar-94
R1	2.78	4.29	4.04	3.96	3.75	3.87
R21	2.25	4.70	4.47	3.57	2.68	2.52
R22	2.25	4.58	3.61	3.95	2.56	2.67
R3	3.41	4.54	3.99	3.37	3.82	4.12
R4	3.79	4.35	4.17	3.83	4.16	4.19
R5	3.54	4.36	4.33	4.29	4.19	4.30
R6	2.97	4.55	4.37	4.26	4.23	4.14
R0	3.92	*	4.26	4.21	4.01	4.00

*) Missing due to WIM installation

Table A.4 IRI in the outside on Left Lane - rigid Section

	Pre-const.	Mar-92	Jul-92	Mar-93	Dec-93	Mar-94
R1	116.99	65.01	69.50	79.93	72.31	79.12
R21	86.67	46.83	54.66	76.06	65.48	65.78
R22	86.67	74.62	89.73	65.02	115.34	116.41
R3	92.39	81.26	77.22	79.15	93.33	91.84
R4	70.71	53.44	52.86	76.85	55.91	87.98
R5	89.13	59.19	58.47	49.15	62.30	63.00
R6	90.01	63.87	66.91	64.36	70.47	71.98
R0	96.01	*	95.41	73.27	86.53	88.01

*) Missing due to WIM installation

Table A.5 IRI in the inside on Left Lane - rigid Section

	Pre-const.	Mar-92	Jul-92	Mar-93	Dec-93	Mar-94
R1	114.55	66.15	75.48	92.73	76.92	74.04
R21	82.91	51.48	51.74	84.32	74.39	70.12
R22	82.91	67.22	76.70	66.48	109.98	113.14
R3	78.66	60.73	73.02	77.37	76.25	74.48
R4	74.09	53.09	49.87	69.23	51.83	72.83
R5	81.19	54.95	63.84	47.11	52.07	63.43
R6	86.82	63.63	65.40	65.35	62.25	74.30
R0	74.93	*	72.33	78.84	74.68	77.18

*) Missing due to WIM installation

Table A.6 PSI on the Left Lane - rigid Section

	Pre-const.	Mar-92	Jul-92	Mar-93	Dec-93	Mar-94
R1	3.49	4.39	4.34	4.08	4.28	4.26
R21	4.19	4.79	4.76	4.16	4.47	4.49
R22	4.19	4.30	4.14	4.40	3.61	3.61
R3	4.26	4.26	4.24	4.22	4.13	4.10
R4	4.33	4.71	4.76	4.30	4.77	4.12
R5	4.18	4.62	4.54	4.83	4.66	4.60
R6	4.19	4.56	4.54	4.56	4.55	4.46
R0	4.10	*	4.12	4.41	4.17	4.18

*) Missing due to WIM installation

• Flexible Section

Table A.7 IRI in the outside on Right Lane - Flexible Section

	Pre-const.	Mar-92**	Jul-92	Mar-93	Dec-93	Mar-94
F1	65.19		63.66	55.60	68.23	64.94
F2	62.22		51.46	51.79	58.42	61.30
F3	67.75		63.78	68.85	63.60	72.55
F4	78.89		57.92	61.91	59.91	71.83
F5	77.12		63.72	114.88	161.53	176.20
F6	62.48		70.63	68.38	71.77	84.96
F01	58.14		68.43	67.97	75.52	71.83
F02	58.14		73.75	75.24	75.90	78.62

**) Missing due to construction

Table A.8 IRI in the inside on Right Lane - Flexible Section

	Pre-const.	Mar-92**	Jul-92	Mar-93	Dec-93	Mar-94
F1	66.22		58.53	56.88	60.25	67.93
F2	64.76		54.49	55.41	57.33	65.07
F3	73.75		76.75	72.58	78.10	83.23
F4	78.43		67.10	69.50	67.26	81.91
F5	78.03		75.90	99.92	136.82	159.82
F6	67.47		71.68	65.10	71.73	85.72
F01	62.70		75.23	77.53	72.99	81.90
F02	62.70		65.14	67.46	67.38	80.03

**) Missing due to construction

Table A.9 PSI on the Right Lane - Flexible Section

	Pre-const.	Mar-92**	Jul-92	Mar-93	Dec-93	Mar-94
F1	4.62		4.72	4.77	4.66	4.62
F2	4.63		4.73	4.75	4.67	4.62
F3	4.49		4.44	4.43	4.43	4.36
F4	4.32		4.53	4.48	4.52	4.34
F5	4.31		4.42	3.64	2.95	2.76
F6	4.59		4.50	4.59	4.46	4.29
F01	4.63		4.34	4.38	4.41	4.29
F02	4.63		4.41	4.35	4.39	4.32

**) Missing due to construction

Table A.10 IRI in the outside on Left Lane - Flexible Section

	Pre-const.	Mar-92**	Jul-92	Mar-93	Dec-93	Mar-94
F1	55.12		72.01	73.81	78.49	87.70
F2	54.12		61.10	64.90	71.53	68.64
F3	68.26		67.56	72.22	74.80	78.38
F4	55.10		73.70	72.70	81.14	87.98
F5	56.81		64.21	69.03	96.58	97.47
F6	56.39		70.23	68.04	71.83	67.17
F01	65.50		75.19	76.44	82.55	86.28
F02	65.50		75.31	77.49	77.65	84.01

**) Missing due to construction

Table A.11 IRI in the inside on Left Lane - Flexible Section

	Pre-const.	Mar-92**	Jul-92	Mar-93	Dec-93	Mar-94
F1	53.87		67.98	62.23	67.43	72.14
F2	53.86		46.79	49.76	54.23	60.97
F3	54.53		59.05	58.26	61.76	68.03
F4	50.35		64.07	62.36	68.80	72.83
F5	48.88		58.09	67.12	75.27	72.54
F6	53.96		55.64	58.85	62.64	61.39
F01	62.15		91.27	82.14	96.82	94.28
F02	62.15		97.77	106.27	91.47	94.09

**) Missing due to construction






Table A.12 PSI on the Left Lane - Flexible Section

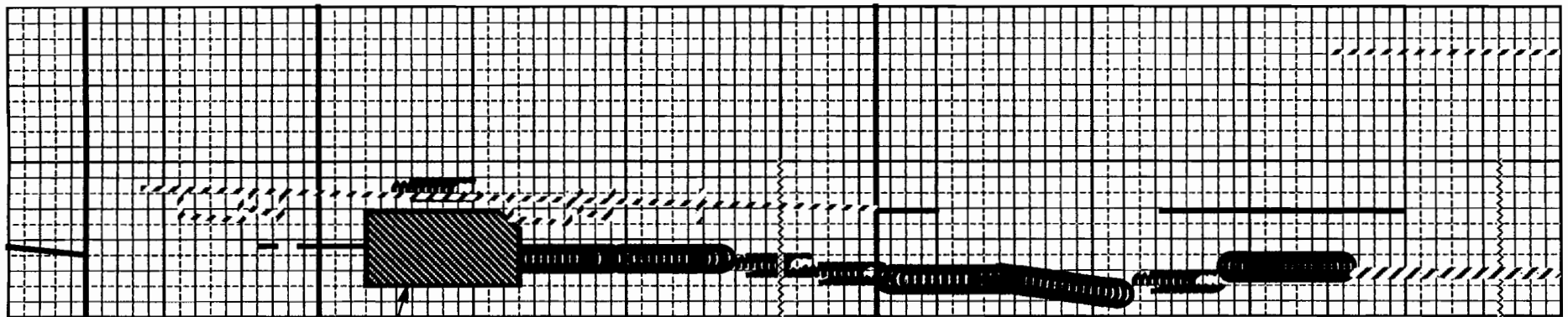
	Pre-const.	Mar-92**	Jul-92	Mar-93	Dec-93	Mar-94
F1	4.74		4.57	4.58	4.50	4.41
F2	4.72		4.73	4.67	4.60	4.56
F3	4.55		4.52	4.52	4.44	4.41
F4	5.03		4.36	4.34	4.31	4.16
F5	4.78		4.55	4.44	4.15	4.15
F6	4.77		4.58	4.56	4.54	4.57
F01	4.52		4.04	4.09	4.01	3.95
F02	4.52		4.12	4.04	4.16	4.11

**) Missing due to construction

APPENDIX B:

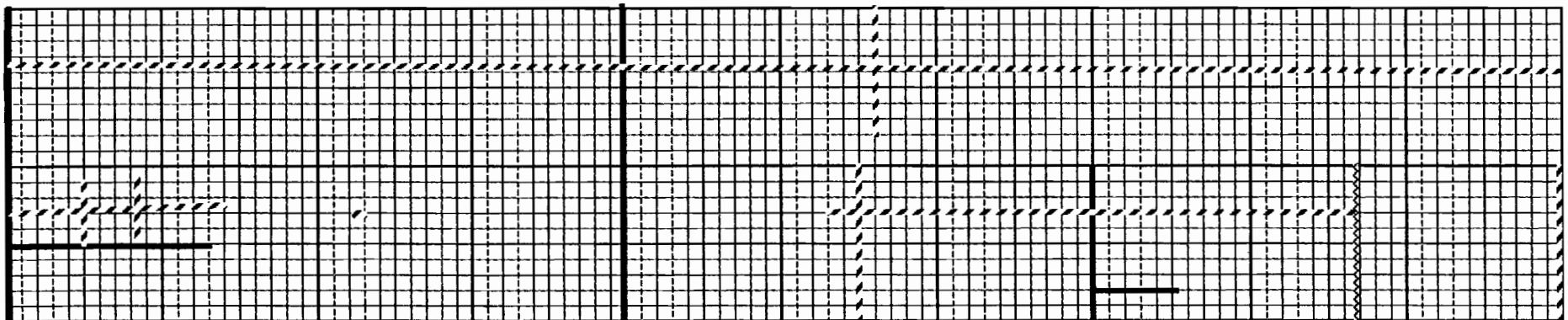
CONDITION SURVEY SAMPLE

Project 987 Condition Survey Conducted by The Center for Transportation Research January, 1994		 Holes (Unpatched)
Section R 2		 Patches
	December, 1992 May, 1993 October, 1993 January, 1994	Cracks
	December, 1992 May, 1993 October, 1993 January, 1994	Alligator Cracking
		 Core Locations



Failing

300



400

